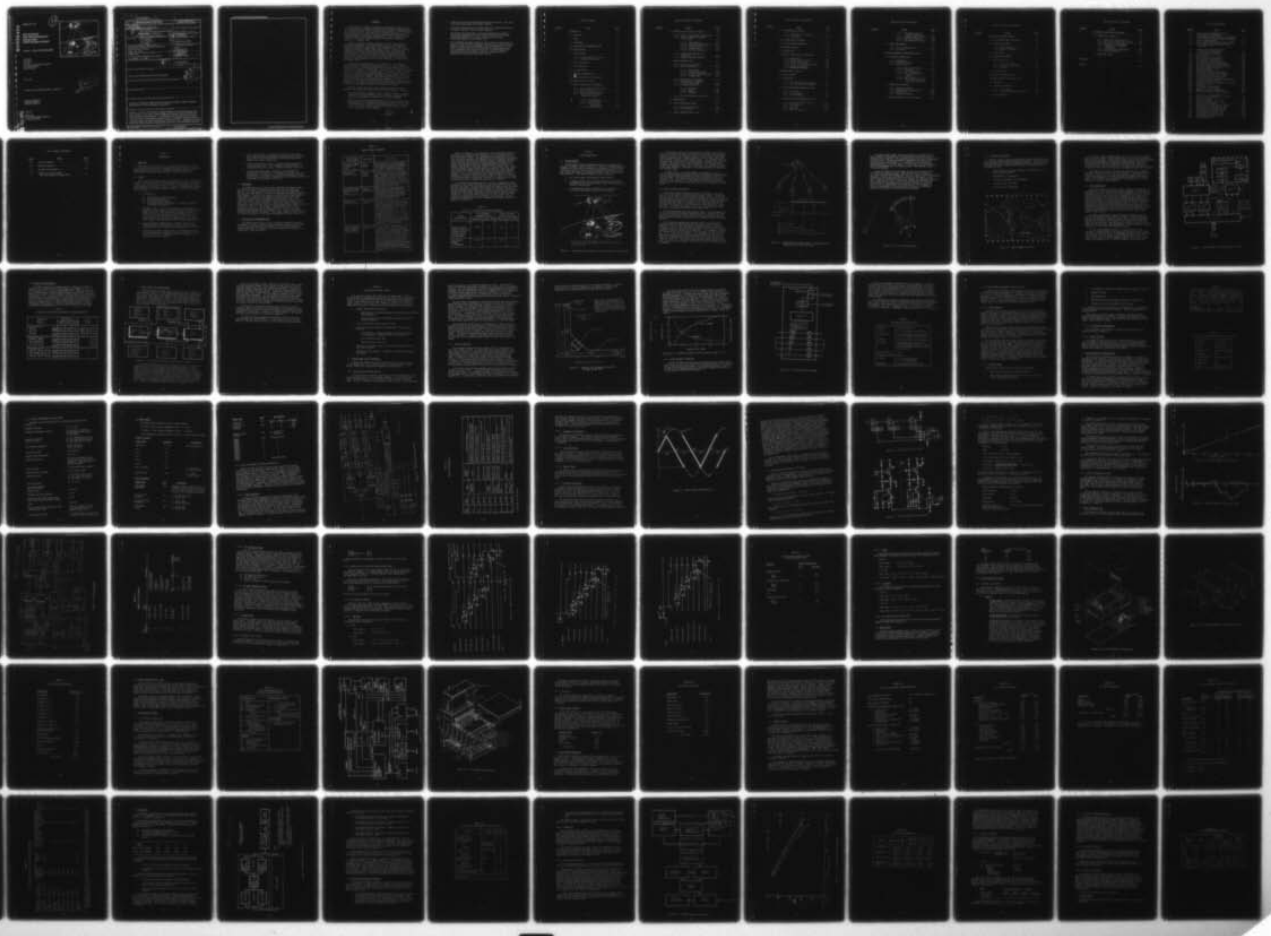
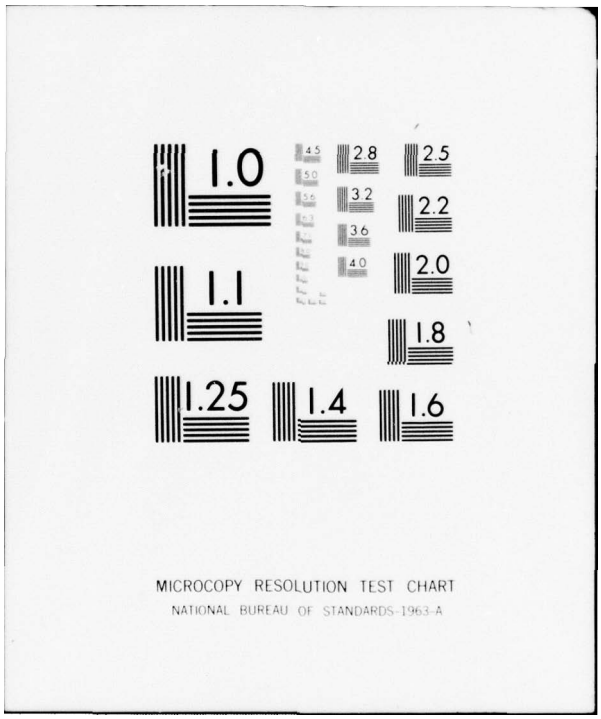
AD-A038 489 IBM FEDERAL SYSTEMS DIV OWEGO N Y F/G 17/7
SELF-CONTAINED, HIGH-ALTITUDE NAVIGATION SYSTEM STUDY: PRAIS NA--ETC(U)
JAN 77 D H ALDRICH, J W SIMMONS, N F TODA F04701-76-C-0106
UNCLASSIFIED IBM-77-D04-002S SAMSO-TR-77-57-VOL-2 NL

1 OF 2
AD A038489

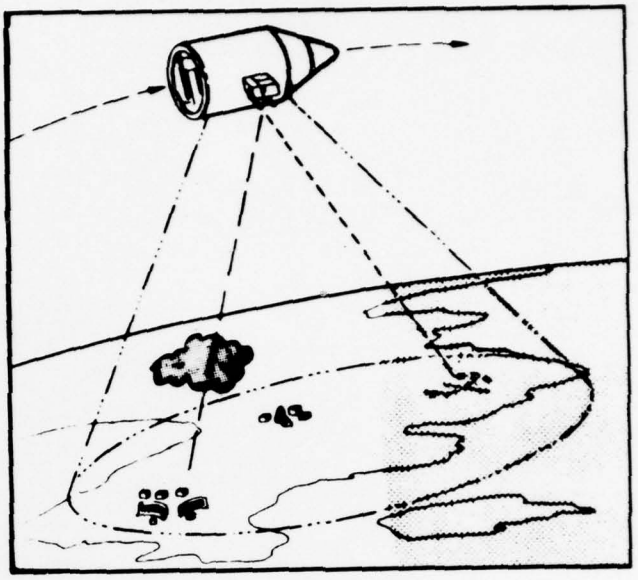



1.0
1.1
1.25
1.4
1.6
1.8
2.0
2.2
2.5
2.8
3.2
3.6
4.0
4.5
5.0
5.6
MICROCOPY RESOLUTION TEST CHART
NATIONAL BUREAU OF STANDARDS-1963-A

AD A038489

SAMSO TR No. 77-57

Self-Contained, High-Altitude Navigation System Study: PRAIS Navigation System



Volume II — System Technical Description

D.H. Aldrich
J.W. Simmons
N.F. Toda
International Business Machines Corporation
Federal Systems Division
Owego, NY 13827

January 1977

DDC
APR 20 1977

Final Report for Period 8 December 1975 — 1 January 1977

Approved for Publication,
Distribution Unlimited

Prepared for

SAMSO YAD
PO Box 92960 Worldway Postal Center
Los Angeles, CA 90009

DDC FILE COPY

PRAIS Navigation System.

UNCLASSIFIED

SECURITY CLASSIFICATION OF THIS PAGE (When Data Entered)

REPORT DOCUMENTATION PAGE

READ INSTRUCTIONS BEFORE COMPLETING FORM

1. REPORT NUMBER: SAMSO TR-77-57-Vol-2	2. GOVT ACCESSION NO.
3. RECIPIENT'S CATALOG NUMBER	
4. TITLE (and Subtitle): Self-Contained, High-Altitude Navigation System Study; Final Report, Volume II, System Technical Description,	5. TYPE OF REPORT & PERIOD COVERED: Final —12/8/75 — 1/1/77
	6. PERFORMING ORG. REPORT NUMBER: IBM-77-D04-002
7. AUTHOR(s): D. H. Aldrich, J. W. Simmons, N. F. Toda	8. CONTRACT OR GRANT NUMBER(s): F04701-76-C-0106
9. PERFORMING ORGANIZATION NAME AND ADDRESS: International Business Machines Corporation, Federal Systems Division, Owego, NY 13827	10. PROGRAM ELEMENT, PROJECT, TASK AREA & WORK UNIT NUMBERS: 63401F, Program 681D
11. CONTROLLING OFFICE NAME AND ADDRESS: SAMSO YAD, P.O. Box 92960 Worldway Postal Center, Los Angeles, CA 90009	12. REPORT DATE: January 1977
	13. NUMBER OF PAGES: 184
14. MONITORING AGENCY NAME & ADDRESS (if different from Controlling Office): 182 p.	15. SECURITY CLASS. (of this report): UNCLASSIFIED
	15a. DECLASSIFICATION/DOWNGRADING SCHEDULE

16. DISTRIBUTION STATEMENT (of this Report)

Approved for publication, distribution unlimited

DDC RELEASED APR 20 1977

17. DISTRIBUTION STATEMENT (of the abstract entered in Block 20, if different from Report)

18. SUPPLEMENTARY NOTES

19. KEY WORDS (Continue on reverse side if necessary and identify by block number)

Autonomous Navigation, High Altitude, Attitude Determination, Passive Ranging, Interferometer, Direction Finding, Kalman Filter

20. ABSTRACT (Continue on reverse side if necessary and identify by block number)

Abstract: Circuits to add a passive ranging capability to the Interferometric Landmark Tracker (ILT) to form a Passive Range Interferometer Sensor (PRAIS) were built and tested in the laboratory. The laboratory test data were used in a Monte Carlo simulation to demonstrate the performance of the PRAIS Navigation System in a highly eliptical orbit and a synchronous (1° inclination) orbit. Navigation accuracies better than 1000 ft and attitude accuracy better than 10 sec were indicated by the analyses.

DD FORM 1 JAN 73 1473 EDITION OF 1 NOV 65 IS OBSOLETE

UNCLASSIFIED

SECURITY CLASSIFICATION OF THIS PAGE (When Data Entered)

409 206

FOREWORD

This report is Volume II of the three-volume final report on the Self-Contained High Altitude Navigation System (SCHANS) study published by the IBM Corporation Federal Systems Division under Air Force Contract No. F04701-76-C-0106. The final report describes the results of studies, design activities, laboratory tests and system simulations performed from 8 December 1975 through 30 December 1976. It is submitted to the USAF Space and Missile Systems Organization (SAMSO) for review by Captain R. A. Lawhern, USAF.

Volume I provides a summary description of the system concept, operation, performance and configuration as well as a statement of application potential, conclusions, and recommendations. This volume describes results of SCHANS contract work by task. Volume III contains circuit level electrical design description of the Interferometric Landmark Tracker (ILT) Receiver and the Pulse Conversion Unit (PCU); it also contains an operational software Computer Program Development Specification. This final report is also supported by several other documents produced under this and previous contracts, as listed in the References section.

This report was authored by D. H. Aldrich and J. W. Simmons of Electromagnetic Development Engineering and by N. F. Toda of Advanced Tactical Systems. The authors acknowledge with gratitude the support of their fellow technical investigators: H. W. Hill, L. O. Smith, R. E. Dreska, L. Fulk, E. E. Kroman, C. J. Standish, and R. L. Smith. Special thanks are due the Staff of the Engineering Administrative Systems Center, under the coordination of Sherry Underwood: Suzanne Crowley, Gae Errigo, Ellen Pulver and Lorrie Zembery. They cheerfully and tirelessly typed and retyped reams of text from manuscripts prepared by a variety of authors. We also appreciate the energetic direction and control provided by Captain R. A. Lawhern of SAMSO YAD and by John Barnes, Aldo Brigante, Eugene Farr and Howard Hendrickson of Aerospace Corporation.

There are a few terms used in this report that deserve some explanation and comment for the sake of clear understanding, as follows:

- ILT (Interferometric Landmark Tracker) denotes a sensor, including antenna array and multichannel receiver, capable of making interferometric measurements on signals received from landmarks.

- PRAIS (Passive Ranging Interferometric Sensor) is an ILT with the added capability of accurately measuring the times of arrival (TOA) of landmark pulses. Additional processing capability is required to use a series of TOA measurements to derive an estimate of the line of sight range to the landmark.

- SCHANS (Self-Contained High Attitude Navigation System) is the name given the program under the present contract.

- PCU (Pulse Conversion Unit) is that part of the PRAIS that provides a digital interface with an external computer.

- SPU (Signal Processing Unit) is the microprocessor with memory, timing and input/output functions chosen to provide the on-board processing capability for signal, navigation and attitude processing needed for space flight test.

- The term PRAIS Navigation System is used in parts of this report to denote the IBM system for autonomous navigation and attitude determination in high altitude spacecraft, using the capabilities of the PRAIS to measure the line of sight direction and estimated ranges to ground based radars of known location. The PRAIS Navigation System consists of the PRAIS, a processor (digital computer), appropriate software and (optionally) an IRU.

TABLE OF CONTENTS

Section	Title	Page
1	INTRODUCTION	1-1
	1.1 OBJECTIVE	1-1
	1.2 SCOPE	1-1
	1.3 BACKGROUND	1-2
	1.4 CONCLUSIONS AND RECOMMENDATIONS	1-2
2	SYSTEM DESCRIPTION	2-1
	2.1 SYSTEM CONCEPT	2-1
	2.1.1 Passive Ranging Description	2-2
	2.1.2 Landmark Distribution	2-5
	2.2 PRAIS DESCRIPTION	2-6
	2.3 SPU DESCRIPTION	2-8
	2.4 IRU DESCRIPTION	2-9
	2.5 PHYSICAL CHARACTRISTICS	2-10
	2.6 SPACE FLIGHT TEST SYSTEM DESIGN	2-11
3	SYSTEM DESIGN (TASKS 1 AND 6)	3-1
	3.1 ANTENNA ARRAY AND RF CALIBRATOR	3-1
	3.1.1 Array/Calibrator Configurtion	3-1
	3.1.2 Antenna Selection	3-2
	3.1.3 Radio Frequency Calibrator	3-4
	3.1.4 Antenna Array/Calibrator Mechanical Design	3-7
	3.1.4.1 Array Material	3-7
	3.1.4.2 Antenna Cables	3-7
	3.1.4.3 RF Calibrator Configuration	3-8
	3.1.4.4 Weight Estimate	3-8

Table of Contents (Continued)

Section	Title	Page
3.2	PRAIS Receiver Electrical Design	3-8
3.2.1	Receiver Performance Specification .	3-12
3.2.2	Receiver Summary Functional Description.	3-14
3.2.2.1	Phase Detector	3-14
3.2.2.2	Frequency Discriminator . .	3-17
3.2.2.3	Local Oscillator.	3-17
3.2.2.4	Control Logic	3-17
3.2.2.5	RF Phase Calibrator	3-17
3.2.3	Compensated Logarithmic IF Amplifier.	3-19
3.2.4	Adaptive Threshold Detector.	3-22
3.3	PULSE CONVERSION UNIT	3-22
3.3.1	PCU Inputs and Outputs	3-25
3.3.2	Modes of Operation	3-25
3.3.2.1	Normal Mode	3-25
3.3.2.2	RF Calibration Mode	3-28
3.3.2.3	IF Phase Calibrator Mode. .	3-28
3.3.2.4	Standby Mode.	3-28
3.3.3	PCU Process Cycle Timing	3-28
3.3.4	Changing Bits in Mode and Tuning Control Words	3-29
3.3.5	PC Processing Errors	3-29
3.3.5.1	Amplitude	3-29
3.3.5.2	Phase	3-34
3.3.5.3	Frequency	3-34
3.3.6	PCU Detailed Design Description. . .	3-34
3.4	POWER SUPPLY.	3-34
3.5	ILT-PCU MECHANICAL DESIGN	3-35
3.5.1	Physical Description	3-35
3.5.2	ILT-PCU WEight	3-38
3.6	SIGNAL PROCESSING UNIT (SPU).	3-41

Table of Contents (Continued)

Section	Title	Page
	3.7 SPU MECHANICAL DESIGN	3-41
	3.7.1 SPU Physical Description	3-41
	3.7.2 SPU Weight	3-45
	3.8 SYSTEM WEIGHT ESTIMATE	3-45
	3.9 SYSTEM POWER CONSUMPTION	3-45
	3.10 THERMAL ANALYSIS	3-47
	3.11 RELIABILITY	3-55
	3.12 NUCLEAR SURVIVABILITY ASSESSMENT	3-57
	3.12.1 Methodology	3-59
	3.12.2 SCHANS Hardness Levels	3-59
	3.12.3 Natural Environment	3-63
	3.12.4 Natural Environment Hardening	3-64
	3.12.5 Nuclear Environment	3-64
	3.12.6 Hardening Assessment	3-64
4	LABORATORY TESTS (TASK 2)	4-1
	4.1 TEST CONCEPTS	4-2
	4.2 CONCLUSION	4-6
	4.2.1 TOA Counter/Buffer Error Rate	4-6
	4.2.2 Time of Arrival Measurements	4-6
	4.3 TOA COUNTER/BUFFER ERROR RATE TEST	4-7
	4.3.1 Test Setup	4-7
	4.3.2 Test Procedure	4-9
	4.3.3 TC/B Test Results	4-9
	4.4 PRECISION TIME MEASUREMENT UNIT TEST	4-12
	4.4.1 Test Premises and Criteria	4-12
	4.4.2 Test Conditions	4-13
	4.4.3 Test Setup	4-13
	4.4.4 Operation	4-13
	4.4.5 PTMU Test Results	4-16

Table of Contents (Continued)

Section	Title	Page
	4.4.5.1 Chi-Square Test for Normal Distribution . . .	4-16
	4.4.5.2 PTMU Measurement Results. .	4-16
	4.4.5.3 TOA Bias Variations	4-19
	4.4.5.4 TOA Standard Deviations . .	4-19
	4.5 PRAIS ERROR BUDGET.	4-25
	4.5.1 Passive Ranging Error	4-25
	4.5.2 ILT Errors	4-25
5	SYSTEM PERFORMANCE DEMONSTRATION (TASK 3). . . .	5-1
	5.1 SIMULATION DESCRIPTION	5-2
	5.1.1 Background	5-2
	5.1.2 Simulation Format.	5-4
	5.1.3 Dynamic Module	5-4
	5.1.3.1 Real World Dynamics	5-4
	5.1.3.2 Gyro Model.	5-6
	5.1.3.3 ILT Error Models	5-6
	5.1.3.4 Passive Ranging Error Model	5-6
	5.1.3.5 Clock Model	5-7
	5.1.3.6 Passive Ranging Measurements Bias Correction . .	5-8
	5.2 SIMULATION VALIDATION	5-9
	5.2.1 Program Validation	5-9
	5.2.2 Algorithm and Approximations	5-9
	5.2.3 Observability.	5-10
	5.2.4 Eigenvalue Analysis	5-11
	5.3 PRAIS Navigation System Performance	5-16

Table of Contents (Continued)

Section	Title	Page
6	FLIGHT TEST PLANNING (TASK 4)	6-1
	6.1 PRELIMINARY FLIGHT TEST PLAN	6-1
	6.2 FLIGHT TEST CONCEPT	6-1
	6.2.1 Normal Operation	6-2
	6.2.2 Real Time Operation	6-2
	6.3 INSTALLATION	6-2
	6.4 COMMAND REQUIREMENTS	6-5
	6.5 DATA ACQUISITION	6-7
	6.5.1 Pulse Data Samples.	6-7
	6.5.2 Navigation Data Samples	6-7
	6.5.3 Telemtry.	6-7
	6.6 DATA REDUCTION	6-10
7	FLIGHT TEST SOFTWARE (TASK 5)	7-1
8	ATTITUDE DETERMINATION DESIGN (TASK 7)	8-1
	8.1 APPROACH	8-1
	8.2 ATTITUDE PROPAGATION	8-2
	8.2.1 Filter Update	8-3
	8.2.2 Filter Covariance Propagation	8-5
	8.3 IRU DESCRIPTION	8-7

Table of Contents (Continued)

Section	Title	Page
9	RECOMMENDED ADDITIONAL DEVELOPMENTS	9-1
	9.1 COMPLETION OF DESIGN	9-1
	9.1.1 Operational Systems Design.	9-1
	9.1.2 Early Space Flight Test Planning. . .	9-3
	9.1.3 Antenna Array Development	9-4
	9.1.4 Reliability and Equipment Redundancy.	9-4
	9.1.5 Flight Software Development	9-4
	9.1.6 System Engineering.	9-5
	9.2 SUBSEQUENT PHASES.	9-6
REFERENCES		R-1
GLOSSARY		G-1

LIST OF ILLUSTRATIONS

Figure	Title	Page
2-1	Passive Range Interferometer Sensor Navigation System Concept	2-1
2-2	Representative Problem Geometry, Autonomous Passive-Ranging Timing at Each Observation	2-3
2-3	Passive Ranging Geometry	2-4
2-5	Passive Range Interferometer Sensor (PRAIS)	2-7
2-6	System Block Diagram with Host Vehicle Interfaces	2-11
3-1	Antenna Array Configuration for 1978 STP Space Flight Test	3-3
3-2	RF Calibrator Block Diagram	3-5
3-3	RF Calibrator	3-10
3-4	PRAIS Receiver Block Diagram	3-15
3-5	Phase Detector Characteristics	3-18
3-6	Log Amplifier Block Diagram	3-20
3-7	Log Amplifier Simplified Schematic	3-20
3-8	Log Video Output Versus Input Power	3-23
3-9	Log Video Linearity Versus Input Power	3-23
3-10	Adaptive Threshold Detector	3-24
3-11	PCU Block Diagram	3-26
3-12	Normal Mode Process Cycle Timing	3-30
3-13	RF Frequency Cal Mode Cycle Timing	3-31
3-14	IF Cal Mode Processor Cycle Timing	3-32
3-15	ILT-PCU Mechanical Organization	3-36
3-16	IF Module Assembly of Preamplifier/Limiter	3-37
3-17	Power Supply Configuration	3-39
3-18	Pluggable Electronic Subassembly (4 Pi Page)	3-39
3-19	SPU Signal Flow	3-43
3-20	SPU Mechanical Organization	3-44
3-21	Reliability Model Diagram	3-56
3-22	Hardness Assessment Methodology	3-60
3-23	Piece Part Radiation Effects Example	3-61
4-1	SCHANS Critical Component Test Concept	4-3
4-2	ILT Receiver Block Diagram	4-4
4-3	PCU Block Diagram	4-5
4-4	TOA Counter/Buffer Test Concept	4-8
4-5	PTMU Test Block Diagram	4-14
4-6	Rador Signal Simulator Block Diagram	4-15
4-7	TOA Deviation of the Mean at -5°C	4-20
4-8	TOA Deviation of the Mean at 20°C	4-20
4-9	TOA Deviation of the Mean at 75°C	4-21
4-10	TOA Standard Deviation at -5°C	4-22
4-11	TOA Standard Deviation at 20°C	4-23
4-12	TOA Standard Deviation at 75°C	4-24
4-13	PRAIS TOA Accuracy	4-26

List of Illustrations (Continued)

Figure	Title	Page
5-1	Simulation of the Gyros and Estimated Attitude Quaternion	5-3
5-2	Measurement Residual Simulation Showing the Real and Filter World Relationships	5-5
5-3	RMS Position Error, Synchronous Orbit	5-13
5-4	Minimum Eigenvalue	5-14
5-5	Condition Number	5-15
5-6	PRAIS Navigation System RSS Position Error in Synchronous (1^{o}) Orbit	5-17
5-7	PRAIS Navigation System RSS Attitude Error in Synchronous (1^{o}) Orbit	5-18
5-8	PRAIS Navigation System RSS Position Error in the Molniya Orbit	5-19
5-9	PRAIS Navigation System RSS Attitude Error in the Molniya Orbit	5-20
6-1	Normal Operation	6-3
6-2	Real Time Operation	6-3
6-3	Prospective Host Vehicle Installation	6-4
6-4	SCHANS Space Flight Test System Cabling	6-6
6-5	Space Flight Test Data Interfaces	6-8
6-6	Navigation Data Sample Generation	6-9
6-7	Real Time Data Transmission	6-11
7-1	SCHANS Operational Program Structure	7-2
8-1	Navigation Error	8-9
8-2	Attitude Error	8-10

LIST OF TABLES

Table	Title	Page
1-1	SCHANS Program Background	1-3
1-2	PRAIS vs. ILT Navigation System Performance	1-4
2-1	SPU Performance Characteristics	2-8
2-2	PRAIS Navigation System Requirements	2-8
2-3	PRAIS Navigation System Strapped Down IRU Characteristics	2-9
2-4	PRAIS Navigation System Physical Characteristics	2-10
3-1	Calibrator Specifications	3-6
3-2	Comparison of Candidate Structural Material	3-9
3-3	RF Cable Mechanical Characteristics (ERI)	3-9
3-4	Antenna Array Weight Estimate	3-11
3-5	Receiver Subassemblies	3-16
3-6	SCHANS I/O Bit Formation	3-27
3-7	Errors of Each Function in the Analog Processing Chain	3-33
3-8	ILT-PCU Weight Calculation	3-40
3-9	Signal Processing Unit Principal Characteristics	3-42
3-10	SPU Weight Calculation	3-46
3-11	Typical Single-Orbit Power Consumption	3-48
3-12	ILT-PCU Power Consumption	3-49
3-13	SPU Power Consumption	3-50
3-14	ILT-PCU Subassembly Mounting Temperature	3-51
3-15	ILT-PCU Electrical Piece Part Case/Junction Temperatures	3-52
3-16	SPU Subassembly Power Dissipation Distribution and Subassembly Mounting Temperatures	3-53
3-17	SPU Electrical Piece Part Case/Junction Temperatures	3-54
3-18	Comparison of Reliability Requirements	3-58
3-19	μA471 Op-Amp Dose Data	3-62
3-20	SCHANS Estimated Hardness	3-65
4-1	TOA Test Summary	4-11
4-2	TC/B Error Rates	4-11
4-3	PTMU Data Statistical Distribution Test Results (Chi-Square Goodness of Fit Test for Normality)	4-17
4-4	PTMU Test Results	4-18
4-5	Passive Ranging Error Budget	4-27

List of Tables (Continued)

Table	Title	Page
4-6	ILT Error Budget	4-27
5-1	Orbital Parameters	5-1
6-1	Navigation Data Sample	6-9
9-1	Comparison of Space Flight Test and Operational Requirements	9-2

Section 1

INTRODUCTION

1.1 OBJECTIVE

The objective of this report is to describe in detail the results of a design study and critical component development phase of a program aimed ultimately at operational autonomous navigation and attitude determination for high altitude (500 nm or greater) spacecraft.

1.2 SCOPE

This volume of the final report is organized, after the introductory sections, to present results of the contract effort by task. The exception is that Task 6 (Signal Processing Unit Design) is discussed with Task 1 (System Design) in Section 3. Tasks 5, 6 and 7 were added to the contract scope after work was started on tasks 1 through 4. The tasks addressed are as follows:

1) System Design

   a) PRAIS Receiver Electrical Design
   b) PCU Electrical Design
   c) ILT-PCU Mechanical Design
   d) System Engineering and Analyses, including reliability and nuclear survivability

2) Laboratory Tests: Tests in the laboratory of breadboard precision time measurement circuits and time of arrival counter/buffer error rate. The former tests yielded statistical characteristics of time-of-arrival measurement errors to be used in the system simulations of Task 3. The latter tests provided assurance that the TOA counter/buffer error rate is small enough to have negligible effect on system performance.

3) System Performance Demonstration: Computer simulation of PRAIS Navigation System performance in two simulated high-altitude orbits, with realistic environment and error sources.

4) Flight Test Planning: Preparation of a preliminary plan to include spacecraft interfaces and support requirements, flight test plan objectives, command and control, telemetry, data acquisition and data reduction.

5) Flight Test Software: Preparation of top-level flow charts and a computer program development specification for Executive, Signal Processing and Navigation and Attitude Determination software for a space flight test.

6) Signal Processor Unit Design: Specification and paper design to logic diagram levels: microprocessor, memory, timing, input/output and power supply. Mechanical design of the unit.

7) Attitude Reference Design: Definition of algorithms for determination of attitude of a stabilized spacecraft using ILT measurements. Incorporation of attitude determination in the system simulation program. Demonstration of attitude determination performance in conjunction with Task 3.

1.3 BACKGROUND

The SCHANS design study and critical component development effort was the latest phase in a program started more than five years ago. In mid-1971, the IBM Corporation's Federal Systems Division undertook a preliminary design (Phase 0) study of the Autonomous Navigation Technology (ANT) program. The basic ANT concept is based on using interferometric measurements of emissions from known but noncooperative ground-based radars for determination of spacecraft position and velocity. The preliminary design concept included use of an inertial reference sensor and a star tracker in the spacecraft. Additional studies, analyses, simulations, and laboratory tests have been performed under SAMSO contracts, as shown in Table 1-1. The changes in program names (and acronyms) reflect the changes in system concept and characteristics as system design has been refined and new techniques (e.g., passive ranging and attitude determination) introduced. The system concept has been developed to a state of readiness for prototype development and space flight test.

1.4 CONCLUSION AND RECOMMENDATIONS

The SCHANS contract caps a series of applied research, laboratory development, analysis, simulation and preliminary design activities that (1) show the practicability and flexibility of the PRAIS Navigation System concept and (2) provides a baseline from which development of an operational system can proceed.

TABLE 1-1

SCHANS PROGRAM BACKGROUND

Program Name & Contract Number	Time Period	Scope & Results
Autonomous Navigation Technology (ANT) Phase 0 F04701-71-C-0339	June 71 through Feb 72	Study of spacecraft autonomous navigation with interferometric landmark tracking (ILT) in combination with inertial reference and star tracker. Feasibility demonstrated
ANT Phase 1A F04701-73-C-0221	March 73 through June 74	Laboratory evaluation of ILT sighting accuracy and computer simulation of ANT performance. Navigation errors within 550 ft were demonstrated with convergence time of 50 minutes in a worst-case orbit. Interferometer performance was measured in an anechoic chamber using two orthogonal baselines of 10 λ each. Accuracy was near 1 $\widehat{\text{min}}$
High-Altitude Navigation System (HANS) Study F04701-74-C-0565	June 74 through Jan 75	Study of utility of passive ranging (PAR) measurements in conjunction with ILT. System sensitivity and error budget analyses. Simulations demonstrated distinct improvement with PAR tracking landmarks with stable pulse repetition intervals
ANT Phase 1B F04701-75-C-0046	Oct 74 through Nov 75	ILT Receiver design study, analyses, and breadboard tests to yield design specification and preliminary physical configuration suitable for space flight test. Design of three-channel superheterodyne receiver for measurement of landmark pulse arrival angle in two orthogonal baselines, received signal strength, time-of-pulse arrival (TOA), signal quality, and calibration (i.e., measurement of inter-channel phase errors). Description of signal processing functions needed to input ILT measurements into a spaceborne navigation program in an onboard computer.
Self-Contained High-Altitude Navigation System (SCHANS) F04701-76-C-0106	Dec 75 through Dec 76	Critical component breadboard tests: TOA counter error rate and TOA measurement error statistics. Preliminary part 1 development specification. Paper design of principal units: Interferometric Landmark Tracker-Pulse Conversion Unit (ILT-PCU) and Signal Processing Unit (SPU). Preliminary space flight test planning. Space flight software design specifications through top level flows (Part 1 specifications). Demonstration of high-altitude navigation and attitude system performance through simulation. Reliability prediction and preliminary Nuclear Survivability analyses.

Table 1-2 summarizes the performance of the autonomous navigation system with and without passive ranging in the two design reference orbits provided by SAMSO. This performance was demonstrated in simulation runs using realistic environmental factors and hardware measurement error statistics determined by laboratory tests. Comparison of these results indicate that the passive range measurements significantly improve both navigation and attitude determination accuracies. Performance improvement is much more dramatic in the Molniya orbit. This is to be expected, since passive ranging estimation of the time difference between the landmark (radar PRI) and spacecraft clocks requires relative motion of the line-of-sight between the spacecraft and the landmark. In a truly synchronous orbit, PRAIS navigation accuracy is essentially limited by the ILT navigation shown in Table 1-2. However, as can be seen even in inclinations as small as 1 degree, passive range measurements provide a significant improvement in accuracy.

A continuing development program is strongly recommended to take advantage of the design, technology and experience base constructed over the past five years. The next phase should see completion of the system, prototype hardware and software design aimed at a space flight test at the earliest practicable date; next, hardware fabrication, qualification testing, software coding, validation and verification; third, a space flight test. Successful demonstration of the space flight model will provide the starting point for operational system design. The key technical considerations of such a recommended development program are addressed in Section 9.

Table 1-2

PRAIS vs. ILT NAVIGATION SYSTEM PERFORMANCE

Orbit Characteristics	ILT Navigation 1-sigma rms Errors		PRAIS Navigation 1-sigma rms Errors	
	Position (ft)	Attitude ($\widehat{\text{sec}}$)	Position (ft)	Attitude ($\widehat{\text{sec}}$)
Molniya altitude: Apogee 21,406 nmi; Perigee 390 nmi Period: 12 hours 63° Inclination	7,080	26	225	10
Synchronous altitude 1° Inclination	8,316	16	3,000	10

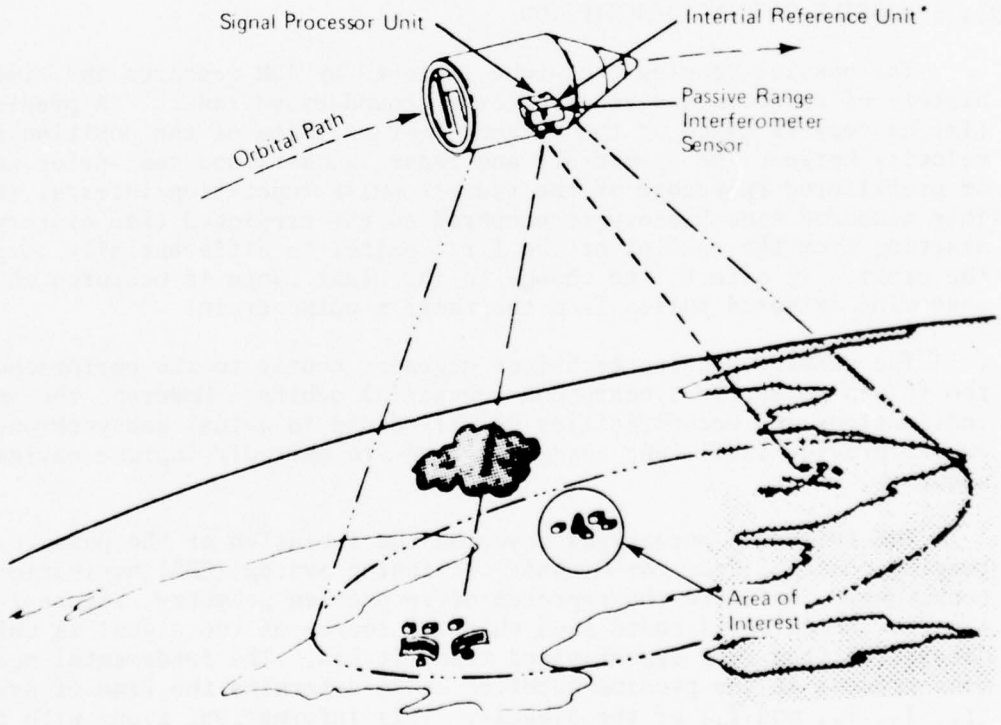
Section 2

SYSTEM DESCRIPTION

2.1 SYSTEM CONCEPT

The IBM Passive Range Interferometer Sensor Navigation System Concept for SCHANS, shown in Figure 2-1, utilizes a strapped-down dual orthogonal baseline phase interferometer augmented by precision time-of-arrival circuits to derive line-of-sight angle and passive (one-way) range measurements to ground-based radars of known location and characteristics. The PRAIS Navigation System consists of

- The Passive Range Interferometer Sensor (PRAIS)
- A Signal Processor Unit (SPU) which processes the PRAIS measurements in a 24-state Kalman filter to derive position, velocity, and attitude
- A strapped-down inertial reference unit (optional) to provide attitude memory between ILT measurements.



*This function can be provided by PRAIS in orbits where at least two landmarks are continuously visible or on spacecraft with independent local vertical-oriented attitude control systems.

Figure 2-1. Passive Range Interferometer Sensor Navigation System Concept

In operation, angle data are received by the PRAIS from such landmarks as air traffic control, defense early-warning and coastal-search radars operating in the frequency range of 2.5 to 2.9 GHz. These angle data are processed with a Kalman navigation filter to determine spacecraft position, velocity, and attitude vectors. The latitude, longitude, altitude, PRI, and frequency of selected radars of known position are stored in the computer to be used as landmarks. Any of these stored landmarks within the field-of-view of the ILT can be acquired by tuning to the radar frequency. Day/night, all-weather operation is inherent in this frequency band.

The PRAIS and its associated computer algorithms also provide passive ranging between the spacecraft and the landmarks, using unsynchronized emissions from ground radars that have stable pulse repetition intervals (PRI). The PRAIS Navigation System estimates the time of emission of the radar pulses in the Kalman filter and does not require synchronization of ground or spacecraft clocks nor time tagging of radar pulses.

2.1.1 PASSIVE RANGING DESCRIPTION

The passive-ranging technique employed by IBM measures the time history of radar pulses received from ground-based radars. A predicted time history is based on the current best estimate of the position and velocity between the spacecraft and radar landmark and some prior knowledge or prefiltered knowledge of the radar's pulse repetition interval (PRI). This measured time history is compared to the predicted time history, starting from the receipt of the first pulse, to differentially correct the orbit. In effect, the change in the slant range is measured while observing selected pulses from the radar's pulse train.

The passive-ranging technique degrades nearly to the performance of the ILT in perfectly synchronous equatorial orbits. However, the small inclinations and eccentricities usually found in actual geosynchronous orbits provide sufficient change in range to markedly improve navigation accuracy.

The following paragraphs describe the evolution of the passive-ranging concept, from the Global-Positioning System (GPS) navigation techniques. Refer to the representative problem geometry, Figure 2-2. A narrow RF pulse is coded such that the source of the signal is uniquely determined from four synchronized transmitters. The fundamental measurement process at the passive receiver is to determine the time of arrival (T_1, T_2, T_3, and T_4) of the signals. This information, along with the known emitter locations, provides sufficient data for the spacecraft computer to determine the position of the passive vehicle and the spacecraft time error, ΔT. The GPS provides such pseudo-range navigation for users in near-earth environments, using four satellites of known positions as landmarks.

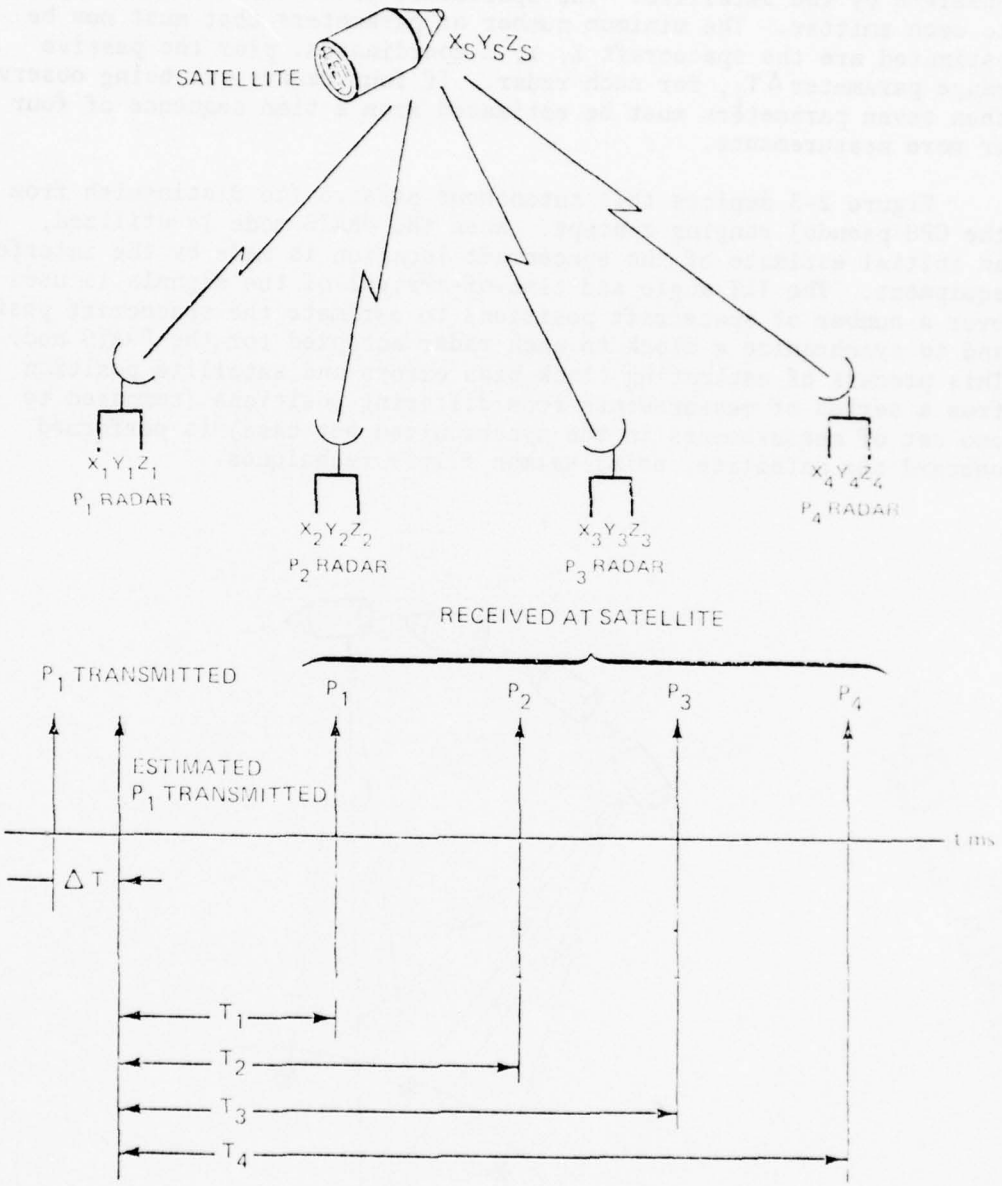


Figure 2-2. Representative Problem Geometry, Autonomous Passive-Ranging Timing at Each Observation

The pseudo-range concept can now be extended to include the case where a number of noncooperative, nonsynchronized radars are being observed by the satellite. The spacecraft processor now must "synchronize" to each emitter. The minimum number of parameters that must now be estimated are the spacecraft X, Y, Z coordinates, plus the passive range parameter ΔT_i, for each radar. If four radars are being observed, then seven parameters must be estimated from a time sequence of four or more measurements.

Figure 2-3 depicts this autonomous passive (to distinguish from the GPS pseudo) ranging concept. When the PRAIS mode is utilized, an initial estimate of the spacecraft location is made by the interferometer equipment. The ILT angle and time-of-arrival of the signals is used over a number of spacecraft positions to estimate the spacecraft position and to synchronize a clock to each radar accepted for the PRAIS mode. This process of estimating clock bias errors and satellite position from a series of measurements from differing positions (compared to one set of measurements in the synchronized net case) is performed onboard the satellite, using Kalman filter techniques.

BEST AVAILABLE COPY

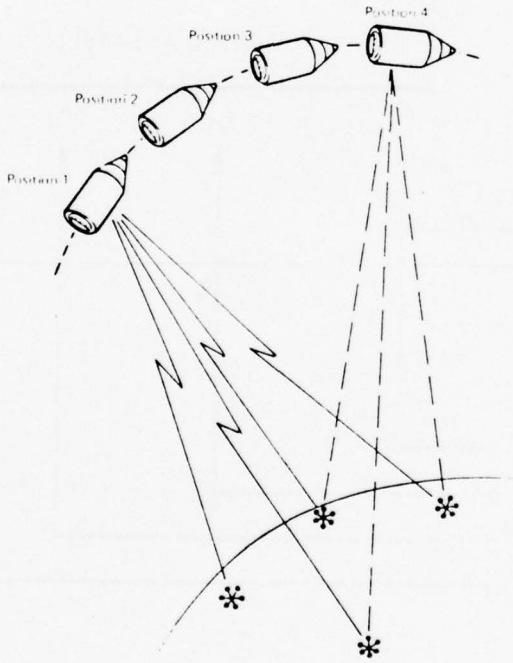


Figure 2-3. Passive Ranging Geometry

2.1.2 LANDMARK DISTRIBUTION

Figure 2-4 shows a typical world-wide distribution of PRAIS landmarks suitable for high-altitude orbital navigation. Analyses indicate that approximately 32 radars distributed world-wide at accessible sites (primarily air traffic control) are sufficient for navigation on the five orbits listed:

- Apogee 21,406 nmi, perigee 390 nmi, 63° inclination, 12-h period (Molniya orbit)
- Synchronous, 1° inclination
- Circular, 10,000 nmi, 63° inclination
- Circular polar, 68,000 nmi
- Circular polar, 150,000 nmi.

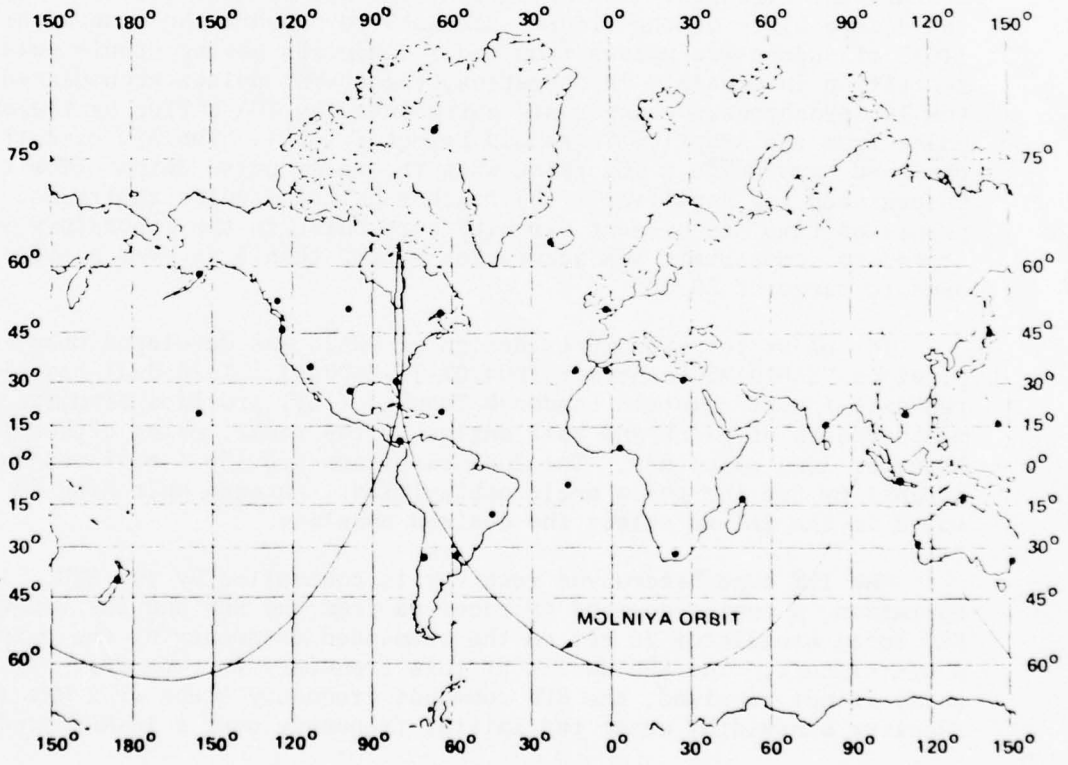


Figure 2-4. PRAIS Landmark Locations

The selected radar landmarks operate in the 2.5- to 2.9-GHz frequency band, and have at least a 400-kW output power. The effective radiated power from these radars is sufficient to permit navigation beyond synchronous orbit with no interruption of the normal radar function. The radars in this frequency band are so numerous (exceeding 5,000) and are so depended upon for critical military and air safety functions they have, in essence, become part of the natural electromagnetic radiation environment.

Only three 32-bit words of storage are required to store landmark latitude, longitude, altitude, PRI, and frequency. Assuming that the 32 landmarks in the figure are stored, 96 words will permit PRAIS Navigation System operation over the mission envelope defined by the listed orbits. This landmark set can accommodate any length mission without additional storage or storage update.

2.2 PRAIS DESCRIPTION

The passive range interferometer sensor (Figure 2-5) consists of a strapped-down, two-axis phase interferometer augmented by precision time measurement circuits. The precision time measurement circuits, shown in the dashed block of the figure, are used to measure the time-of-arrival (TOA) of successive pulses from radar landmarks having stable pulse repetition intervals. In operation, the 60-MHz pulses accumulated in the TOA synchronous counter are gated into the TOA buffer by the output pulse from the Adaptive Threshold Detector (ATD). The ATD circuit is designed to provide a TOA pulse when the radar pulse output from the Compensated Log Amplifier (CLA) reaches half the pulse amplitude. These precision time measurement circuits were built in the laboratory and tested to demonstrate TOA accuracies better than 5 ns over a signal dynamic range of 55 dB.

The phase interferometer design of PRAIS was developed under a previous USAF/SAMSO contract (F04701-75-C-0046). This dual-baseline, two-axis Interferometric Landmark Tracker (ILT) provides simultaneous measurements of pitch and roll angles to the radar, using either the short or long baselines. The dual baselines provide a self-resolving capability for the phase angle ambiguities. Antenna switching is incorporated in the ILT to select the desired baseline.

The ILT superheterodyne receiver is controlled by the SPU. In operation, a tuning command is received from the SPU and the YIG-tuned VCO local oscillator is set on the commanded frequency by the output of a D/A circuit. The SPU dwells at this frequency for one PRI. If a pulse is not received, the SPU commands frequency steps of 2 MHz (the receiver bandwidth) about the initial frequency over a 10-MHz band.

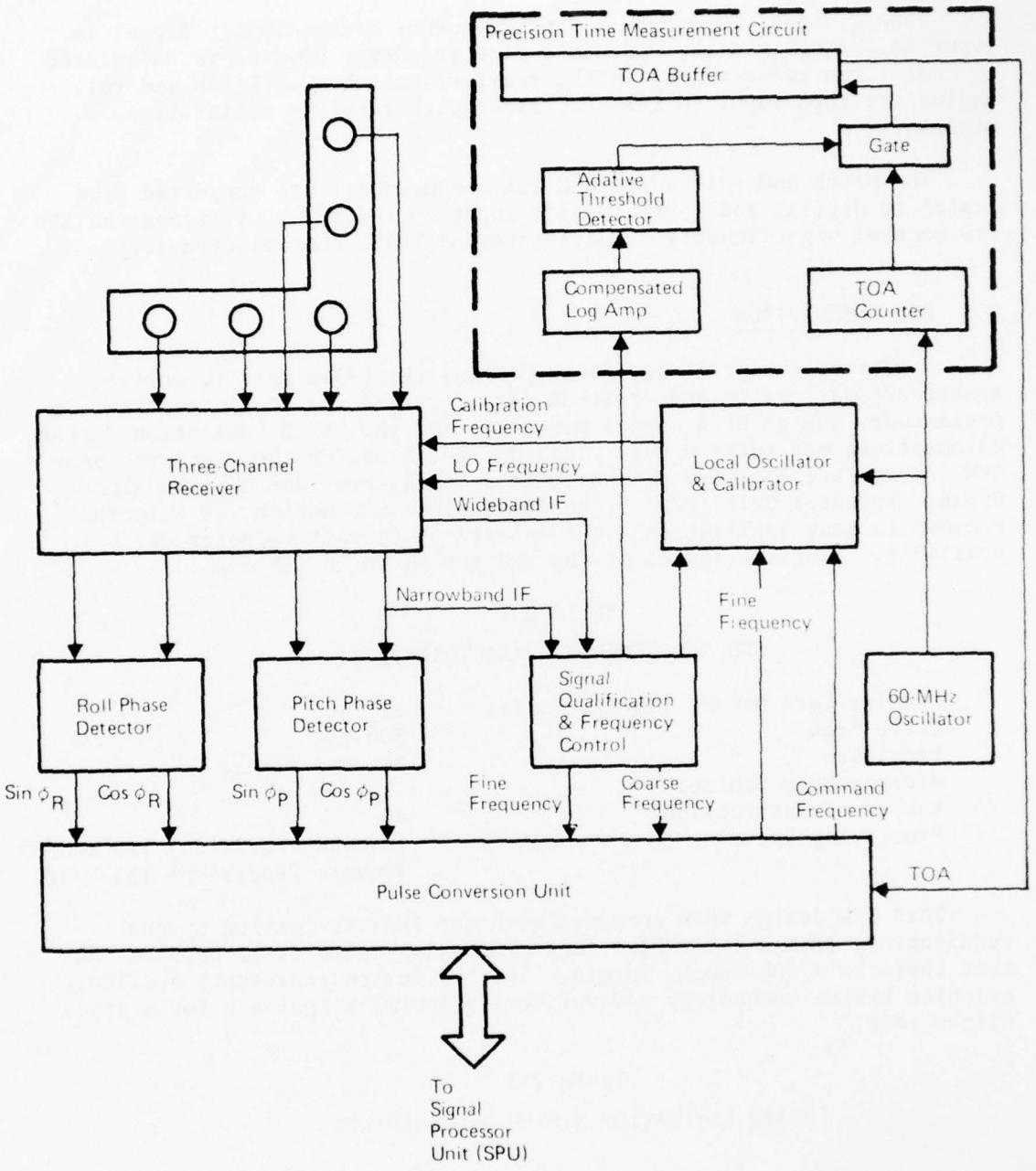


Figure 2-5. Passive Range Interferometer Sensor (PRAIS)

When a signal is found, a fine frequency discriminator signal is input to the SPU via the PCU and a fine frequency command is calculated to center the radar signal in the receiver pass band. Pitch and roll angles are then input to the SPU, along with receiver calibration signals.

The pitch and roll angle and TOA measurements are converted from analog to digital and formatted for input to the SPU. Utilizing the SPU for control significantly reduces internal PRAIS control circuitry.

2.3 SPU DESCRIPTION

A microprocessor is needed to process the PRAIS data to derive spacecraft navigation and attitude data. During the SCHANS contract, a preliminary design of a signal processor for the PRAIS Navigation System calculations was carried out. This design, based on the microprocessor IBM incorporates in many of their ESM systems, provides a stand-alone Signal Processor Unit (SPU). The stand-alone SPU design was selected because in many applications, the onboard spacecraft computer may be available. Characteristics of the SPU are shown in Table 2-1.

Table 2-1

SPU PERFORMANCE CHARACTERISTICS

Modular Core Memory (16-Bit Words)	32,768
Cycle Time	300 ns
Precision	16- and 32-bit
Microprogram Control	
Number of Instructions	40
Processing Speed	(Single Precision) 175 kad/s*
	(Double Precision) 135 kad/s

This SPU design when compared with the PRAS Navigation System requirements (Table 2-2) shows that processing speed is no problem and that there is a 30% memory margin. The SPU design represents available avionics system technology and reflects a low-risk approach for a space flight test.

Table 2-2

PRAIS NAVIGATION SYSTEM REQUIREMENTS

	Requirement	% SPU Use
Memory (16-Bit Words)	23,300	70.0
Processing Speed	4,350 kad/s*	2.8

*kiloadds/second

2.4 IRU DESCRIPTION

The Inertial Reference Unit characteristics are shown in the Table 2-3. The IRU performance shown was used in the simulation during the SCHANS contract. As indicated, this performance can be met with either a laser gyro package or with conventional gyros. To meet reliability goals on long missions, the laser gyro is preferred, but even this unit will require redundancy.

Analysis of operation with only the ILT in a low earth orbit and estimating spacecraft attitude rates instead of using gyros, showed that gyros improved navigation accuracy by only 8% and attitude accuracy by only 20%. These results indicate that in orbits where measurements can be made to three or more landmarks at a rate compatible with spacecraft attitude rates, a gyro package is not required. Alternately, if rate gyros are used in the spacecraft attitude control system, those gyro data could be used to provide attitude memory to reduce the PRAIS measurement rate. The IRU is therefore considered an optional system element.

Table 2-3

PRAIS NAVIGATION SYSTEM
STRAPPED DOWN IRU CHARACTERISTICS

PERFORMANCE		
Gyro Drift		0.001°/h
Correlated Gyro Drift		0.0005°/h
Correlation Time		72,000 s
PHYSICAL CHARACTERISTICS		
	Conventional	Laser
Weight	22 lb	15 lb
Power	60 W	40 W
Size	0.52 ft^3	0.22 ft^3
MTBF	23,000 h	TBD

2.5 PHYSICAL CHARACTERISTICS

The PRAIS, including its antenna array as indicated in Table 2-4, weighs 42 lbs, occupies 1.18 ft^3 and consumes an average of 17 W of electrical power in a typical high-altitude orbit. When the spacecraft has available onboard a digital computer and an optional IRU, only the PRAIS need be added to provide onboard autonomous navigation and attitude determination. If a signal processor is not available, then adding the PRAIS Navigation System capability increases physical characteristics to 71 lbs, 1.69 ft^3 and 35 W. Finally, when mission precision requires maximum performance the full PRAIS System should be added as shown on the bottom line of Table 2-4. The full PRAIS System has a peak power requirement of approximately 272 W (117 for ILT-PCU and 155 for SPU).

Table 2-4

PRAIS NAVIGATION SYSTEM PHYSICAL CHARACTERISTICS

PRAIS Navigation System Configuration		PRAIS Navigation System Requirements			Available Spacecraft Equipment
		Weight (lb)	Volume (ft^3)	Average Power (W)	
Minimum Configuration					
PRAIS	PRAIS	42	1.18	17	Digital Computer — IRU
	Total	42	1.18	17	
Flight Test Configuration					
PRAIS — SPU	SPU	29	0.51	18	IRU
	Total	71	1.69	35	
Maximum Configuration					
PRAIS — SPU — IRU	IRU	15	0.22	40	None
	Total	86	1.91	75	

2.6 SPACE FLIGHT TEST SYSTEM DESIGN

The PRAS Navigation System design concept for space flight test is represented in Figure 2-6. The interfaces shown are those identified for a space flight test, with regard for the operational high-altitude application. For example, if a highly stable frequency standard is accessible in the host vehicle (HV), its use could enhance performance. But if it is not available, as in the low-altitude space flight test, then space allocated in the Pulse Conversion Unit (PCU) can be used to house a 60-MHz crystal oscillator.

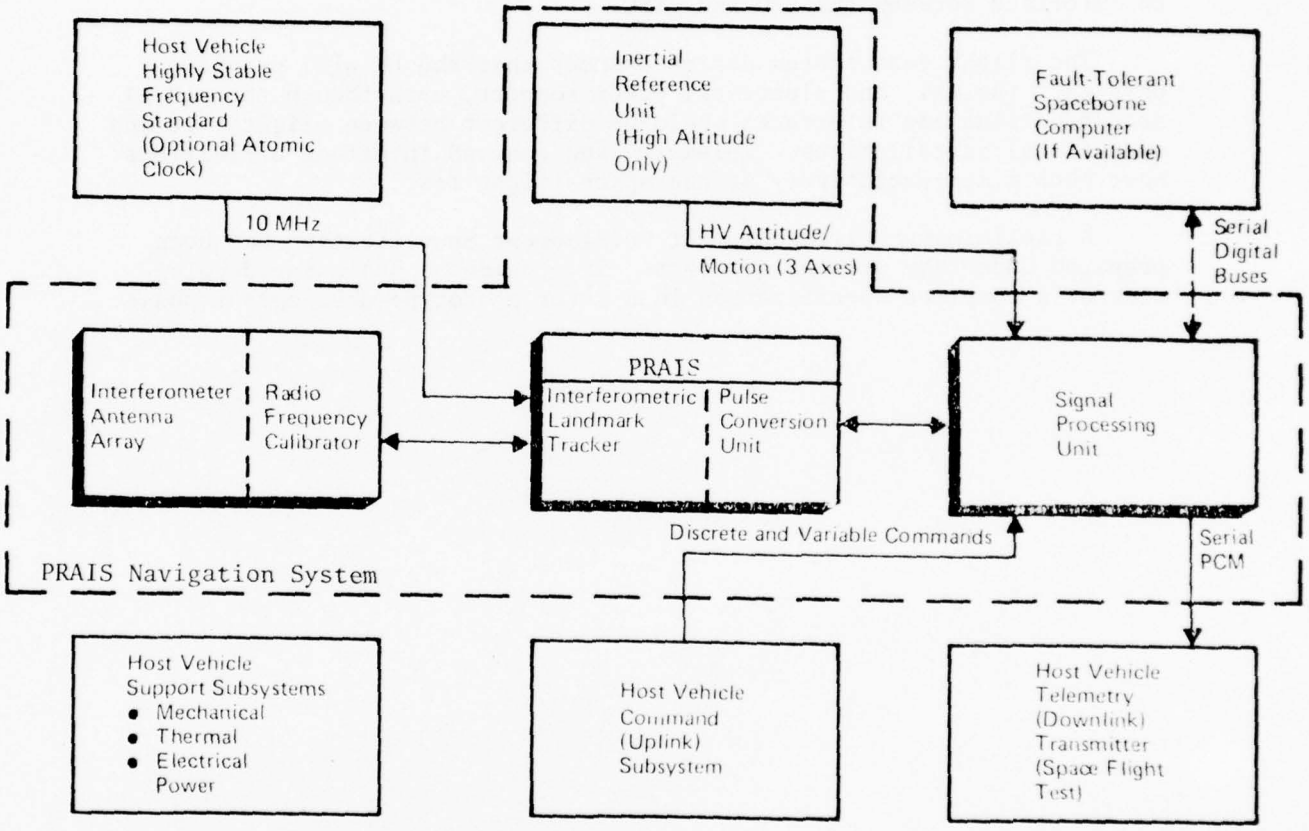


Figure 2-6. System Block Diagram with Host Vehicle Interfaces

The Inertial Reference Unit (IRU) included in Figure 2-6 preferably represents access to the host vehicle attitude determination system (ADS) or at least to measurements of HV attitude and motions. When it became known that such measurements would not be available from the HV, inclusion of an IRU in the SCHANS flight test configuration was considered, and an appropriate off-the-shelf unit was tentatively selected. However, a modification to the flight test navigation program to provide attitude determination was conceived and shown by analysis and partial simulation to be feasible and produce acceptable results in low earth orbit. The space flight test configuration therefore does not include an IRU.

Early in the SCHANS contract, there was a possibility that a Fault-Tolerant Spaceborne Computer (FTSC) would be on the same host vehicle for space flight test, and it was considered worthwhile to provide an interface between SCHANS and the FTSC so that the latter could be exercised by processing ILT measurements. Because both SCHANS and the FTSC would be under test, neither could be allowed to depend upon the other for successful performance. It was therefore necessary to make SCHANS self-sufficient, including signal processing and navigation software. The Signal Processing Unit (SPU) was introduced into the system to meet this need. The present space flight test configuration does not include an interface between the SPU and FTSC.

The flight test system design assumes that the HV will provide physical, thermal, and electrical power support, even though the actual accommodations and interfaces would be different between flight test and operational installations. Telemetry and command interface definitions have been aimed exclusively at the space flight test.

A preliminary Prime Equipment Development Specification has been prepared under the present contract. It provides a basis for development of a complete specification in a later prototype development phase.

Section 3

SYSTEM DESIGN (TASKS 1 AND 6)

This section discusses the results of two design tasks. Task 1, System Design, was predominantly concerned with electrical and mechanical design of an integrated ILT-PCU but also encompassed system engineering. Task 6, Signal Processor Unit (SPU) Design, was added to the contract scope of work in the Spring of 1976, after the need for such a unit for flight test was proven. Together the two tasks addressed the following:

- o Overall system design including
  - Specification of system performance requirements and objectives (See Reference 2)
  - Definition and control of external interfaces and intra-system interfaces
- o System design analyses and tradeoff studies
- o Electrical and logic design, including power supply requirements for
  - PRAIS Receiver - usually referred to in previous reports as Interferometric Landmark Tracker (ILT) Receiver
  - Pulse Conversion Unit (PCU)
  - Signal Processing Unit (SPU)
- o Mechanical design and packaging of the ILT-PCU and SPU, including weight estimates
- o Supporting system analyses: reliability, nuclear survivability and thermal.

3.1 ANTENNA ARRAY AND RF CALIBRATOR

Although the antenna array and RF calibrator designs were not part of the design task, it was necessary always to consider them in system design, flight test planning and planning for future phases.

3.1.1 ARRAY/CALIBRATOR CONFIGURATION

In the ANT Phase 1A contract, performance of an interferometer antenna array was measured in a 40 foot anechoic chamber. The array used four spiral antennas mounted in two orthogonal baselines of ten wavelengths each. This was a laboratory demonstration of the technique; space conditions

were not simulated, and breadboard equipment was used. Since mid 1974, modest attention has been given to design of an antenna array for operation in space. This was appropriate, since the design problems are principally mechanical and are constrained by physical accommodations in the spacecraft. A tentative design approach was conceived, predicated on installation in a space test program vehicle, in accordance with the results of a payload accommodation study performed by one possible host vehicle integration contractor (HVIC) in 1976.

The provisional interferometer antenna array design uses five precision, phase-tracking antennas mounted on an L-shaped structure with a diagonal member to support the Radio Frequency Calibrator, as shown in Figure 3-1. The two baselines are orthogonal, for directional measurements in two dimensions. One baseline will closely parallel the spacecraft roll axis; the other will be in the roll plane displaced approximately 15^{o} from the pitch axis. The baselines (A-P2 and A-R2) will be as long as spacecraft installation constraints permit, for precise arrival-angle measurement. The shorter baselines (A-P1 and A-R1) are used for resolution of ambiguities in the longer-baseline measurements. The optimum length for each shorter baseline is half the long baseline ± a half wavelength.

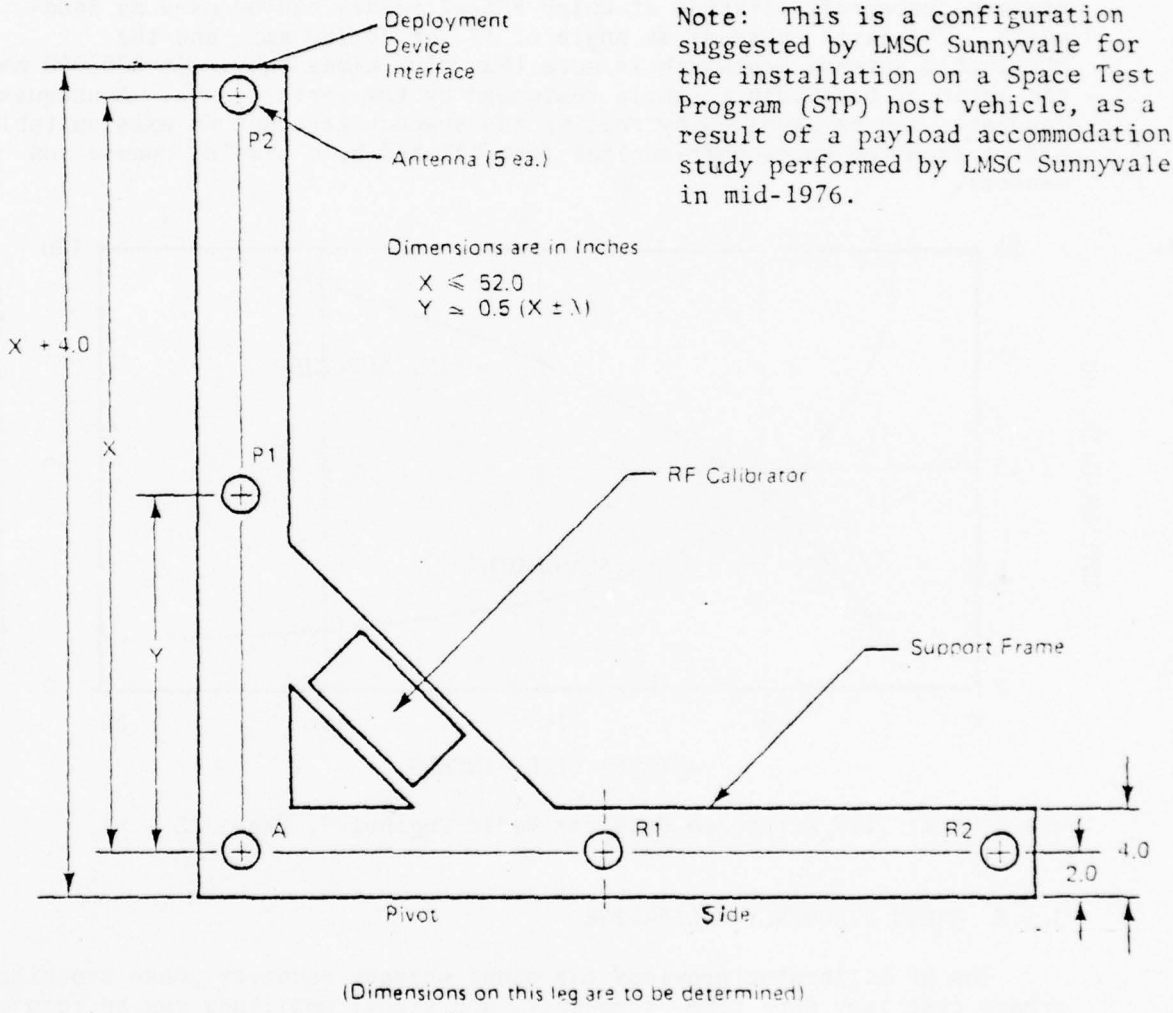
For operational installation in a different host vehicle, the configuration, installation and deployment considerations would be different. Baselines need not be mutually orthogonal, but the angle between them should be between 60 and 120 degrees. The baselines need not be coplanar, and each should be 24 to 60 inches long, but they need not be of equal length. The individual antenna boresights should be mutually parallel within ± one degree. Alignment with spacecraft pitch and roll axes is not necessary but the actual alignment should be known within about one degree.

3.1.2 ANTENNA SELECTION

The principal antenna selection criteria are (1) a high front-to-back ratio (20 dB or more); (2) predictable phase-center movement with input signal direction, or close phase tracking between antennas to $\pm 45^{o}$ off boresight; and (3) suitability of construction and materials for long-term operation in space after launch, boost, and injection into orbit. Suitability of the spiral antenna selected before the SCHANS contract, a cavity-backed spiral housed in a Teflon radome 2.15 inches in diameter, the same as that used in ANT phase 1A, deserves reconsideration. Because of its low front-to-back ratio (10 to 15 dB), reflections from the spacecraft structure behind the array could be unacceptably disturbing.

A circularly polarized horn antenna (such as used in the ATS-6 interferometer) could be used. A typical optimum horn antenna has a 20 dB front-to-back ratio. By incorporating chokes at the aperture and loading the aperture with one or more septa, the front-to-back ratio can be improved beyond 20 dB. A polarizer grid mounted on the open aperture of the antenna

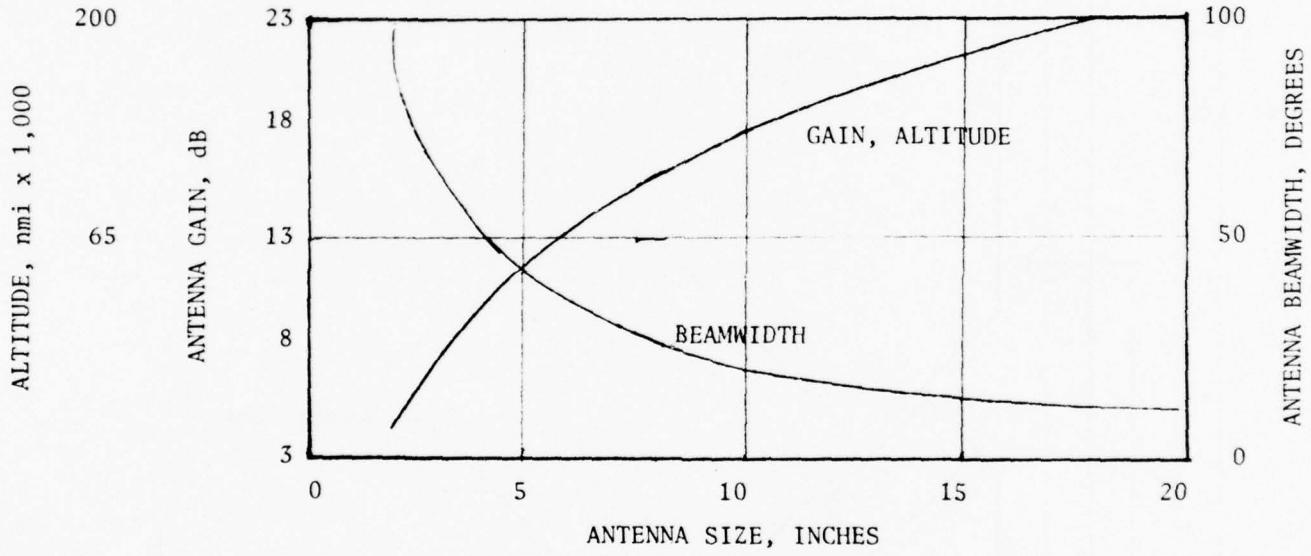
would change the linear polarization to circular polarization. The horn antenna is able to receive signals that are linearly or elliptically polarized in any sense and circularly polarized in one sense.



Note: This is a configuration suggested by LMSC Sunnyvale for the installation on a Space Test Program (STP) host vehicle, as a result of a payload accommodation study performed by LMSC Sunnyvale in mid-1976.

Figure 3-1. Antenna Array Configuration for 1978 STP Space Flight Test

The wide field-of-view (120°) of the spiral antenna is ideal for low earth orbit, and its gain (3 dB) is sufficient for operation up to synchronous altitude. At higher altitudes, higher gain (and consequently narrower beamwidth) will be required. The figure below indicates the relationship between the size (one side of the aperture) of a square 3 GHz horn antenna, gain and beamwidth. It also shows the corresponding maximum spacecraft altitude at which FPS-47 radars can be used as landmarks. The earth subtends an angle of 17° at 20,100 nmi, and the obtainable antenna beamwidth is more than five times that. At 200,000 nmi, the ratio of beamwidth to angle subtended by the earth is ten. Consequently landmarks can be acquired by rolling the spacecraft about an axis suitably offset from the spacecraft-sunline (established by a simple, coarse sun sensor).



(Data Source: ITT Reference Data for Radio Engineers, Pages 25 - 37.)

3.1.3 RADIO FREQUENCY CALIBRATOR

The RF Calibrator provides the means whereby receiver phase tracking errors that vary with time, frequency, and signal amplitude can be removed from the phase angle measurements. The block diagram shown in Figure 3-2 is that of a five-channel calibrator developed by Anaren Microwave, Inc., for IBM under the ANT Phase 1B contract.

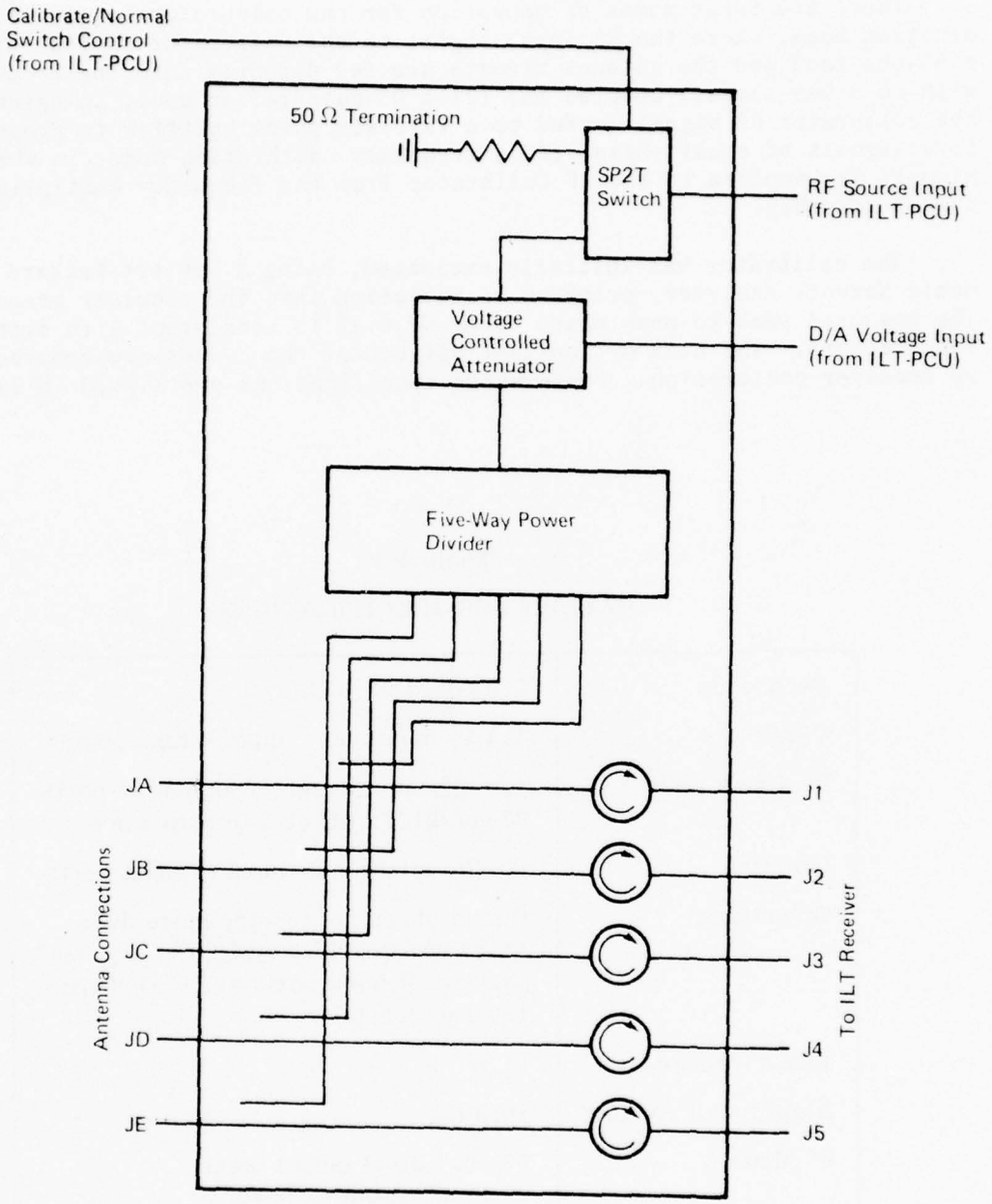


Figure 3-2. RF Calibrator Block Diagram

There are three modes of operation for the calibrator: (1) a termination mode, where the RF input signal to the calibrator is fed into a 50 ohm load and the antenna signals are fed directly into the receiver with no other signals coupled in; (2) a 0^{o} calibration mode, in which the calibrator RF signal is fed to a five-way power splitter to produce five signals of equal phase; (3) a frequency calibration mode, in which signals are applied to the RF Calibrator from the frequency multiplier/calibrator assembly.

The calibrator was initially evaluated, using a Hewlett-Packard Automatic Network Analyzer, prior to installation into the receiver breadboard. The measured peak-to-peak phase error of 0.8^{o} is consistent with system requirements. The bias or constant offsets of the curves are removed by receiver calibration. Performance specifications are listed in Table 3-1.

Table 3-1

CALIBRATOR SPECIFICATIONS

Frequency	2.5 GHz to 2.9 GHz
VSWR	1.4:1, maximum: input/output ports
Insertion Loss	1.0 dB, maximum: input/output ports 37-40 dB: calibrator to output ports
Isolation	50 dB, minimum: input to input ports
Directivity	Output phase not to vary more than ±1.2° when VSWRs applied to any input port or all input ports are varied from 1.0:1 to 2.0:1
Phase Tracking	±1.0°
Amplitude Tracking	±0.2 dB
0° Mode	0° ±0.4 dB at output ports 0° ±1.0° at output ports
Attenuation	60 dB continuous dynamic range

3.1.4 ANTENNA ARRAY/CALIBRATOR MECHANICAL DESIGN

The purpose of the antenna array structure is to hold and position a set of five identical antennas. The manner in which this is accomplished is critical to subsystem performance. Measurement accuracy requirements can be met only if each antenna position is known. Environmental forces affecting the array and its members vary widely from assembly, through launch, to orbit. Forces of acceleration, vibration, and shock dominate through launch, and temperature variations dominate in orbit.

3.1.4.1 Array Material

Selection of the structure material is critical to the design of the array structure. The structure must be light, strong, and thermally stable. The relative position of the antennas must be maintained within a small tolerance. In orbit, the array structure will experience radiation conditions including direct solar radiation, sunlit earth albedo, dark earth, and open space. Temperature changes and their effects can be controlled by thermal shielding and insulation, material selection and design of mounting points.

Thermal shielding and insulation design should maintain temperature excursions to less than $100^{o}C$. The array material must possess a sufficiently low coefficient of thermal expansion (α) that position is maintained within acceptable limits. Additionally, the array must be kinematically mounted to prevent stresses from being transmitted from the host vehicle, through the attachment points, to the array.

Two low expansion materials could be used to fabricate the structure. Invar is shown primarily as a basis for comparison. Use of invar would result in a higher assembly weight. Table 3-2 compares the materials. It should be noted that over a temperature range of $100^{o}C$, a graphite laminate structure would change in length by 2.5×10^{-5} inches per inch, which is tolerable for system operation without baseline temperature compensation. In the special case of a sun-synchronous orbit, solar radiation impinges continuously on one edge, producing a temperature gradient along the baseline. Since the gradient should reach a steady state after hours in orbit, its effects can be estimated in the navigation filter in flight and largely calibrated out.

3.1.4.2 Antenna Cables

Antenna cables should meet the following requirements.

- Phase match between any two cables within 2.0^{o}
- Phase tracking between any two cables within 1.0^{o} over the entire temperature range (TBD)

- o Not affected in electrical characteristics by shock or vibration
- o Hermetic sealing
- o High reliability
- o Repeated flexure without change in phase or insertion loss
- o Minimal or precisely measurable insertion loss.

A cable that meets or exceeds all those requirements is manufactured by ERI Corporation, Los Angeles, California. Table 3-3 summarizes its characteristics.

These cables can endure repeated deformation without measurable effect on performance or reliability. There are less advanced (and less costly) cables available, and a comparison/trade study should be executed before a firm selection is made.

3.1.4.3 RF Calibrator Configuration

The calibrator, which weighs five pounds, has the physical configuration shown in Figure 3-3.

3.1.4.4 Weight Estimate

The weight of the Antenna Array/RF Calibrator Assembly is conservatively estimated as shown in Table 3-4. This is for the configuration shown in Figure 3-1 and assumes an arduous launch environment mounted hard to the spacecraft; other configuration designs indicate an operational antenna array weight of 12 pounds can be achieved.

3.2 PRAIS RECEIVER ELECTRICAL DESIGN

The ILT receiver is described in detail in Appendix A, Volume III. The PRAIS receiver operates in the same way with respect to interferometric measurements. It receives and processes landmark pulses to produce signals representing sine and cosine of arrival phase-angles along each baseline, log video (pulse amplitude), frequency and signal qualification. The additional capabilities incorporated in the PRAIS receiver are those needed to measure pulse time of arrival (TOA) accurately. Sequences of TOA measurements allow incorporation of passive ranging (PAR) in the Navigation and Attitude Determination Program (NADP). The concept orginated in the High Altitude Navigation System (HANS) Study, as reported in Reference 13.

The SCHANS design effort entailed designing certain circuits, testing them in the laboratory and updating the ILT receiver and PCU designs. The circuits involved are a Compensated Log Amplifier (CLA), an Adaptive Threshold Detector (ATD) and a TOA Counter Buffer (TC/B). In this report, the CLA is described functionally with the receiver and the others with the PCU. Results of laboratory tests appear in Section 4.

Table 3-2

COMPARISON OF CANDIDATE STRUCTURAL MATERIALS

Material	Density (lb/in^3)	Tensile Strength (Ksi)	Strength-to-Weight Ratio	Coefficient of Expansion (α) (in/in/°C)
Invar	0.289	65-85	225-294	1×10^{-6}
Graphite Laminate	0.07	212	3029	0.25×10^{-6}

Table 3-3

RF CABLE MECHANICAL CHARACTERISTICS (ERI)

Thermal	-180°C to 925°C
Vibration	250g (31-2000 Hz)
Shock	600g (0.5 ms)
Hermetic Seal	10^{-9} cm^3/s He/min
Dielectric	SiO_2
Weight per Foot	0.04 lb (0.142 dia.)
Axial Twist	1°/in
Bend Radius	0.5 in
Life	10^6 hours MTBF

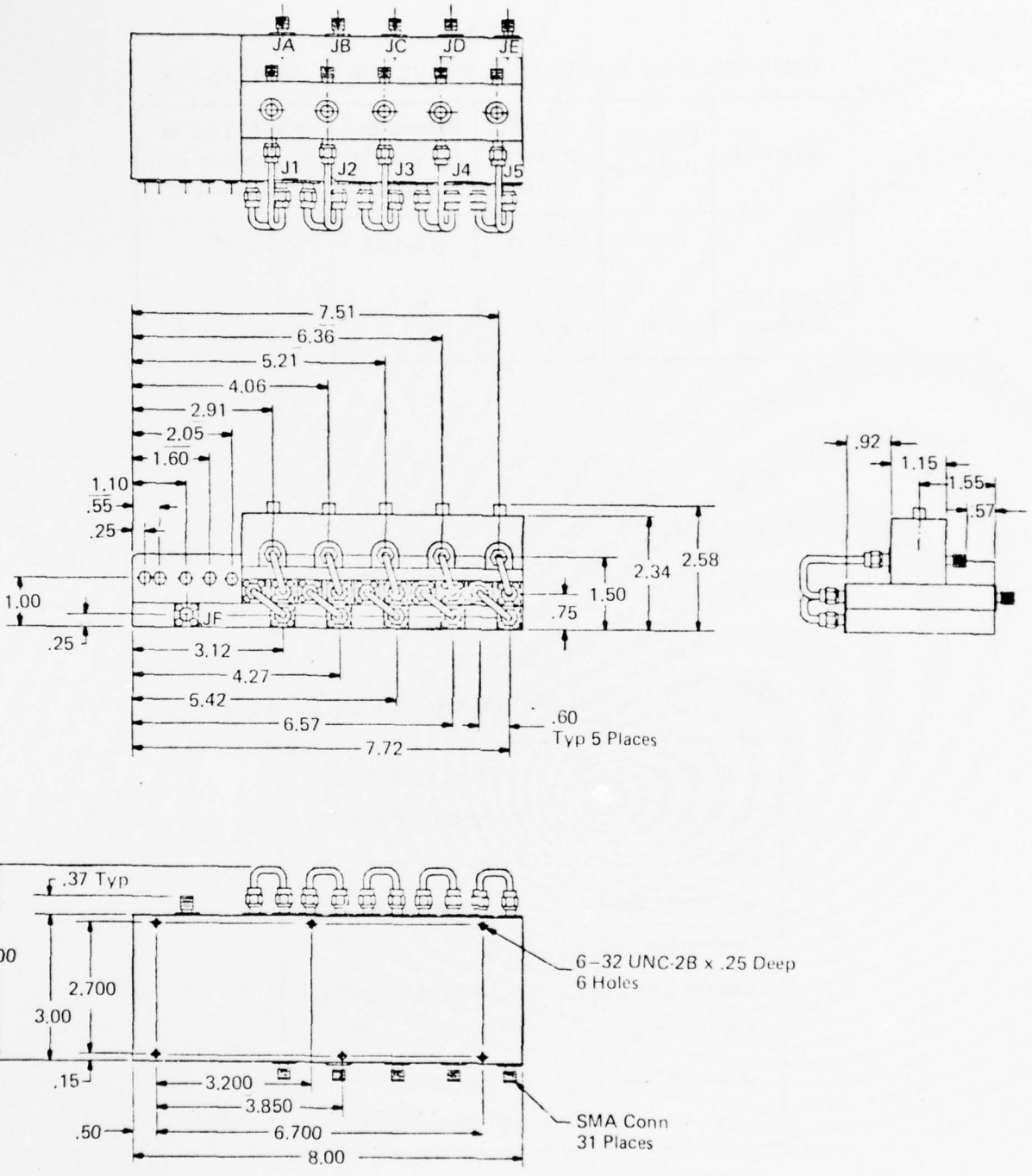


Figure 3-3. RF Calibrator

Table 3-4

ANTENNA ARRAY WEIGHT ESTIMATE

Component	Unit Weight (lb)	Total Weight (lb)
Array Structure*	8	8
Antenna	1.5	7.5
RF Cable	0.25	2.5
RF Calibrator	5	5
Total Assembly		23
*Assumes the use of graphite lamina		

3.2.1 RECEIVER PERFORMANCE SPECIFICATIONS

The PRAIS receiver design meets the following performance specifications.

Frequency Coverage	-	2.5 - 2.9 GHz
Frequency Measurement Accuracy	-	0.4 MHz error (including LO uncertainty) when smoothing 100 pulses
Frequency Variation (Pulse to Pulse)	-	At -76.5 dBm 600 kHz p-p max At -66.5 dBm 180 kHz p-p max At -56.5 dBm 60 kHz p-p max
Instantaneous Bandwidth	-	2 MHz-1 dB points 3 MHz-3 dB points
Sensitivity (MDS)	-	-96.0 dBm min
Dynamic Range (Operating)	-	50 dB min
Spurious Rejection	-	60 dB min for signals 2 MHz or more away from the desired frequency. Image rejection by dither acceptable.
Phase Accuracy	-	1^{o} max error between channels
Phase Detector Linearity	-	$\pm.25^{o}$ (-45^{o} to $+45^{o}$)
Phase Variation	-	At -76.5 dBm 34.0^{o} p-p max At -66.5 dBm 11.4^{o} p-p max At -56.6 dBm 3.4^{o} p-p max
Input Pulsewidth	-	0.5 μs to CW
Log Video Response		
Dynamic Range	-	54 dB min
Linearity of Video Response	-	±.6 dB
Time Delay Bias Error Versus Input Power (Over Specified Dynamic Range)	-	±10 ns
Slope	-	33 mv/dB
Max Video Rise Time (Log Video, Phase Video and FRF Video)	-	300 ns (To within 1 dB of final amplitude for a rectangular input pulse).
RF Calibration Signal	-	CW signal within ±0.1 MHz and ±2.0 dB of received input signal

LO Tuning Speed

For steps from any frequency to any other frequency:

To within ±2 MHz of final frequency within - 10 ms max

To within ±.1 MHz of final frequency within - .1 sec max

Final frequency is defined as that occuring 1 sec after tuning command.

Outputs Required

Signal Name	Amplitude	Description
Log Video	0 - 2.5 V	95 Ohm Termination
Sin A	±2 V	"
Cos A	±2 V	"
Sin B	±2 V	"
Cos B	±2 V	"
Fine RF	±1 V	"
RCVR. Blanking	TTL	1 = Processing 0 = No Processing
Qualification	TTL	1 = In Band 0 = Out of Band

Inputs Required

Signal Name	Type	Description
Freq Change (FREQ CHG)	TTL	Normally a logic 1 goes to logic 0 a minimum of 100 ns before the tuning word is going to change. Goes back to logic 1 when tuning word changes.
RF ϕ CAL Mode (CALRCV)	TTL	1 = RF Phase Cal mode 0 = Normal mode
RF Freq Cal Mode (RF FREQC)	TTL	1 = Normal mode 0 = RF Freq Cal mode
IF Cal Mode (IFCAL)	TTL	1 = IF Cal mode 0 = Normal mode

Signal Name	Type	Description		
		Sel 1	Sel 2	IF Cal Sel
IF Cal Sel 1 (IFCALS1)	TTL	0	0	-45^{o}
IF Cal Sel 2 (IFCALS2)	TTL	0	1	$+45^{o}$
		1	0	$+135^{o}$
		1	1	$+225^{o}$
Antenna Select (ANTSEL)	TTL	0 = Antenna #1 1 = Antenna #2		
TUNB04	TTL	Tuning Word MSB		
TUNB05				
TUNB06				
TUNB07				
TUNB08				
TUNB09				
TUNB10				
TUNB11				
TUNB12				
TUNB13				
TUNB14				
TUNB15		Tuning Word LSB		

3.2.2 RECEIVER SUMMARY FUNCTIONAL DESCRIPTION

Figure 3-4 shows the PRAIS receiver block diagram and indicates its partitioning into modules or subassemblies (e.g., A7 at the lower left), which are listed in Table 3-5. It is basically a three channel superheterodyne receiver. Outputs from the Antenna/RF Calibrator Unit are switched at RF into three receiver channels. Phase measurements are made between the center channel and the two adjacent channels. A receiver channel is composed of an input bandpass filter, mixer, preamplifier/bandpass filter and limiter. Following the receiver channels are two phase detectors, a frequency discriminator and qualification circuitry, and a logarithmic amplifier. The basic receiver functions are to provide RF to IF (60 MHz) conversion, filtering, gain, and phase, RF and amplitude measurement.

3.2.2.1 Phase Detectors

The phase detectors generate 360 degrees of unambiguous video. The phase detectors are implemented at the receiver IF, and output voltage is a function of input phase angle difference as indicated in Figure 3-5. The portions of the sine and cosine curves used for phase measurements are indicated by the heavy lines and are assumed linear. To accurately determine which phase detector segment to use for a phase measurement, IF calibration is done periodically. The SPU controls activation of the IF calibration mode and selection of a 45^{o}, 135^{o}, 225^{o}, or 315^{o} phase CW calibration signal to be input to both pairs of phase difference channels of the IF circuitry. The phase detector voltages for each input

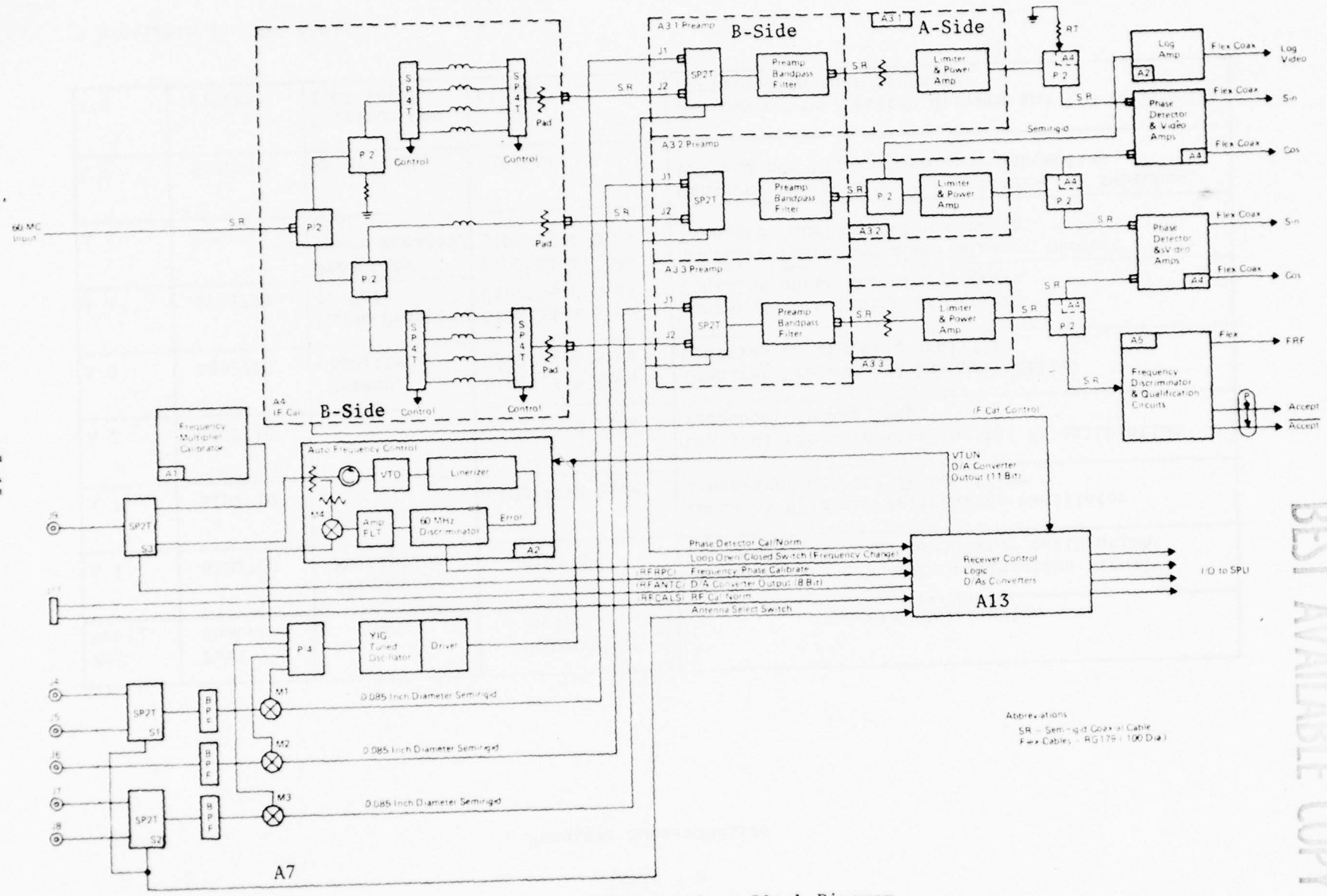


Figure 3-4. PRAIS Receiver Block Diagram

BEST AVAILABLE COPY

Table 3-5

Receiver Subassemblies

Ref. Desig.	Part Number	Name	Schematic * Number	Function Description
A 1	6102700	Frequency Multiplier	6102703	Generates the frequency calibration signal necessary for local oscillator calibration
A 2	6102710		6102714-A Side	Contains RF phase calibration oscillator linearizer and log IF amplifier
A 2	6102710		6102715-B Side	Contains the circuitry for the RF calibration frequency locked loop
A 3	6102720	Preamp/ Limiter	6102724-B Side 6102725-A Side	Contains Pre amp and bandpass filter Contains IF limiting amplifier
A 4	6102730	Phase Detector IF Cal.	6102734-A Side 6102735-B Side	Contains IF calibration network Contains phase detector circuit
A 5	6102740	Frequency Discriminator/ QUAL	6102744-A Side 6102745-B Side	Contains frequency discriminator circuit Frequency qualification circuit
A 7	6102650	RF Assembly	6102664	Contains the mixers, B.P. filters, RF switches, P/4 and the YTO and isolator assemblies
A13	6102869	Receiver Control Logic	6102877	D/A converters, switch drivers and I/O to PCU are contained on this assembly

* Available in CDRL #A013

condition are sampled and held at 25 μsec intervals and transmitted to the SPU where the data from each input condition is averaged to determine phase detector segment end points (circled in Figure 3-5). In addition, the phase detectors are calibrated as a function of IF frequency on a monopulse basis. Phase versus IF frequency characteristics are stored in software for each phase detector.

3.2.2.2 Frequency Discriminator

The frequency discriminator generates an analog voltage proportional to the input IF frequency. The frequency qualification circuits are used to reject receiver generated spurious signals. When a signal satisfies the frequency qualification criteria in the hardware, an accept signal is generated.

3.2.2.3 Local Oscillator

A fast tuned YIG oscillator is used for the local oscillator. The oscillator frequency is controlled by a 12-bit D/A converter. To achieve the required frequency accuracy, the local oscillator is calibrated with a combline generator referred to in Figure 3-4 as the frequency multiplier calibrator. The combline generator provides calibration signals at 100 MHz increments in the 2.5 - 2.9 GHz range.

3.2.2.4 Control Logic

The control logic assembly provides the interface between the analog signal processing circuitry and receiver, the D/A converter circuits for control of the local oscillator and Antenna/RF Calibrator Unit attenuator, and the switch drivers providing current to the RF and IF switching networks.

3.2.2.5 RF Phase Calibration

Because the phase performance of the receiver channels is important, a monopulse calibration signal of 0^{o} phase is injected via the Antenna/RF Calibrator Unit. The calibration signal amplitude is set by ILT/PCU hardware control to the same amplitude as the signal pulse. Since the phase of the calibration signal is 0^{o}, the receiver can be calibrated on a pulse-to-pulse basis for phase fluctuations due to signal amplitude.

The Antenna/RF Calibrator Unit provides the means whereby receiver phase tracking errors that vary with time, frequency, and signal amplitude can be removed from the phase angle measurements. There are three modes of operation for the calibration circuitry: a termination mode in which the calibration signal is fed into a 50 ohm load and the antenna signals fed

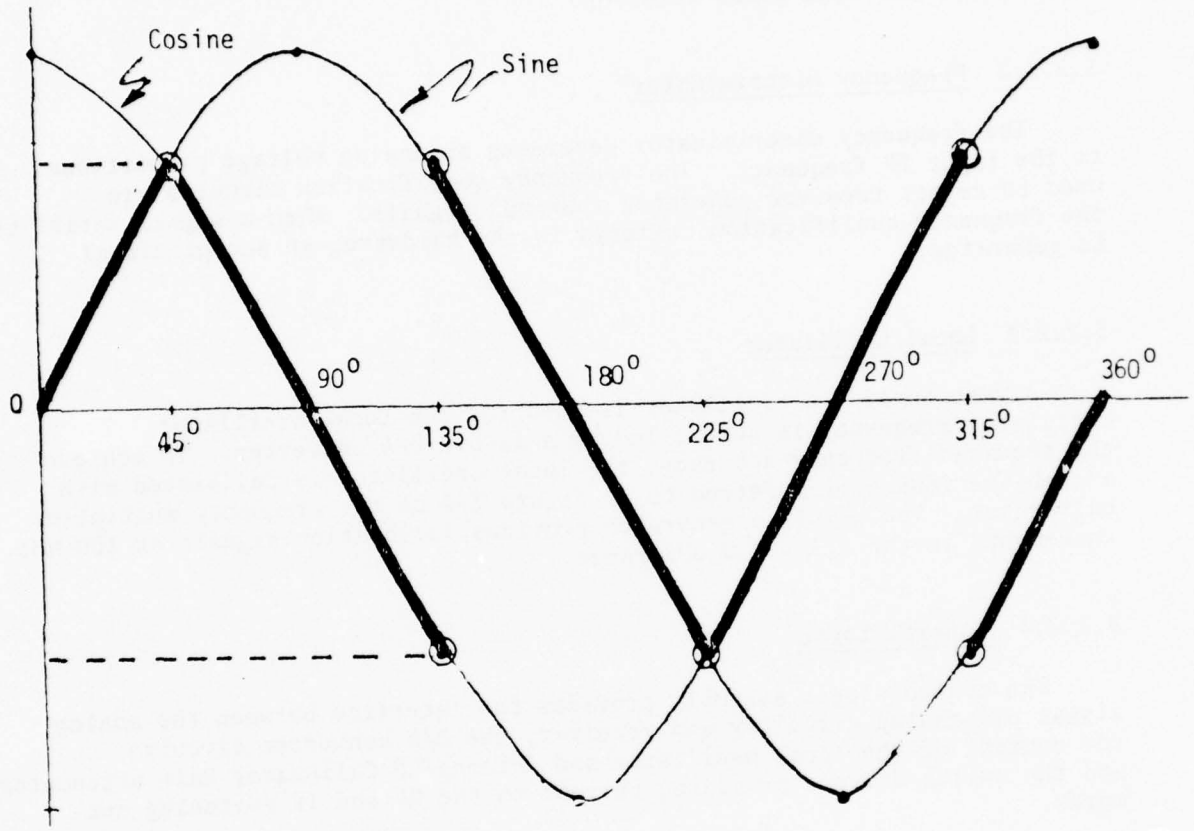


Figure 3-5. Phase Detector Characteristics

directly into the receiver with no other signals coupled in; a 0^o calibration mode in which the calibration signal is fed to a 5-way power splitter to produce four signals of equal phase; a frequency calibration mode in which a calibration signal is applied to the Antenna/RF Calibrator Unit from the frequency multiplier calibrator assembly. Mode control is provided by a switch internal to the Antenna/RF Calibrator Unit and an external switch to select the RF source or frequency multiplier. 0^o phase detector outputs are desired for 0^o input signals over the input frequency range and signal dynamic range. The calibration is inserted following each signal pulse and is adjusted to the amplitude and frequency of the incoming preceding pulse. The amplitude of the calibration signal is controlled by a voltage controlled attenuator with the RF Calibrator Unit. The attenuator is controlled by an 8-bit D/A converter in the ILT/PCU Unit. Frequency control is provided by a frequency locked loop, which is discussed in a later paragraph of this section. In order to minimize the phase error contribution of the Antenna/RF Calibrator Unit, a software calibration compensates for its phase error as a function of frequency based on laboratory measurements of individual Antenna/RF Calibrator Units.

The auto frequency control loop is a frequency locked loop whose function is to lock the voltage tuned oscillator exactly 60 MHz above the local oscillator frequency. This oscillator is tuned in conjunction with the LO and is used to provide the RF signal for the RF calibration circuitry.

3.2.3 COMPENSATED LOGARITHMIC IF AMPLIFIER

The log IF amplifier generates a video signal proportional to the logarithm of the IF signal power. This video signal is used by the signal processor to derive signal strength information and for TOA measurements with the Precision Time Measurement (PTMU) circuitry.

The Log IF Amplifier design is based on the successive summation of a number of straight line segments to approximate a logarithmic curve. Figure 3-6 is a block diagram of the amplifer. Each stage is designed to have the same gain and limit at the same point. The output for each stage can be expressed as:

$$k_1 \log (k_2 e_i) = k_1 \log e_i + k_2 \log k_1$$

where k_1 is the slope constant and k_2 is the offset constant. The output from the summing amplifier is:

$$e_o = e_1 + e_2 + e_3 + \text{---} + e_n$$

The signal level out of the summing amplifier when the last stage just limits is:

$$e_L (1 + A^{-1} + A^{-2} + \text{---} + A^{-N}),$$

where e_L is the saturated output voltage for each stage and the output obtained when each succeeding stage saturates is:

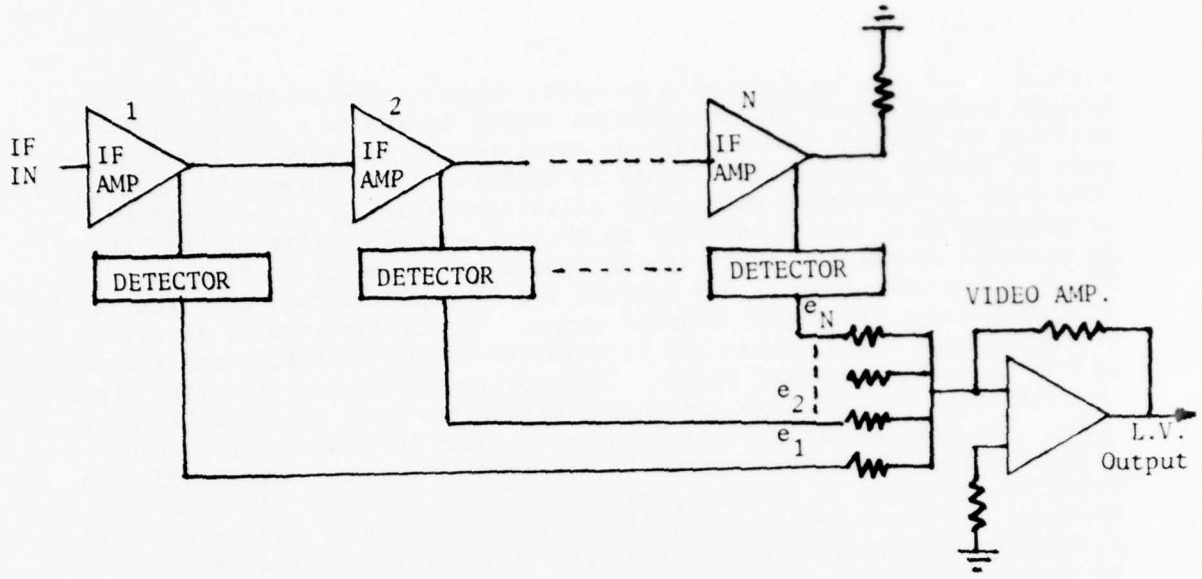


Figure 3-6. Log Amplifier Block Diagram

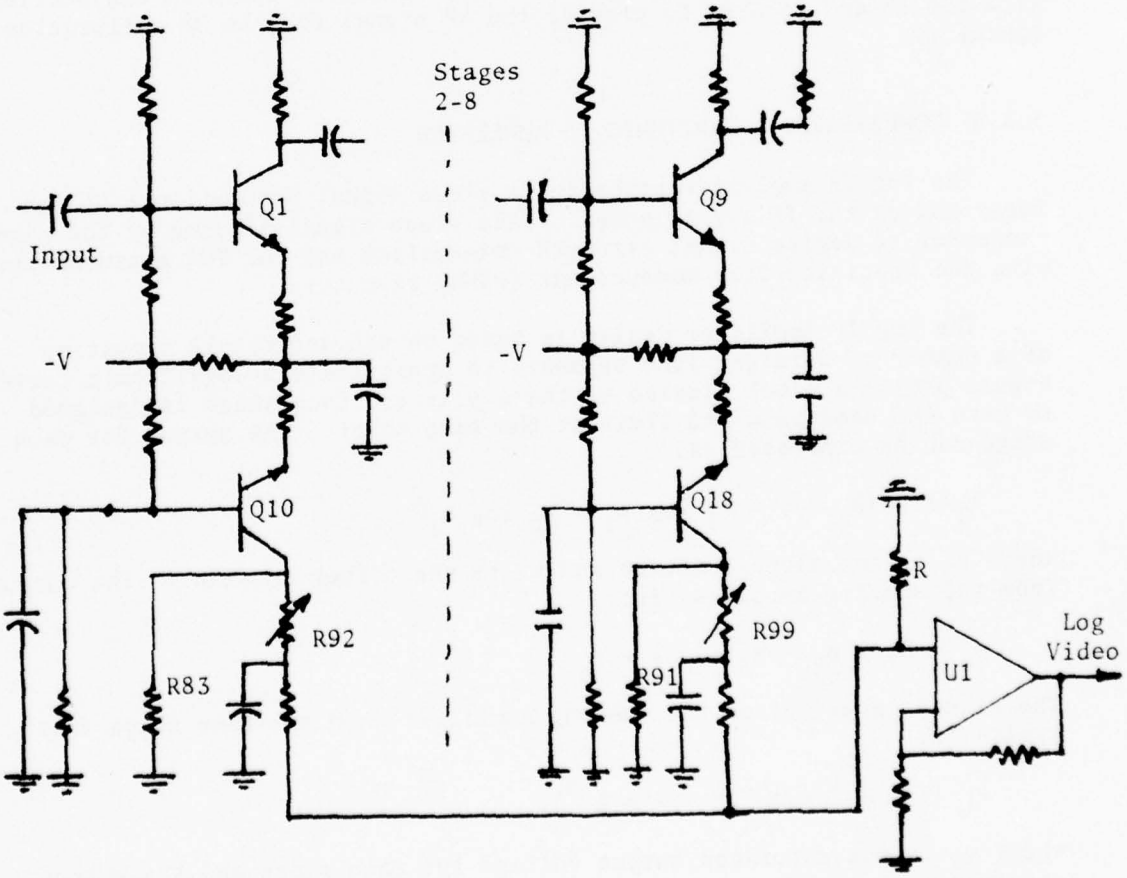


Figure 3-7. Log Amplifier Simplified Schematic

$$e_o = e_L (2 + A^{-1} + A^{-2} + \text{---} + A^{-N+1}),$$

$$e_o = e_L (3 + A^{-1} + A^{-2} + \text{---} + A^{-N+2}), \text{ etc.}$$

If A>>1, then the terms in powers of A^{-1} are neglected. The output increases by constant steps e_L as the input increases by a ratio of A, a logarithmic relationship.

The use of the log amplifier introduces some errors into the time measurements. The amplifier has absolute time delays of one to two nsec per stage and therefore an overall delay of 9 - 18 nsec depending on input power. The video rise time varies as a function of input level due to effective bandwidth variations as the signal propagates thru the amplifier. In addition non linearities in the log video output also effect the TOA measurement as illustrated below:

Linearity - ±.3 dB

Slope - 30 mV/dB

-1 to -10 dB rise time - 150 ns (measured)

Time delay change due to non linearity error is:

non linearity error (mV) = ±.3 x 30 = ±9 mV

$$\Delta\text{time delay} = \frac{\text{Non Linearity Error (mV)}}{\text{Change in Log Video (mV)}} \times \text{Risetime (ns)}$$

Δtime delay = ±9/270 x 150 = +5 NS

Based on the above discussion it is necessary to incorporate circuitry to control and reduce the effect of these error sources.

Techniques used to minimize time variation errors are use of wide stage bandwidth to reduce rise time effects over the dynamic range and reduction of the stage gain and use of additional stages to approximate the log curve with more straight line segments.

The log amplifier design goals are as follows:

Center Frequency - 60.0 MHz

Log Linearity - ±.5 dB

Log Slope - 30 mV/dB

Dynamic Range - -65 to 0 dBm

Time Delay Variation (both absolute delay and linearity) induced variations - ±10 nsec. over specified dynamic range

Figure 3-7 is a schematic of the log amplifier simplified to illustrate the following explanation.

The amplfier functions as follows: Transistors Q1 thru Q9 provide the IF gain. The gain per stage is a compromise between linearity, dynamic range and physical size. The average gain per stage is 7 dB. Nine stages are used yielding a dynamic range of greater than 65 dB. The amplifier is RC coupled with single stage bandwidths exceeding 100 MHz, thereby minimizing circuit delays.

The base-emitter junction of the IF amplifier rectifies the IF signal and an exponential current proportional to the IF signal power is generated. Transistors Q10 thru Q18 are current buffers and resistors R83 thru R91 function as current to voltage converters.

To achieve the desired linearity compensation resistors R92 thru R99 are trimmed. Time delay compensation is provided by the addition of external capacitors CS1 thru CS9 as required.

Video amplification of the log signal is provided by U1. This amplifier has gain control to set the slope to the desired level.

In the actual amplifier, the output does not truly change logarithmically from saturation of one stage to saturation of the next. Furthermore, contribution due to terms in higher powers of A^{-1} are not truly negligible. Trimming is necessary to achieve the best approximation to the desired characteristic. Figures 3-8 and 3-9 show the measured gain characteristic and deviation of the characteristic from linearity.

3.2.4 ADAPTIVE THRESHOLD DETECTOR

The Adaptive Threshold Detector (ATD) actually appears on the block diagram of the PCU in Section 3.3. Its purpose is to generate a pulse ("TOA STROBE") when the log video pulse leading edge reaches half the pulse amplitude, the ATD is used because of the wide dynamic range of the signal. With a fixed threshold detector the time at which leading edge crosses the threshold varies depending on signal levels and rise time.

The ATD compares the output of a peak detector, biased 6 dB down to the delayed output of the Log IF amplifier. As the signal level varies in magnitude the trigger level is maintained at the same point on the leading edge relative to the peak. The 6 dB down point is chosen because it is the point of maximum leading edge slope. The operation is illustrated by Figure 3-10. Details of operation and error analysis appear in 3.4.1 of Appendix B, Volume III.

3.3 PULSE CONVERSION UNIT

The function of the Pulse Conversion Unit (PCU) is to digitize the video pulse outputs of the receiver and output this digital data to the

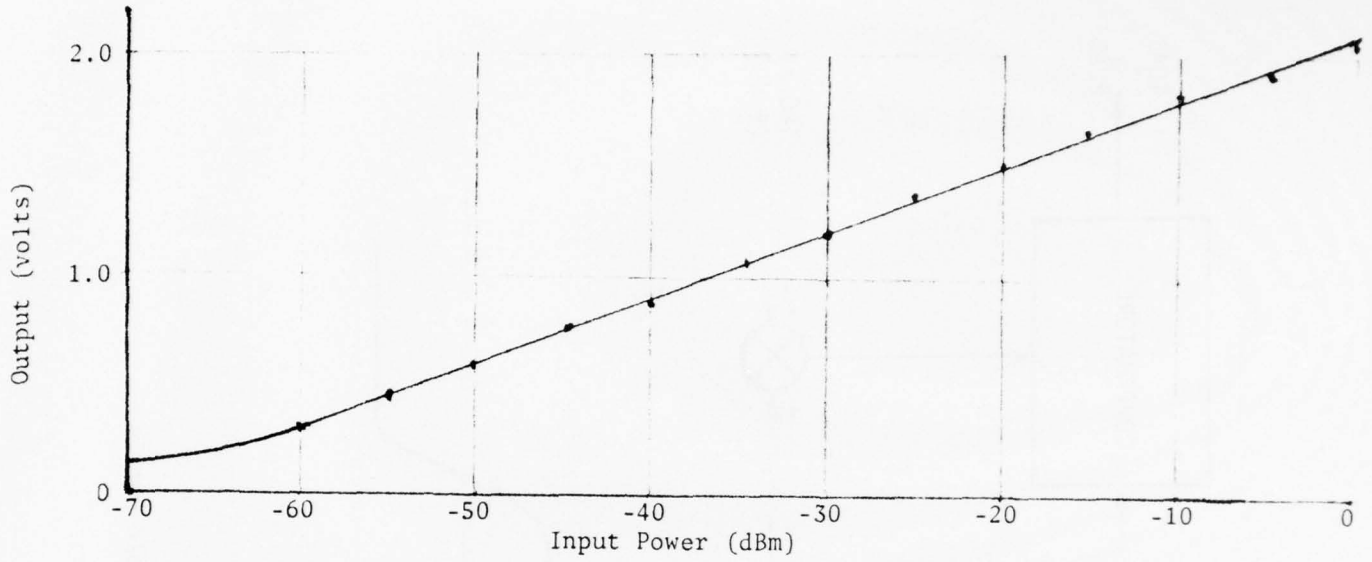


Figure 3-8. Log Video Output Versus Input Power

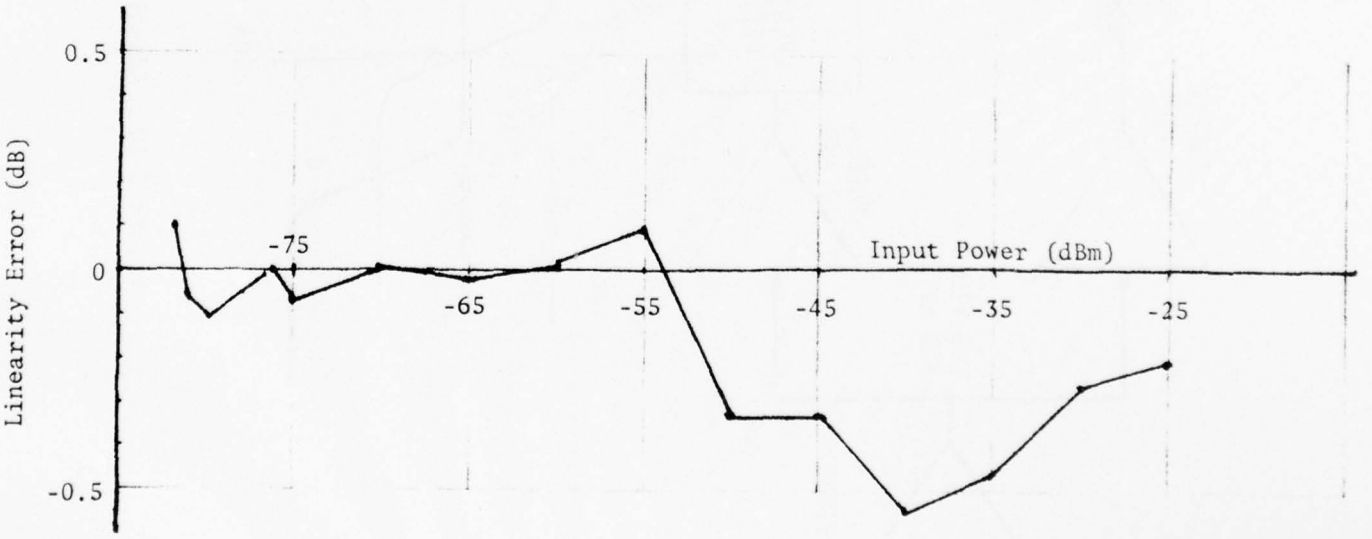


Figure 3-9. Log Video Linearity Versus Input Power

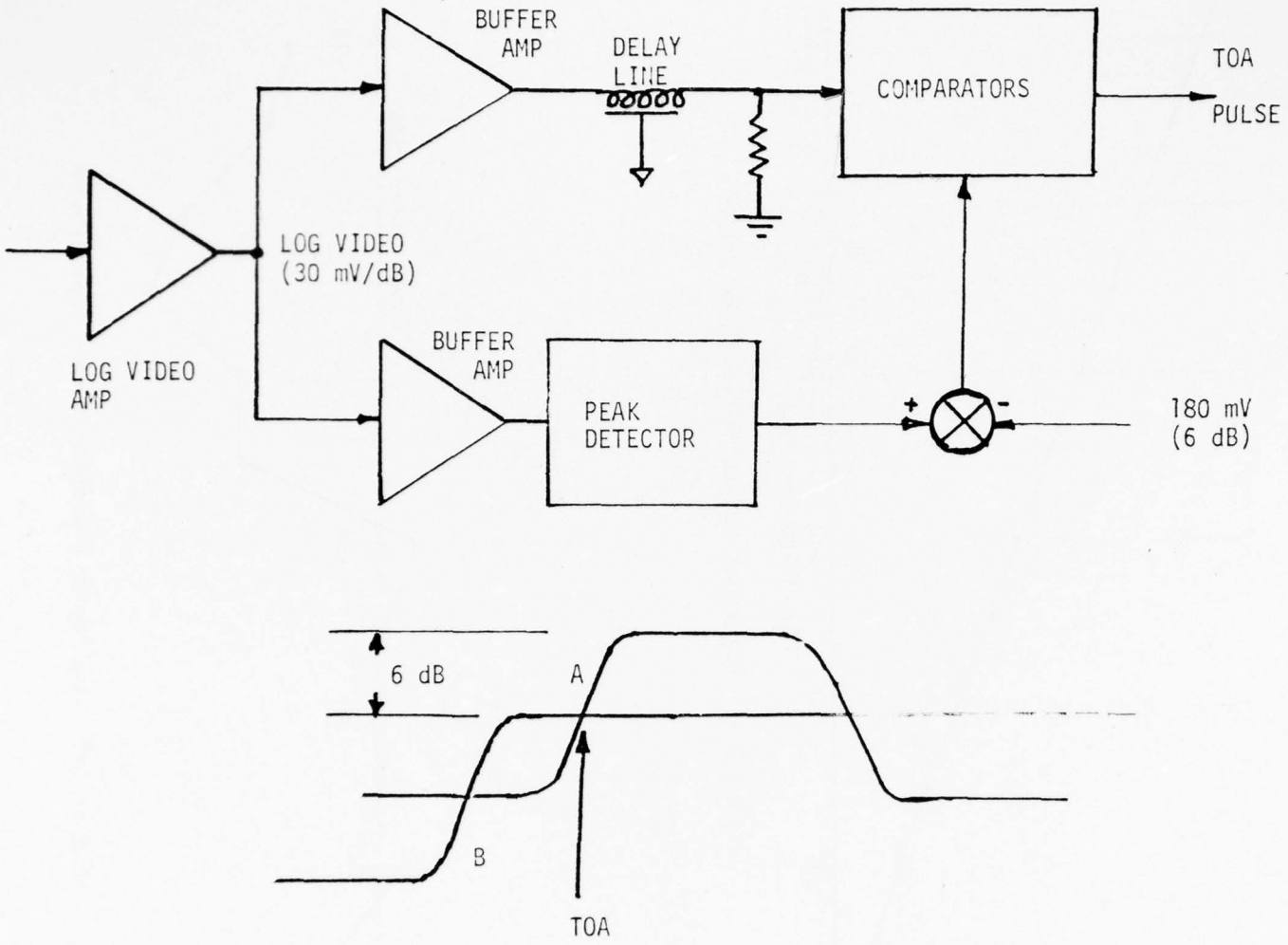


Figure 3-10. Adaptive Threshold Detector

Signal Processing Unit (SPU). The PCU also receives mode control and receiver tuning words from the SPU to control the mode of operation of the ILT and PCU, and to tune the receiver to the proper frequency. Figure 3-11 is its block diagram.

3.3.1 PCU INPUTS AND OUTPUTS

The inputs to the PCU from the receiver are one log video signal (LV), one fine frequency (FRF), one accept pulse (QUAL), and four phase signals (sinA, CosA, SinB, CosB). Signal processing starts upon the receipt of a LV pulse that has sufficient amplitude to exceed the minimum threshold level. When the LV signal has settled to its final level a hold gate and qual strobe are generated. The hold gate causes sample and hold circuits connected to the LV, FRF and phase inputs to hold the value of those input signals at that instant of time. The qual strobe interrogates the qual signal to determine if the input should be accepted or rejected. The held values are serially multiplexed to an eight bit A/D converter whose output is held in a digital register until all the parameters are converted. The Time of Arrival (TOA) of the input RF pulse is also stored in these registers. The TOA is determined by an Adaptive Threshold Detector (ATD) which indicates when the log video is at its minus six dB point on the rise time. At this point, the count of a 32 bit 60 MHz counter is strobed into the storage register to indicate TOA for that particular pulse. When all of this data is in the storage register it is transferred to the SPU via a 16 bit data ready, data acknowledge parallel interface.

The PCU also receives inputs from the SPU via a 16 bit data ready, data acknowledge interface. This interface transfers the mode of operation that the PCU and receiver should be operating in and the tuning word that tunes the receiver to the correct frequency for processing landmarks.

3.3.2 MODES OF OPERATION

The PCU operates in four different modes which are Normal, RF Calibration, IF Calibration and Standby. The SPU commands both the PCU and receiver to operate in a particular mode by issuing a specific mode control word or discrete signal. The mode control word format appears in Table 3-6.

3.3.2.1 Normal Mode

In the normal mode the PCU receives pulse data that represents amplitude, fine frequency and phase from the receiver. It digitizes these data and holds them along with the TOA in storage registers. It then commands the receiver to go into a calibration mode where signals of equal phase shift and of the same power level of the pulsed input are injected into the receiver. After 11 μs the phase inputs are held and digitized. This phase information is also put into storage registers. The SPU is then given a data ready and the data stored in the registers is transferred to the SPU. After all the data is transferred, the PCU is reset and can process another input.

BEST AVAILABLE COPY

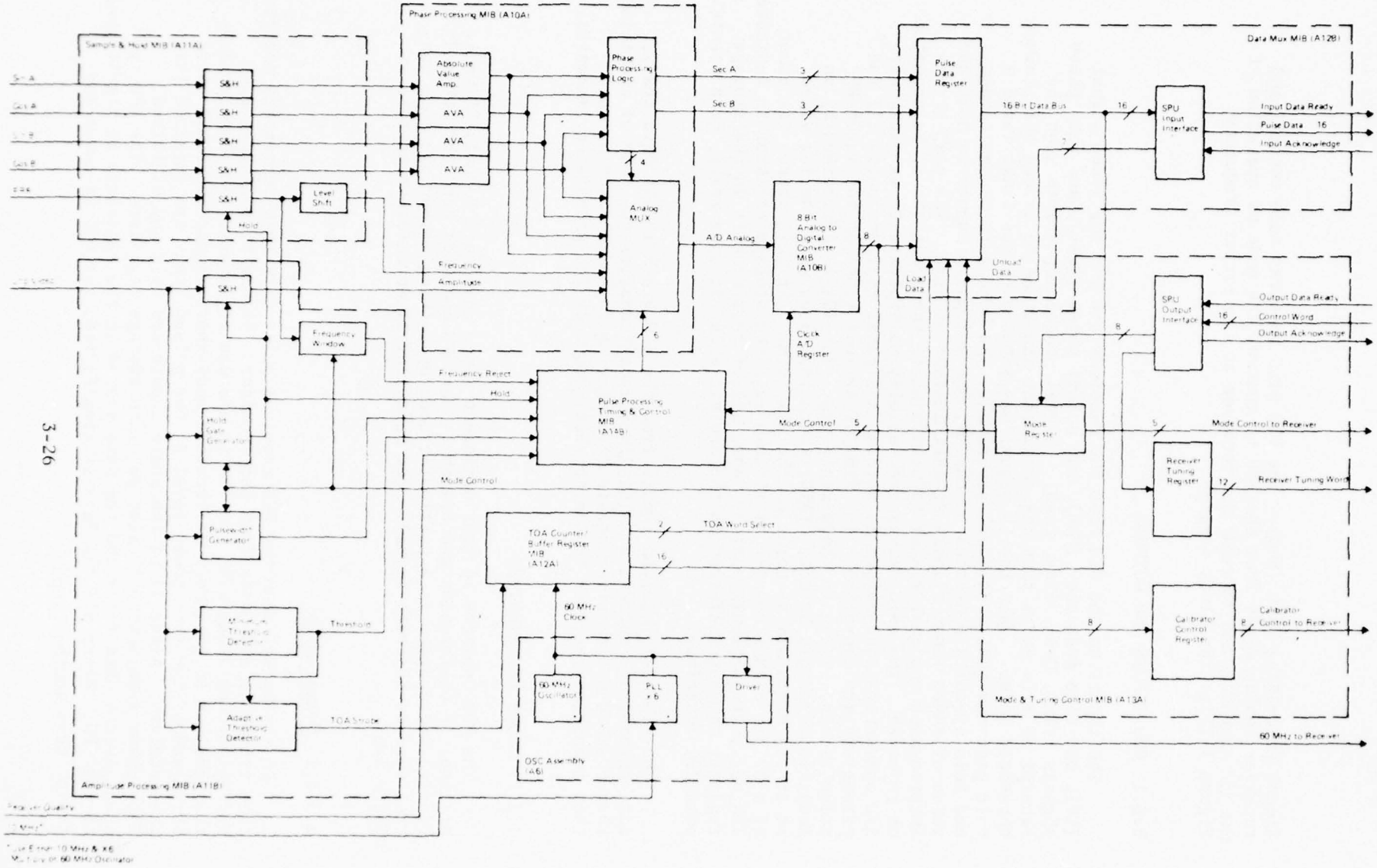


Figure 3-11. PCU Block Diagram

Table 3-6

SCHANS I/O Bit Formation

Bit Position	Signal Name	Definition
15	Process Enable	0 Processing Disabled 1 Processing Enabled
14	Antenna Select	0 Antenna #1 1 Antenna #2
13	RF Freq Cal Mode	0 RF Freq Cal Mode 1 Normal Mode
12	IF Cal Mode	0 Normal Mode 1 IF Cal Mode
11	IF Cal Sel 1 IF Cal Sel 2	Sel 1 / Sel 2 / IF Cal Sec 0 / 0 / -45^{o} 0 / 1 / $+45^{o}$ 1 / 0 / $+135^{o}$ 1 / 1 / $+225^{o}$
9	Wide Pulse Mode	0 Hold at 0.7 μs 1 Hold at 5 μs
8	Use Freq Window	0 Window Disabled 1 Window Enabled

3.3.2.2 RF Calibration Mode

In the RF Calibration Mode a signal with known frequency and known amplitude and with equal phase shift is injected into the input of the receiver channels. Eleven microseconds after the unit is commanded to go into RF Frequency Calibration Mode the PCU will hold the values of amplitude, fine frequency and phase and will digitize these terms. Also the TOA register will store the TOA at hold time. When all terms are in the storage registers the data will be transferred to the SPU via the data ready acknowledge 16 bit interface. After all data is transferred the PCU is reset, another 11 μs time out is generated and the digitizing cycle starts all over again. The PCU will keep cycling in this mode until the SPU commands another mode of operation. This mode can be used for the following functions:

1) RF Frequency Calibration
2) RF Phase Calibration
3) Built In Test
4) Real Time Counter for SPU (using the TOA readings)

3.3.2.3 IF Phase Calibration Mode

In the IF Phase Calibration Mode inputs with known phase shifts of -45^{o}, $+45^{o}$, $+135^{o}$ and $+225^{o}$ are applied to the IF channel inputs. The SPU commands the PCU and receiver to be in the IF Phase Calibration Mode and commands the receiver to apply specific test input. After waiting 11 μs for switching and settling the PCU holds the values of amplitude, frequency and phase. It then digitizes the values of the SinA, CosA, SinB and CosB phase terms. After these terms are in the storage registers the data is transferred to the SPU via the 16 bit data ready/acknowledge interface. When the transfer is complete the PCU is reset, it will resample the inputs after an 11 μs delay and digitize the phase terms again. The PCU will continue to cycle in this mode until commanded to enter a new mode.

3.3.2.4 Standby Mode

This mode is entered by the SPU sending a discrete signal to the power supply. The power supply will then turn off all the PCU power except for the voltages going to the TOA Counter/Buffer mib (A12A) and the Oscillator Assembly (A6). The voltages for the A12A and A6 assemblies are on separate mib layers in the backpanel and are supplied by the standby capability of the power supply. This allows the TOA counter to run while the rest of the unit is off, thus keeping an accurate real time measurement.

3.3.3 PCU PROCESS CYCLE TIMING

The time required to digitize the receiver inputs is dependent upon the mode of operation. For the three modes the time from the generation of hold gate to the time conversion complete is generated is:

Normal	33 μs
RF Frequency Cal	26 μs
IF Cal	26 μs

A timing diagram for these modes is shown in Figures 3-12, 3-13 and 3-14.

3.3.4 CHANGING BITS IN MODE AND TUNING CONTROL WORDS

When the operation of the PCU requires that the Mode or Tuning Control Words be changed, it is required that first just the Process Enable bit be turned off (Bit 15 = "0") and then wait until pending data is transferred to the SPU.

The time to transfer pending data is the sum of the processing time of the PCU plus the I/O time of the SPU. The processing time of the PCU is mode dependent and is as follows for the three modes:

Normal	34 μs for narrow pulse mode, 39 μs for wide
RF Freq Cal	28 μs
IF Cal	28 μs

After this time any number of bits may be changed.

3.3.5 PCU PROCESSING ERRORS

Table 3-7 shows the errors at room temperature and over the $0^{o}C$ to $70^{o}C$ temperature range encountered for SCHANS for each of the functions in the analog processing chain. For each of the terms processed a slightly different processing chain is encountered. Therefore the PCU processing errors are a function of the term being converted.

3.3.5.1 Amplitude

The amplitude term (Log Video) chain contains a Sample and Hold, Multiplexer, and A/D converter.

At $25^{o}C$

Error (max) = 5 + 8 = 13 mV

Error (RSS) = $(5)^2 + (8)^2 = 9.4$ mV

0 to $70^{o}C$

Error (max) = 10 + 1.3 to .4 + 12 = 23.7 mV

Error (RSS) = $(10)^2 + (1.3)^2 + (0.4)^2 = 15.7$ mV

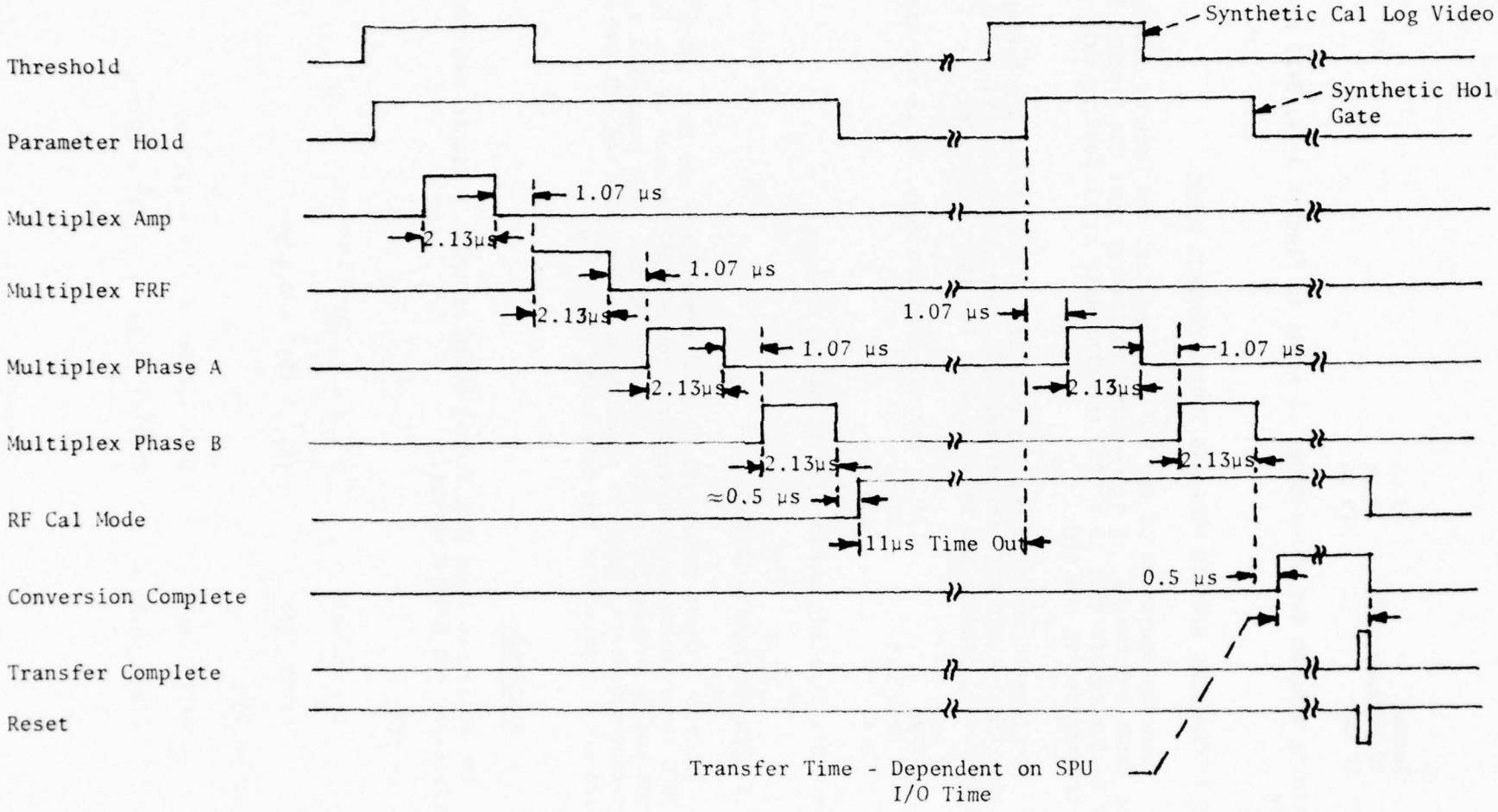


Figure 3-12. Normal Mode Process Cycle Timing

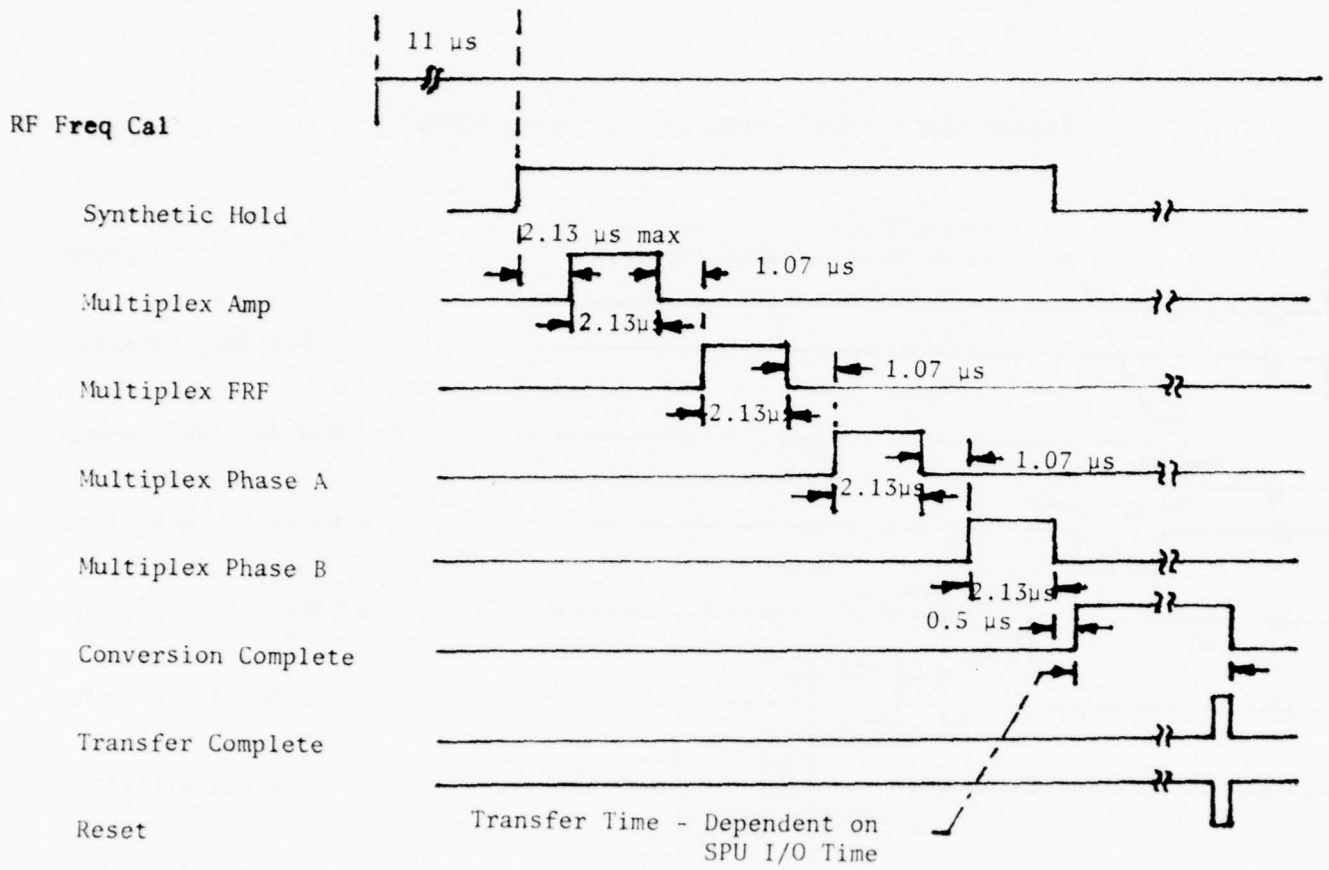


Figure 3-13. RF Frequency Cal Mode Process Cycle Timing

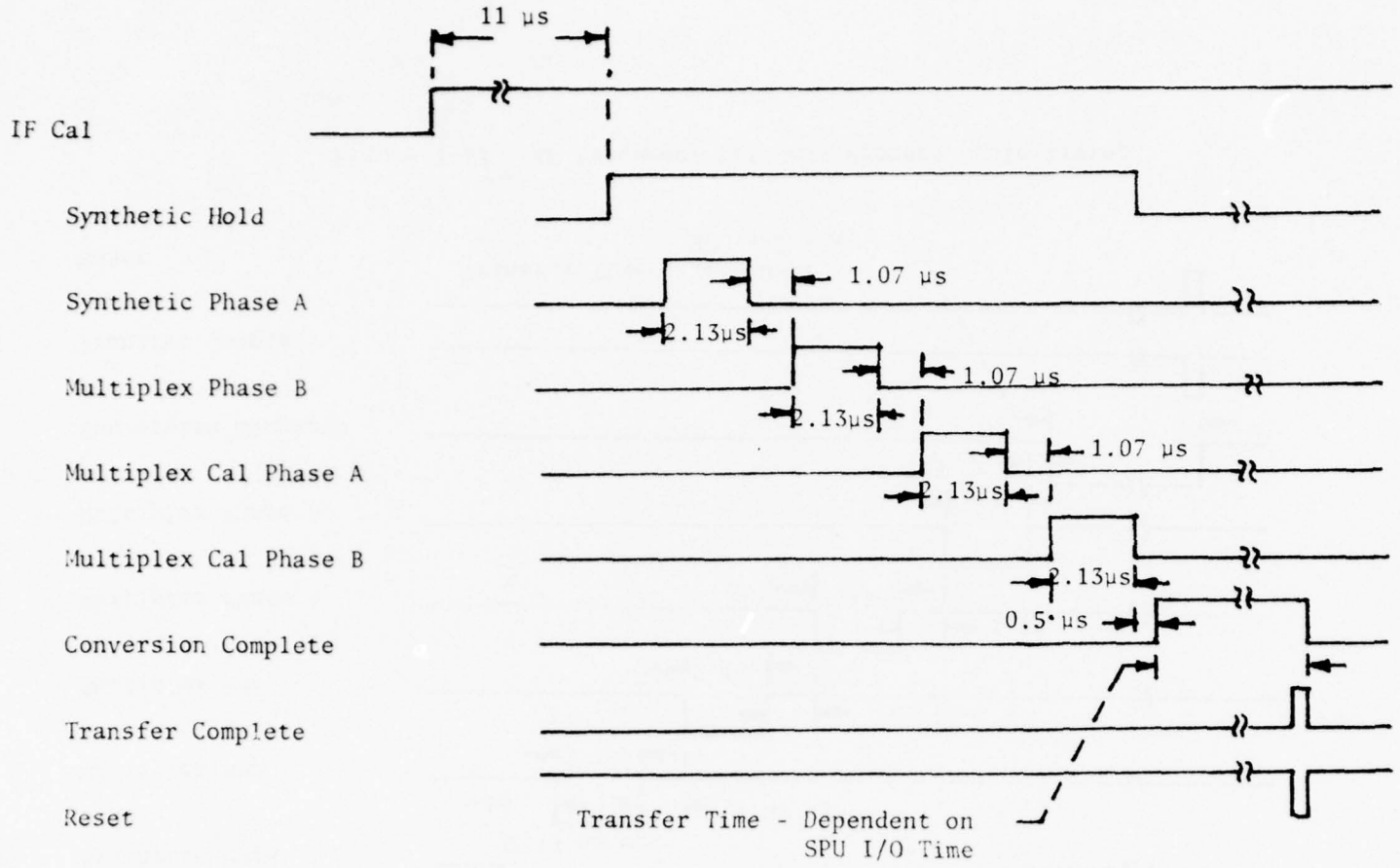


Figure 3-14. IF Cal Mode Process Cycle Timing

Table 3-7

Errors of Each Function in the
Analog Processing Chain

Function	Error In Millivolts	
	25°C	0 to 70°C
Sample and Hold		
Gain	5	10.0
Offset	0	1.3
Absolute Value Amplifier		
Gain	1	1.5
Offset	0	1.0
Multiplexer	0	0.4
A/D	8	12.0
Frequency Level Shift		
Gain	1	1.5
Offset	0	5.0

3.3.5.2 Phase

The phase terms (sine and cosine) have a Sample and Hold, Absolute Value Amplifier, Multiplexer and A/D converter in the processing chain.

At $25^{o}C$

Error (max) = $5 + 1 + 8 = 14$ mV

Error (RSS) = $(5)^2 + (1)^2 + (8)^2 = 9.5$ mV

0 to $70^{o}C$

Error (max) = $10 + 1.3 + 1.5 + 1 + .4 + 12 = 26.2$ mV

Error (RSS) = $(10)^2 + (1.3)^2 + (1.5)^2 + (1)^2 + (0.4)^2 + (12)^2 = 15.8$ mV

3.3.5.3 Frequency

The frequency processing chain is the Sample and Hold, Level Shift, Multiplexer and A/D Converter.

At $25^{o}C$

Error (max) = $5 + 1 + 8 = 14$ mV

Error (RSS) = $(5)^2 + (1)^2 + (8)^2 = 9.5$ mV

0 to $70^{o}C$

Error (max) = $10 + 1.3 + .4 + 1.5 + 5 + 12 = 30.2$ mV

Error (RSS) = $(10)^2 + (1.3)^2 + (0.4)^2 + (1.5)^2 + (5)^2 + (12)^2 = 16.5$ mV

3.3.6 PCU DETAILED DESIGN DESCRIPTION

A detailed description of PCU electrical/logic design and operation appears in Appendix B, Volume III.

3.4 POWER SUPPLY

The power supply selected for the ILT-PCU (and for the SPU as well) is produced by the IBM Federal Systems Division, Huntsville, Alabama, facility for the B-52 Automatic Offset Unit. Some modifications would be required to operate from an unregulated, nominally +28 VDC source. Current output requirements for the ILT-PCU are as follows.

Supply Voltage (V)	Direct Current (Amp.) Standby	Peak
+ 5	0.7	3.2
- 5	0.2	0.8
+15	0.2	1.1
-15		0.9

The power supply has self-control circuitry for sequencing from off to standby to full power to off, as commanded by TTL-level input logic signals. There are short-circuit, input over-voltage and output overload protection provisions. In case of an input over-voltage or failure, power can be sustained to the units long enough for the SPU to execute its own power-down sequence.

3.5 ILT-PCU MECHANICAL DESIGN

3.5.1 PHYSICAL DESCRIPTION

The mechanical organization of the ILT-PCU is shown in Figure 3-15. The overall size of the assembled unit is 10.75 x 5.78 x 22.56 inches. It occupies a swept volume of 0.81 ft^3 and weighs 36.27 lb. The unit contains the following main sections and their subassemblies:

- o Receiver
  - RF Subassembly, consisting of three switches, three bandpass filters, four mixers, a power divider, a coupler, an isolator, and voltage tuned oscillator. All are mounted to an aluminum frame and interconnected by means of semirigid coaxial cable. The power divider is a hybrid package with a ceramic substrate and the voltage tuned oscillator is a hybrid package with an Epsilam-10 substrate.
  - YIG-Tuned Oscillator, a purchased unit mounted directly to the inside wall of the housing.
  - IF Section, consisting of six modules. Each module consists of one or more printed circuit boards populated with discrete components and housed in an aluminum chassis. Sheet aluminum covers are fastened on both sides to prevent RF coupling between the circuits of adjacent modules. Input/output connectors are located at one end of the module in order to conserve space and provide easy removal from the housing. Three limiter circuits, which are hybrid packages with ceramic substrates, are contained within the six modules. Figure 3-16 illustrates the configuration. Connections between IF modules and other subassemblies are implemented with coaxial cabling and light-weight connectors.

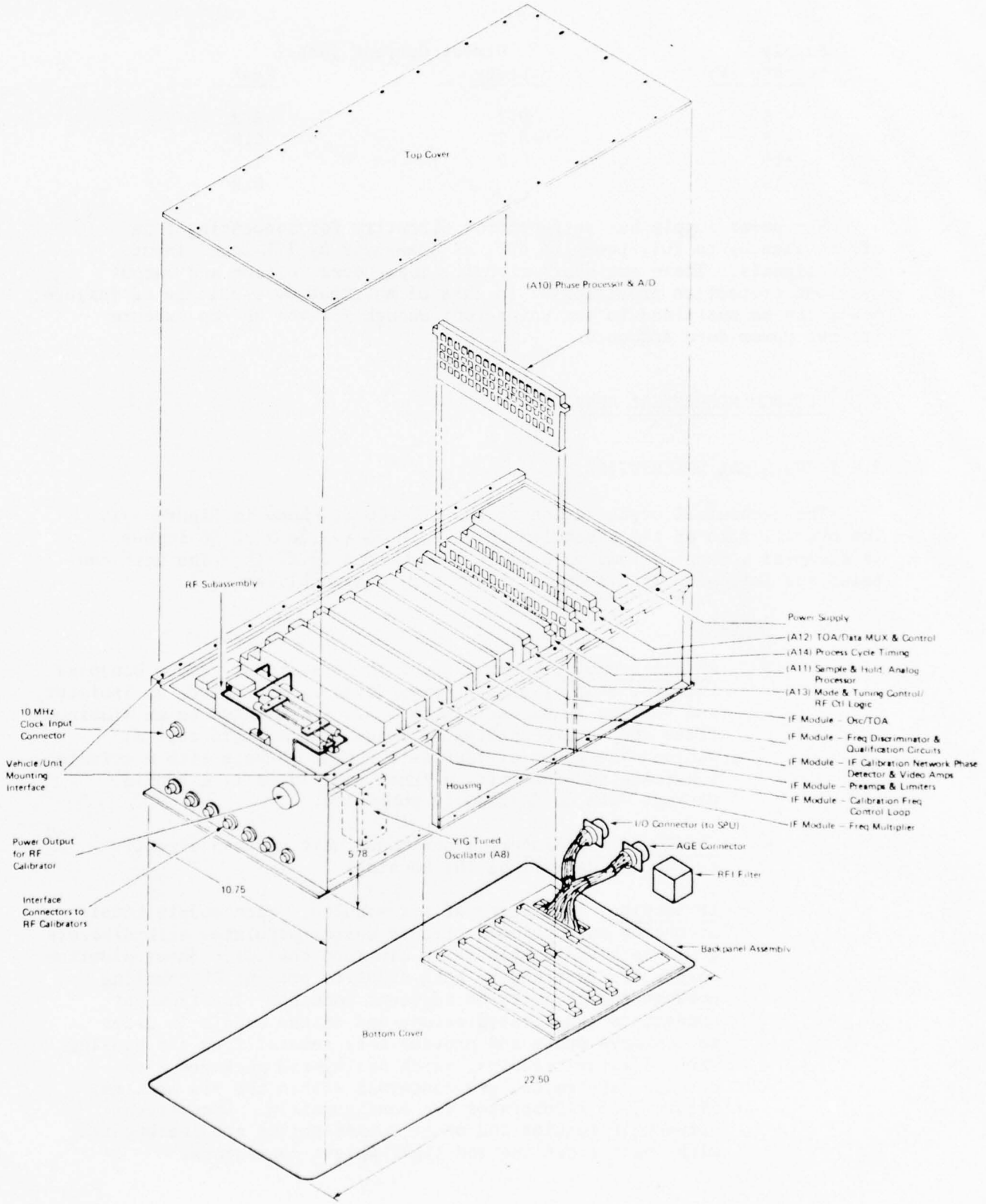


Figure 3-15. ILT-PCU Mechanical Organization

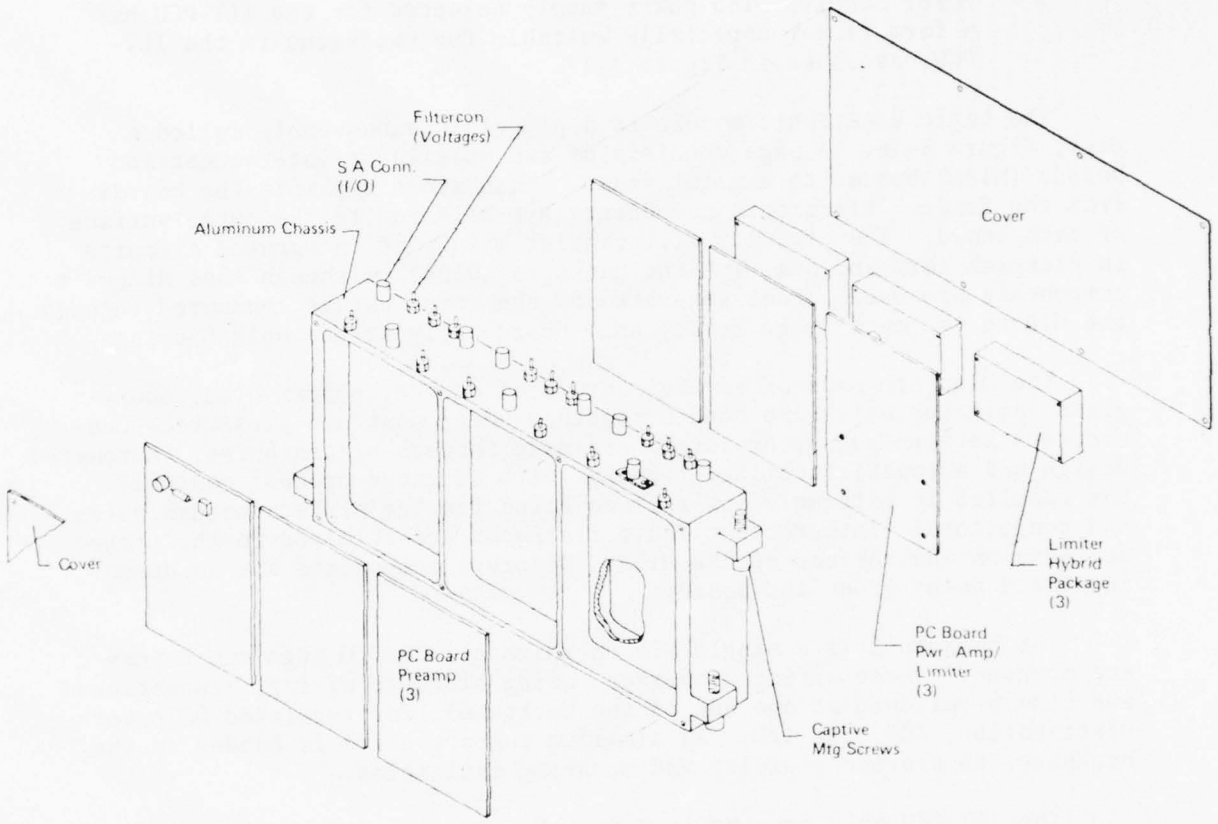


Figure 3-16. IF Module Assembly of Preamplifier/Limiter

- RF Control Logic, packaged on a single IBM 4 Pi page, located in the PCU section.

o Pulse Conversion Unit. The PCU consists of five standard 4 Pi Pages, of which three are analog and two are digital. The backpanel assembly provides connections between pages.

o Power Supply. The power supply selected for the ILT-PCU has a form factor especially suitable for packaging in the ILT-PCU, as shown in Figure 3-17.

The basic electronic module is a pluggable subassembly called a page, Figure 3-18. A page consists of two multilayer interconnection boards (MIBs) bonded to a metal frame. Insulators separate the boards from the frame. Electronic components are soldered to the outer surface of each board. The circuits will consist mainly of integrated circuits in flatpack form and dual in-line packages (DIPs), although some discrete components are used. Heat generated by the component is conducted through the MIB to the metal page frame, and subsequently to the unit housing.

The MIBs are made of several layers of etched, copper-clad, epoxy-glass laminates which are bonded together under heat and pressure. Connections between conductor layers are made through plated holes. Automated design and automatic testing, together with advanced process control, has resulted in extremely low failure rates for the plated-through holes and conductors. Integrated circuit flatpacks are soldered to the etched patterns on the surface of the MIBs. Discrete components are soldered in plated holes or on the board.

The backpanel is a single MIB on which all CPU/IO page connectors are mounted. Three wiring harnesses, using discrete wiring, are attached and strain-relieved at one end of the backpanel, for regulated DC power distribution, AGE, and I/O. An aluminum support plate is bonded to the backpanel to provide rigidity and mounting facilities.

The ILT-PCU main housing is a 6061-T6 aluminum dip brazing which is subsequently machined to provide necessary mounting provisions for the electronics subassemblies. The housing provides a heat transfer path from the electronic subassemblies to the mounting panel or pallet. The mounting flanges will be machined flat with a surface finish of 32 μin to achieve a good thermal connection to the pallet. The top and bottom covers provide easy access to subassemblies and are fabricated from sheet metal aluminum and secured to the main housing with military standard screws.

3.5.2 ILT-PCU WEIGHT

The weight of the ILT-PCU is calculated to be 36.3 pounds, as shown in Table 3-8.

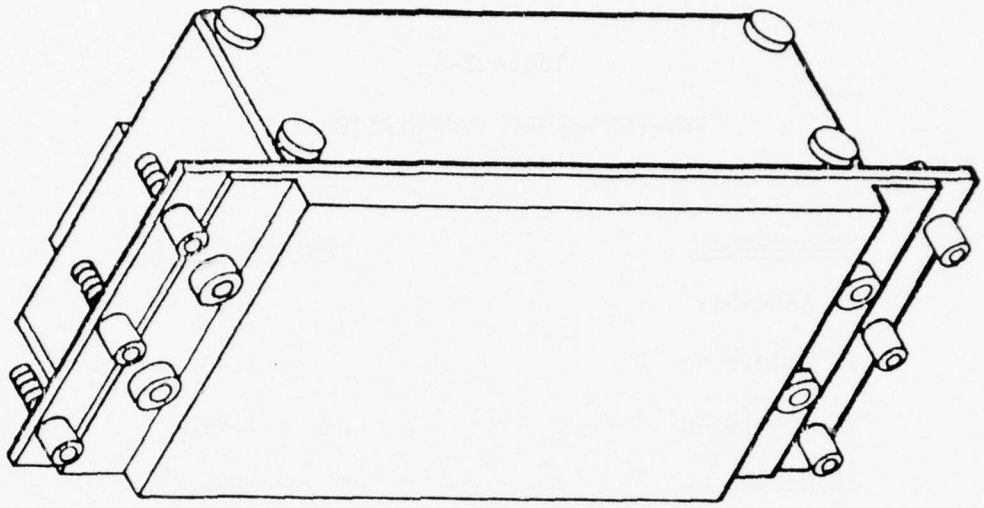


Figure 3-17. Power Supply Configuration

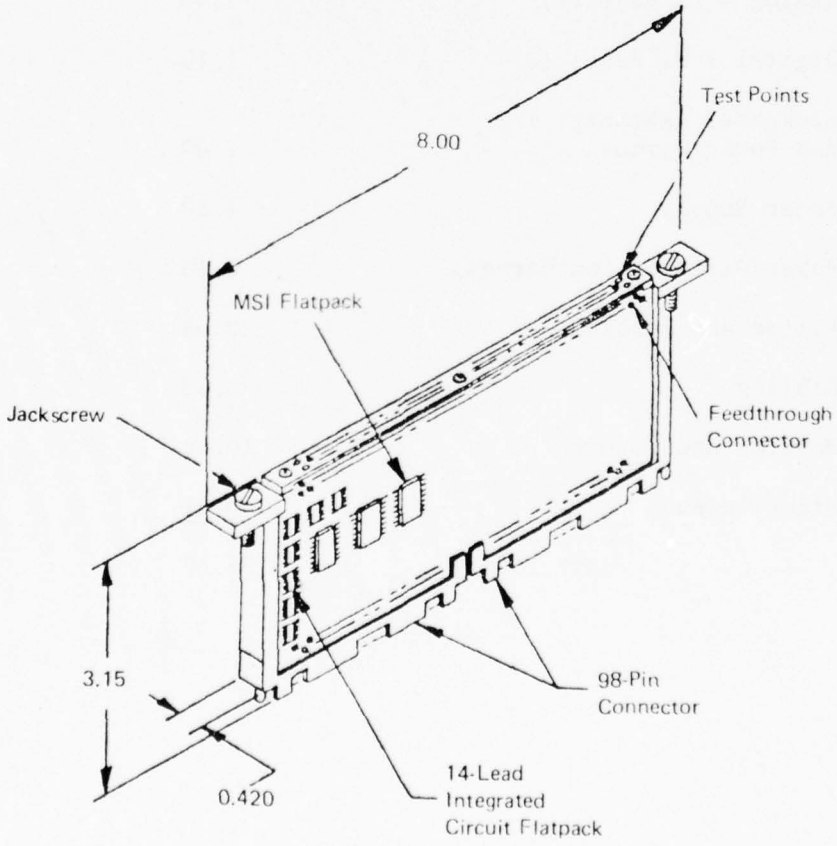


Figure 3-18. Pluggable Electronic Subassembly (4 Pi Page)

Table 3-8

ILT-PCU WEIGHT CALCULATION

Subassembly	Weight (lb.)
RF Assembly	4.23
IF Module No. 1	1.40
IF Module No. 2	1.94
IF Module No. 3	1.43
IF Module No. 4	1.36
IF Module No. 5	1.51
IF Module No. 6	1.40
Analog 4 Pi Page (3)	2.40
Digital 4 Pi Pages (2)	1.10
Backpanel Assembly, I/O and Power Harness	2.00
Power Supply	4.50
Power Distribution Harness	0.50
Filter and Bracket	0.65
Cabling	0.50
Housing and Covers	10.64
Miscellaneous	0.71
Unit Total	36.27

3.6 SIGNAL PROCESSING UNIT (SPU)

The SPU contains an advanced-design, single-page microprocessor designated ML-0, two double modular core memories (DMCM) memory timing page, three input/output (I/O) pages and a power supply. Principal characteristics are listed in Table 3-9. The ML-0 page has been designed and tested with high-speed logic, as has the DMCM, both for other programs. Support software is available to facilitate software development.

The memory design is considered complete. The I/O design to interface the SPU with the PCU is complete through logic diagrams. No automated design has been undertaken, and no multilayer interconnection boards (MIBs) have been detailed. Design of the other I/O functions was undertaken to the point of allocating space (enough for two standard logic pages). Lack of timely definition of external interfaces precluded completion of I/O design. The internal signal flow is indicated in Figure 3-19.

3.7 SPU MECHANICAL DESIGN

3.7.1 SPU PHYSICAL DESCRIPTION

The mechanical organization of the SPU is shown in Figure 3-20. The overall size of the assembled unit is 12.00 x 13.25 x 7.91 inches. It occupies 0.5 ft^3 of swept volume (not including external connectors) and weighs approximately 29 lb. The SPU consists of a memory, power supply, a microprocessor, three input/output subassemblies contained in the same housing and interconnected by a common backpanel.

The memory section consists of 3 pluggable page assemblies. Two of the page assemblies are identical interchangeable storage pages, the third is a timing page.

The timing page is constructed similar to the 4 Pi assemblies in the ILT-PCU but is larger. It consists of two multilayer printed circuit boards bonded to each side of a metal plate frame. Insulators separate the boards from the frame. Components are attached to the outer surface of each board, and two 120 pin connectors are soldered along the bottom edge of the frame between the boards. The assembly is installed and removed by jackscrews in ears on each edge of the frame.

Each storage page assembly consists of two multilayer circuit boards, each bonded to separate heat sink frames. The core mat is soldered to a pattern on the back of these two assemblies, folded, and fastened together. By attaching the core mat between the two separable boards, the outside, and portions of the inside, faces of the circuit boards are left free for component mounting.

A 120-pin connector is soldered to the bottom edge of each circuit board, one on each end of the assembly. These connectors interconnect the pages through the backpanel multilayer board.

Table 3-9

SIGNAL PROCESSING UNIT
PRINCIPAL CHARACTERISTICS

Microprocessor

- Single Page, Low Power Logic
- Microprogram Control
- Cycle Time 300 ns
- Organization
  - Fixed Point, Binary, Fractional
- Instruction Word Length
  - 16 & 32 bits
- Single (16-bit) and Double (32-bit) Precision
- General Registers
  - Set of Eight 16-bit Hardware Registers
- Number of Instructions
  - Over 40

Memory

- Two Double Modular Core Memories (DMCM)
- Total Capacity
  - 32,768 16-bit Words
- Timing Page

Input/Output (3 Pages)

- PCU
  - 16-bit Parallel Control
  - 16-bit Parallel Data
- PCM Telemetry
  - Serial NRZ, 64-128 kb/s
- Command
  - 3 Discrete; 7-bit Variable
  - 22 to 35 V Relay Drives

Power Supply

- Modified AOU (Identical to that of the ILT-PCU)

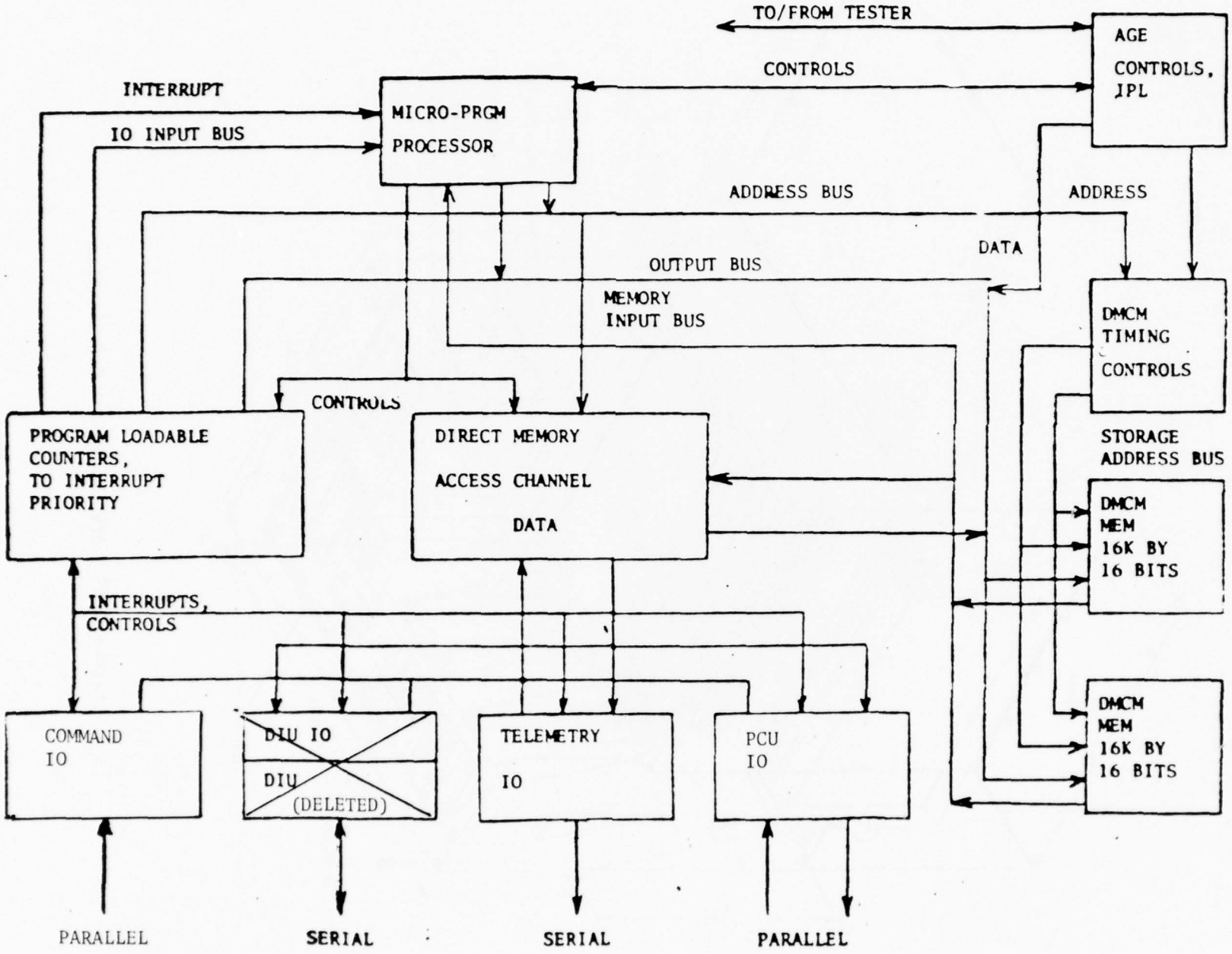


Figure 3-19. SPU Signal Flow

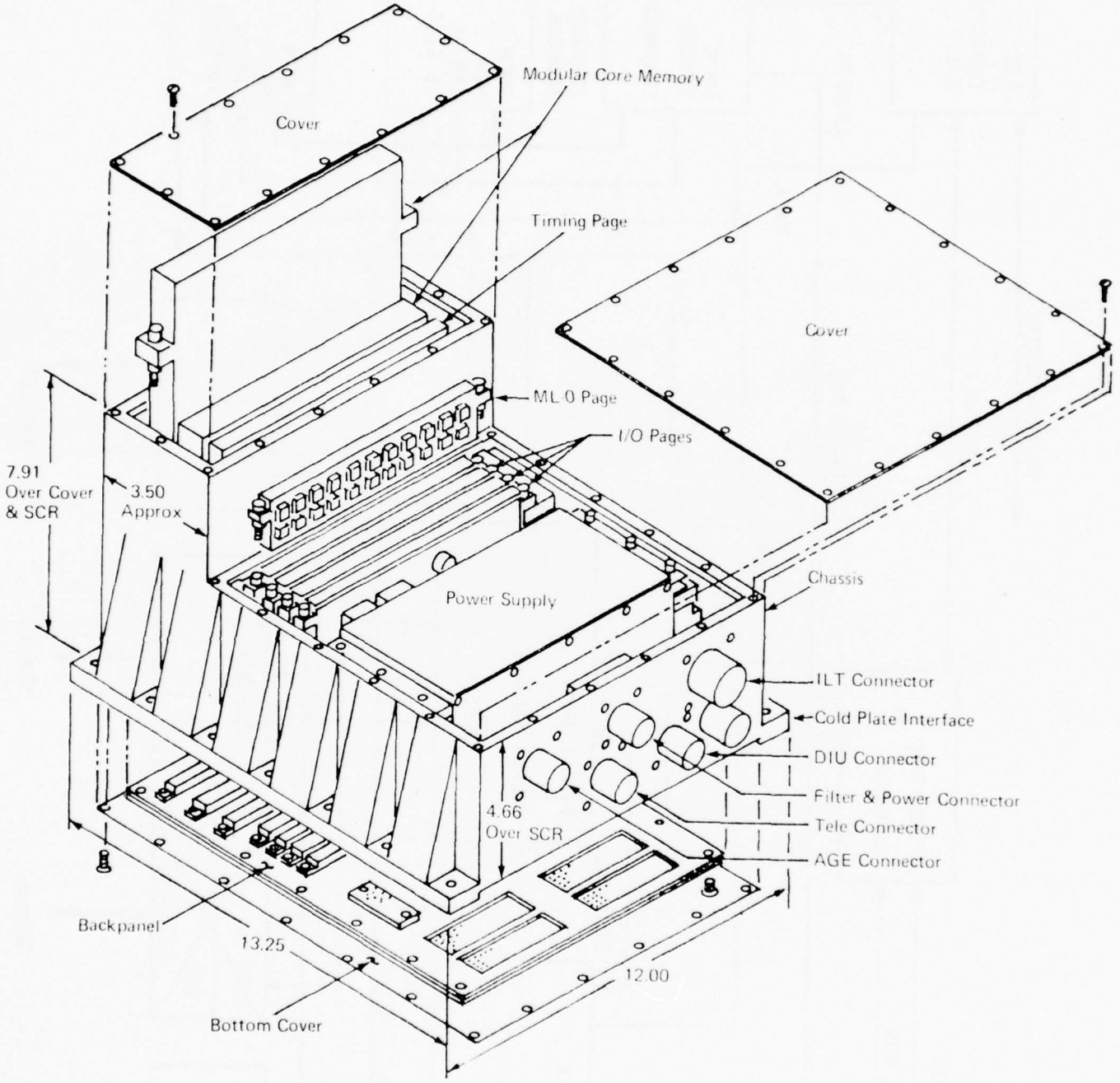


Figure 3-20. SPU Mechanical Organization

The page is fastened to the SPU housing through mounting flanges extending from each side of the page. Additional support is provided by the connectors and the backpanel support plate which also is mounted to the SPU housing.

3.7.2 SPU WEIGHT

The weight of the SPU is calculated as 29 pounds, as shown in Table 3-10. The high chassis weight is based on an early power-dissipation estimate and is designed to provide high thermal conductivity. A redesign based on more recent power estimates will allow a weight reduction of 4.5 pounds.

3.8 SYSTEM WEIGHT ESTIMATE

In the table below, only the weights of the ILT-PCU and SPU are calculated with confidence, as shown in Tables 3-8 and 3-10, respectively. The calibrator weight is based on a design, completed under a previous contract, intended for installation inside another unit. The cable weight depends principally on the type of coaxial cable chosen for connecting the RF Calibrator (in the Antenna Array structure) to the ILT-PCU. The assumed separation distance is ten feet, and the figure shown is for low noise microwave coaxial cable. The weight of the antenna array includes the structure, antennas and semi-rigid coaxial cables connecting the antennas to the calibrator.

Component/Unit	Weight (lb.)
Antenna Array	7.0
Calibrator Assembly	5.0
ILT-PCU	36.3
SPU	29.0
System Cables	12.1
System Total	89.4

3.9 SYSTEM POWER CONSUMPTION

The system is designed to operate from an unregulated (22 to 35 volt) DC primary source. The antenna array and RF Calibrator are, in this respect, passive. Primary power is supplied directly to the ILT-PCU and to the SPU, each of which has three states: off, standby and operating. The ILT-PCU is controlled by the SPU, which initiates power-up and power-down sequence in response to external commands.

The flight test plan contemplates having the system off through launch and injection into earth orbit. At some time after that, depending upon the primary payload schedule, SCHANS would begin intermittent operation: two successive orbits each day. At the beginning of the

Table 3-10

SPU WEIGHT CALCULATION

Subassembly	Weight (lb.)
DMCM Pages (2)	3.30
Timing Page	0.85
Basic Logic Page	0.80
Support Page No. 1	0.75
Support Page No. 2	0.75
Support Page No. 3	0.70
Backpanel and Harnesses	3.50
Power Supply	4.50
Filter and Power Connector	0.65
Chassis and Covers	13.20
Unit Total	29.00

operating period, the system would be turned on and initialized by command. The SPU places itself and the ILT-PCU in standby as the signal processing program in the SPU selects the first set of landmarks. When a predicted landmark encounter time is reached, the ILT receiver is turned on and landmark signal measurements begin. When a number of measurements have been stored, the ILT-PCU is returned to standby, and the measurements are processed by the navigation software to update its Kalman filter. The SPU then returns to standby for the remainder of a ten second interval or until a new landmark is encountered; the cycle then repeats. Twelve such cycles will be executed for each landmark group.

The total duty cycle is complex and depends principally on the number of landmarks encountered. For a particular landmark, the peak operating time for a set of pulses (approximately 50 per landmark per data point) also depends upon the pulse repetition interval of the landmark. Table 3-11 shows average power for a simulated 90 minute orbit (112 Nm polar), using actual landmarks and assuming nominal (28V dc) primary voltage.

ILT-PCU and SPU power consumption are calculated in Table 3-12 and 3-13 respectively.

3.10 THERMAL ANALYSIS

Thermal analyses were performed on the unit designs to estimate subassembly mounting and piece part case or junction temperatures. The results appear in Tables 3-14 through 3-17. The ILT-PCU analysis is an August 1976 update of one performed in October 1975; the SPU analysis was performed in September 1976.

The analyses considered only steady state thermal conduction of internally dissipated power, with no other (i.e., solar) thermal inputs. Each unit was assumed to be mounted on a thermally controlled pallet shielded from sunlight at a pressure of 10^{-5} Torr. A five percent (5%) duty cycle was also assumed. Mounting surface temperature was assumed to vary from minimum to maximum (160^{o}F) and back to minimum in a 90 minute period. The critical reader will note that the minimum SPU temperature is 0^{o}F while the minimum ILT-PCU temperature is 30^{o}F. The latter is a holdover from a previous contract phase and in any case is more conservative from a reliability standpoint.

The highest average piece part temperature is 68^{o}C in the ILT-PCU and 80^{o}C in the SPU.

Unit operations remain satisfactory so long as mounting temperatures remain between 0^{o}F and 160^{o}F and solar irradiance is minimal. Selection of temperature control measures (shielding, active or passive thermal control, etc.) should be worked out in close coordination with the spacecraft contractor, after a host vehicle is selected.

Table 3-11

TYPICAL SINGLE-ORBIT POWER CONSUMPTION

Total Landmark Sightings	33 (9 single, 8 groups of 3)
Data Points/Landmark Group	12
Total Number of Updates	204
ILT/PCU Power Requirements (Table 7-2):	
o Standby Power	17.3 Watts
o Peak Power	116.9 Watts
Total On Time @ .5 Sec./ Landmark/Data Point	198.0 Sec.
o Duty Cycle	.037
o (Peak-Standby) X Duty Cycle	3.7 Watts
o Average Power	20.0 Watts
SPU Power Requirements (Table 7-3):	
o Standby Power	11.5 Watts
o Peak Power	154.7 Watts
o Landmark Data Process Time @ 1.25 Sec./Update	255.0 Sec.
o Clock Reset Time (300 msec/min)	27.0 Sec.
o Total On Time	282.0 Sec.
o Duty Cycle	.052
o (Peak-Standby) X Duty Cycle	7.4 Watts
o Average Power	18.9 Watts
Total System Average Power	38.9 Watts

Table 3-12

ILT-PCU Power Consumption

Subassembly	Power (Watts) Standby	Peak
RECEIVER		
Frequency Multiplier	0.38	2.20
Calibration Frequency Control	0.00	6.61
Preamplifier/Limiter	0.00	4.17
IF Calibrator	0.00	0.00
Frequency Discriminator	0.00	1.73
Oscillator Assembly (VTO)	1.20	1.20
Heater* (on at 70°F, off at 85°F)	1.00	8.00
RF Assembly	0.75	4.20
Oscillator Assembly (YTO)	1.00	8.73
Heater* (on at 70°F, off at 85°F)	2.00	12.00
PCU		
Phase Processing	0.00	1.81
A/D Converter	0.00	3.31
Sample and Hold	0.00	3.58
Amplitude Processing	0.00	3.51
TOA Counter/Buffer	3.26	3.26
Data Multiplexer	0.00	3.00
Mode and Tuning Control	0.00	0.90
Process Cycle Timing	0.00	1.15
Oscillator	0.78	0.78
Sub-Total	10.37	70.14
POWER SUPPLY (60% efficiency)	6.91	46.76
Total	17.28	116.90

*Heater power depends on internal temperature.

Table 3-13

SPU POWER CONSUMPTION

Subassembly	Power (Watts) Standby	Peak
Memory	3.00	38.80
Memory Timing	0.00	9.87
Basic Logic Page	1.40	14.20
Input/Output Pages	2.50	29.95
Sub-Total	6.90	92.82
Power Supply (60% efficiency)	4.60	61.88
Total	11.50	154.70

There are two Double Density Modular Core Memories. Only one is used at a time. Peak power consumption is highly program-dependent, particularly in the memory. The figures given are worst-case estimates.

Table 3-14

ILT-PCU SUBASSEMBLY MOUNTING TEMPERATURES

Subassembly	5% Duty Cycle Power (Watts)	Subassembly Mounting Temperatures (°C) 0°F (-18°C) Vehicle Frame Temperature Aluminum	Magnesium	160°F (71°C) Vehicle Frame Temperature Aluminum	Magnesium
Freq. Multiplier	0.436	-16	-14	73	75
RF Assy.					
Heaters ON	5.602	+4	+30	--	--
Heaters OFF	2.202			80	89
Control Logic	0.607	-15	-13	74	76
Col. Freq. Control Loop & Log Amp	0.330	-16	-15	73	74
Preamp & Limiters	0.208	-17	-16	72	73
IF Cal., Phase Net & Dect. Video Amp	0.025	-17	-17	72	72
Freq. Discm. & Qual. Circuits	0.086	-17	-17	72	72
1) Analog Page(s) 1, 2 & 3	1.005	-16	-15	73	74
Digital Page 1	4.412	0	+20	89	109
Digital Page 2	0.375	-16	-15	73	74
2) Pwr. Supply Assy(s) 1 & 2	5.700	-6	+6	83	95

(1) 0.335 watts each for Analog Page Assemblies

(2) 2.85 watts each for Power Supply Subassemblies

(3) Aluminum: 6061-T6

(4) Magnesium: AZ-31B

Table 3-15

ILT-PCU ELECTRICAL PIECE PART CASE/JUNCTION TEMPERATURES

Subassembly	Piece Part Identification		Average Piece Part Power Dissip. (Watts)	Case Or Junction	Piece Part Temp. (°C) Aluminum Structure (6061-T6) 0°F Veh. Frame	160°F Veh. Frame	Average	Piece Part Temp. (°C) Magnesium Structure (AZ-31B) 0°F Veh. Frame	160°F Veh. Frame	Average
RF Section										
Freq. Mult.	Pwr. Trans Q4		0.02	Junction	-9	80	36	-7	82	38
RF Assy.	VTO Assy.	Heaters ON	1.75	Case	+39	--	68	+65	--	85
		Heaters OFF	0.75		--	96	68	--	105	85
	YTO Assy.	Heaters ON	3.727	Case	+43	--	43	+69	--	55
		Heaters OFF	1.327				43	--	109	55
Control Logic	Flat Pack U1,U9,U15		0.010	Junction	-12	77	33	-10	79	35
	D/A Conv.		0.015	Junction	-12	77	33	-10	79	35
IF Section										
Cal. Freq. Loop Log. Amp.	Hybrid Log. Amp.		0.160	Junction	-8	81	37	-7	82	38
Pre Amp/Limiters	Transistor, Q1		0.008	Junction	-13	76	32	-12	77	33
IF Cal, Phase Net Dect.&Video Amp.	Diodes, CR1-CR16		0.001	Junction	-16	73	29	-16	73	29
Freq. Disc.&Qual. Circuits	Op. Amp. U1, U2 and U5		0.015	Junction	-7	82	38	-7	82	38
Processor Section										
Analog Page Assy(s) 1,2&3	IC, typical 0.5w max. dissipation		0.025	Junction	-15	74	30	-14	75	31
Digital Page Assy. 1	IC, typical 0.5w max. dissipation		0.025	Junction	+9	98	54	+29	118	74
Digital Page Assy. 2	IC, typical 0.5w		0.025	Junction	-15	74	30	-14	75	31
Power Supply Section										
Pwr. Supply Assy(s) 1&2	IC, typical 0.5w max. pwr. transistor		0.025	Junction	-2	87	43	+10	99	55

Notes: (1) Vehicle frame temperature maintained at 160°F (71°C) and 30°F (-1°C)
(2) Conduction only mode of heat dissipation
(3) ILT-PCU structure aluminum 6061-T6

Table 3-16

SPU SUBASSEMBLY POWER DISSIPATION DISTRIBUTION AND SUBASSEMBLY MOUNTING TEMPERATURES

Subassembly Identification	Power Dissipation (Watts) Max.	Standby	Duty Cycle 5%	Subassembly Mounting Temperatures $0^{o}F$ ($-18^{o}C$) Vehicle Panel Temp. (^{o}C)	$160^{o}F$ ($71^{o}C$) Vehicle Panel Temp. (^{o}C)
A2, DMCM Page Assy	37.3	-	1.86	$-13^{o}C$	$76^{o}C$
A3, DMCM Page Assy	1.5	-	0.08	-17	72
A4, Timing Page Assy.	9.9	-	0.50	-16	73
A5, Page Assy. ML-0	14.2	-	0.71	-15	74
A6, Page Assy., 1	8.0	-	0.40	-17	72
A7, Page Assy., 2	10.0	-	0.50	-16	73
A8, Page Assy., 3	7.5	2.5	2.75	-9	80
Power Supply, PSI[1]	54.8	9.0	11.3	-10	79
Total (Watts)	143.2	11.5			

[1] Power Supply Efficiency 62%

Table 3-17

SPU ELECTRICAL PIECE PART CASE/JUNCTION TEMPERATURES

Subassembly Identification	Piece Part Identification	Piece Part Power Dissipation 5% Duty Cycle (Watts)	Piece Part Temperature Type	Piece Part Case or Junction Temperatures		
				0°F (-18°C) Vehicle Panel Temp. (°C)	160°F (71°C) Vehicle Panel Temp. (°C)	Averag (°C)
A2, DMCM Page Assy.	Transistor, Q1	0.179	Junction	-5°C	84°C	40°C
A3, DMCM Page Assy	Hybrid, IC	0.035	"	-3	86	42
A4, Timing Page Assy	Flatpak, U34	0.019	"	-14	75	31
A5, Page Assy, ML-0	Hybrid, IC	0.047	"	-13	76	32
A6, Page Assy, 1	Flatpak	0.010	"	-16	73	29
A7, Page Assy, 2	Flatpak	0.010	"	-15	74	30
A8, Page Assy, 3	Flatpak	0.180	"	0	89	45
Power Supply, PSI(1)	Structure	11.3	Assy. Stru.	-3	79	42

(1) Power Supply evaluated here in subassembly configuration; piece part data not available at time of analysis; assumed typical 4-Pi power supply mounting criteria limit of 95°C for extreme operation with satisfactory piece part temperature values.

3.11 RELIABILITY

A reliability prediction analysis has been performed and reported in detail, with supporting data, in the Design Analysis Report (Reference 17). A summary is given here.

The predicted Mission Phase Reliability for both the SCHANS Space Flight Hardware and the Flight Test Hardware is listed below. Both predictions are for a 32K 16 Bit Memory. The phases of the Mission are defined as follows:

1) Two months storage prior to launch
2) A 0.15 hour (9-minute) launch into orbit
3) A 30 day non-operating period
4) A 90 day period of low duty cycle operation for two orbits per day.

PHASE	1	2	3	4
SPACE FLIGHT HARDWARE	.9621	.9620	.9436	.8897
FLIGHT TEST HARDWARE	.9637	.9636	.9459	.8941

The numbers were derived from the Reliability Block Diagram shown in Figure 3-21. Successful operation of the SCHANS System is defined as follows:

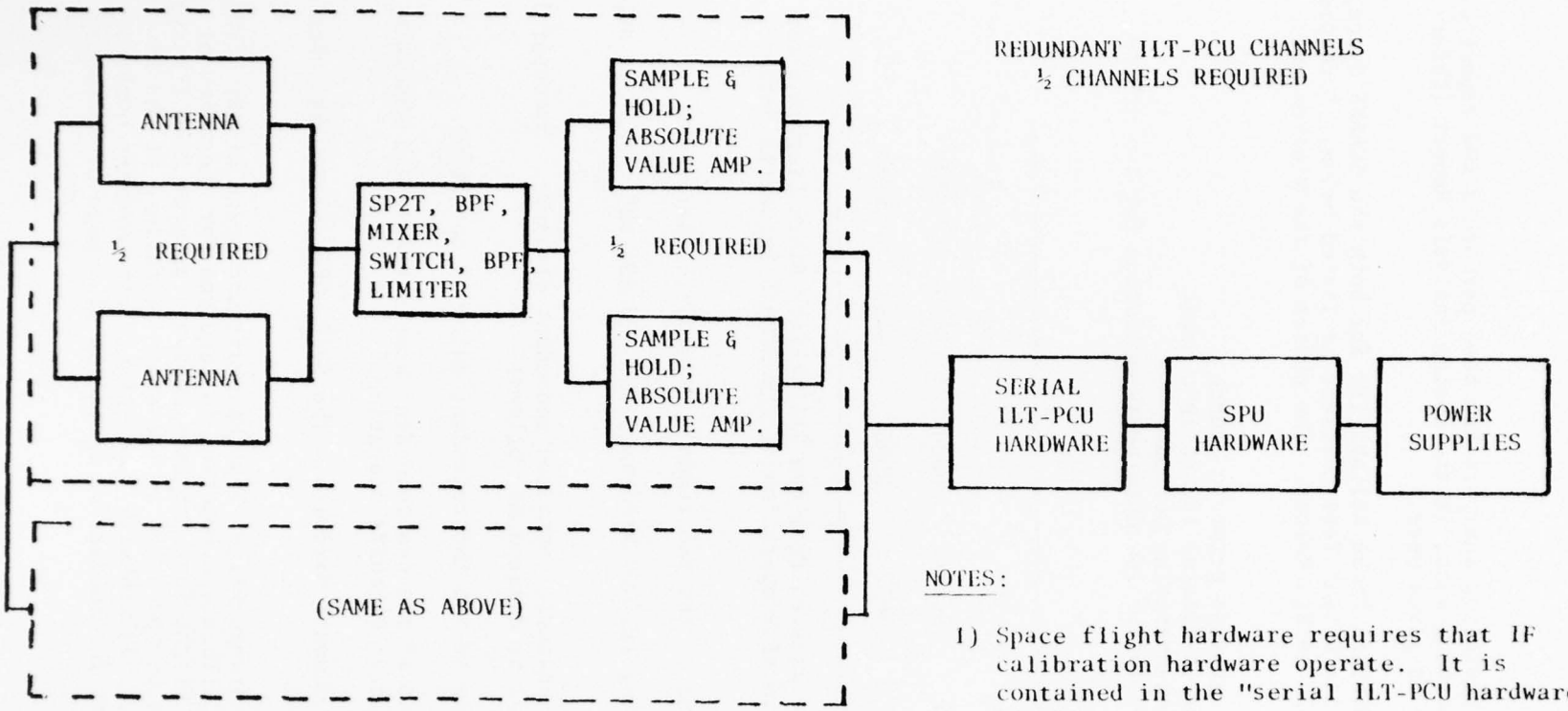
- At least one of the two redundant channels operating.
- The remaining ILT/PCU hardware, the SPU and the two power supplies operating.

Each of the two channels contained redundant elements. Successful operation of a channel is defined as follows:

- At least one of the two redundant antennas operating.
- At least one of the two redundant Sample & Hold and Absolute Value Amplifier Circuits operating.
- The Serial Channel Hardware - The SP2T, BPF, Mixer, Switches - operating.

The difference between Flight Test Hardware and Space Flight Hardware is that the IF Calibration Function is required for operation of the latter while the Flight Test Hardware analysis assumes that the system will still be capable of operation in the event of failure of the IF Calibration Function. Additionally, the Flight Test Hardware numbers includes a requirement for successful operation of a page of Telemetry I/O Hardware.

BEST AVAILABLE COPY



NOTES:

1) Space flight hardware requires that IF calibration hardware operate. It is contained in the "serial ILT-PCU hardware" block.

2) Flight test hardware requires that telemetry I/O be operable. It is contained in the "SPU Hardware" block.

Figure 3-21. Reliability Model Diagram

Interpretation of the results for the space flight hardware tabulated above is as follows:

1) The probability that the System is capable of operation at the time of launch (T = 0) is .9621.

2) The probability that the System is capable of operation 0.15 hours after launch (T = 0.15) is .9620.

3) The probability that the System is capable of operation 30 days after launch is .9436.

4) The probability that the System is capable of operation 120 days after launch is .8897.

Since the system is primarily in a non-operating state, the non-operating failure rates of the hardware are important. For this analysis, non-operate failure rate at the Functional Block Level have been assumed to be 30% of the operate failure rates. A discussion of non-operating failure modes and mechanisms for some piece parts is also included in the Design Analysis Report (Reference 17).

An environmental stress factor of 30 was used for the launch phase. This was primarily a matter of precedence. Even if the factor were 100, the effect on the results shown above would be negligible.

Additional analysis is needed to determine design changes needed to improve reliability for a space flight test. The problem of achieving a system with a 7-year operational life should also be addressed during subsequent phases. To accomplish this, it may be necessary to redefine the flight test hardware design, by adding the redundant hardware where it is required. (The present flight test model design has an operational life of under 1.8 years, assuming a low duty cycle operational profile.) Such an undertaking is more appropriate after space flight test, in support of product engineering. Table 3-18 compares the two sets of requirements.

3.12 NUCLEAR SURVIVABILITY ASSESSMENT

An assessment of SCHANS hardness to nuclear radiation was performed to a limited depth in August 1976 and was based on all design descriptive data available and all piece part radiation effects and hardware data that was obtainable by the investigator in the time allotted. The study results indicate that:

- no special hardening or shielding steps need be taken to protect the equipment from the natural radiation environment, except for orbits that traverse the Van Allen belts frequently over a long period of time (e.g., the Molniya orbit). In the latter case, some piece part changes and shielding equivalent to an additional 1/8 inch of aluminum would suffice.

Table 3-18

COMPARISON OF RELIABILITY REQUIREMENTS

Requirement	120-Day Flight Test	7-Year Design Goal
Program Plan	—	X
Reliability Analysis	X	X
Test Requirement	X	X
System	500- to 2000-hour burn-in	X
Assemblies	—	X
Piece Parts	Selected parts	X
FMEA	—	X
Functional	—	—
Piece Part	—	X
Reliability Prediction	Update	X
Stress Analysis	—	X
Circuit	—	X
Piece Parts	—	X
Failure Detection by Telemetry	—	—
Failure Recurrence Control	X	X
Failure Impact Planning	—	X

X = Required

- more extensive design precautions (not specifically identified) would be required for protection from a weapon-induced environment.

The complete report is presented in the Design Analysis Report (Reference 17) and a classified supplement thereto.

3.12.1 METHODOLOGY

The methodology shown in Figure 3-22, appropriate for a nuclear survivability study of any depth, was followed in the analysis reported below. The radiation levels were obtained from references 21 and 22 for induced and natural environments respectively. Existing radiation effects data and the results of radiation testing by IBM and others in previous efforts (no testing was undertaken under the SCHANS contract) were either on hand or obtained with SAMSO assistance. Examples appear in Figure 3-23 and Table 3-19.

The SCHANS unit parts lists were surveyed and compared to the list of parts on which data were available. There was little exact commonality between the two lists but ample similarities, enough for a preliminary hardness assessment. Piece part and some circuit effects were considered but unit and system effects were not.

3.12.2 SCHANS HARDNESS LEVELS

The estimated ionizing dose, dose rate and neutron fluence hardness levels for the SCHANS semiconductor piece parts are listed in Table 3-20.

Dose hardness was based on radiation effects data on about twenty-five percent of the semiconductor piece parts used and on similarity between parts. Since the CA3100T op amp uses MOS devices, a dose degradation level of 10^4 to 10^5 rads (Si) was used. MOS devices are usually more sensitive than bipolar transistors to ionizing dose effects. Other linear circuits such as op amps and comparators can tolerate relatively large changes in offset voltage, offset and bias current, and in open loop gain. Considering these loose requirements a dose hardness level of 1 to 5 x 10^5 rads (Si) was used. A dose hardness level of 1 to 5 x 10^5 rads (Si) was used for the TTL type logic circuits based on the data in the report "Use of Integrated Circuits in Future Satellites", L. D. Cotter, et al, Intelcom Rad Tech, March 1975 (AFWL7494).

A much larger radiation data base for dose rate and neutron fluence effects than for total dose effects was available for estimating part hardness levels. IBM has tested or analyzed many of the parts and circuits used in the SPU and power supply.

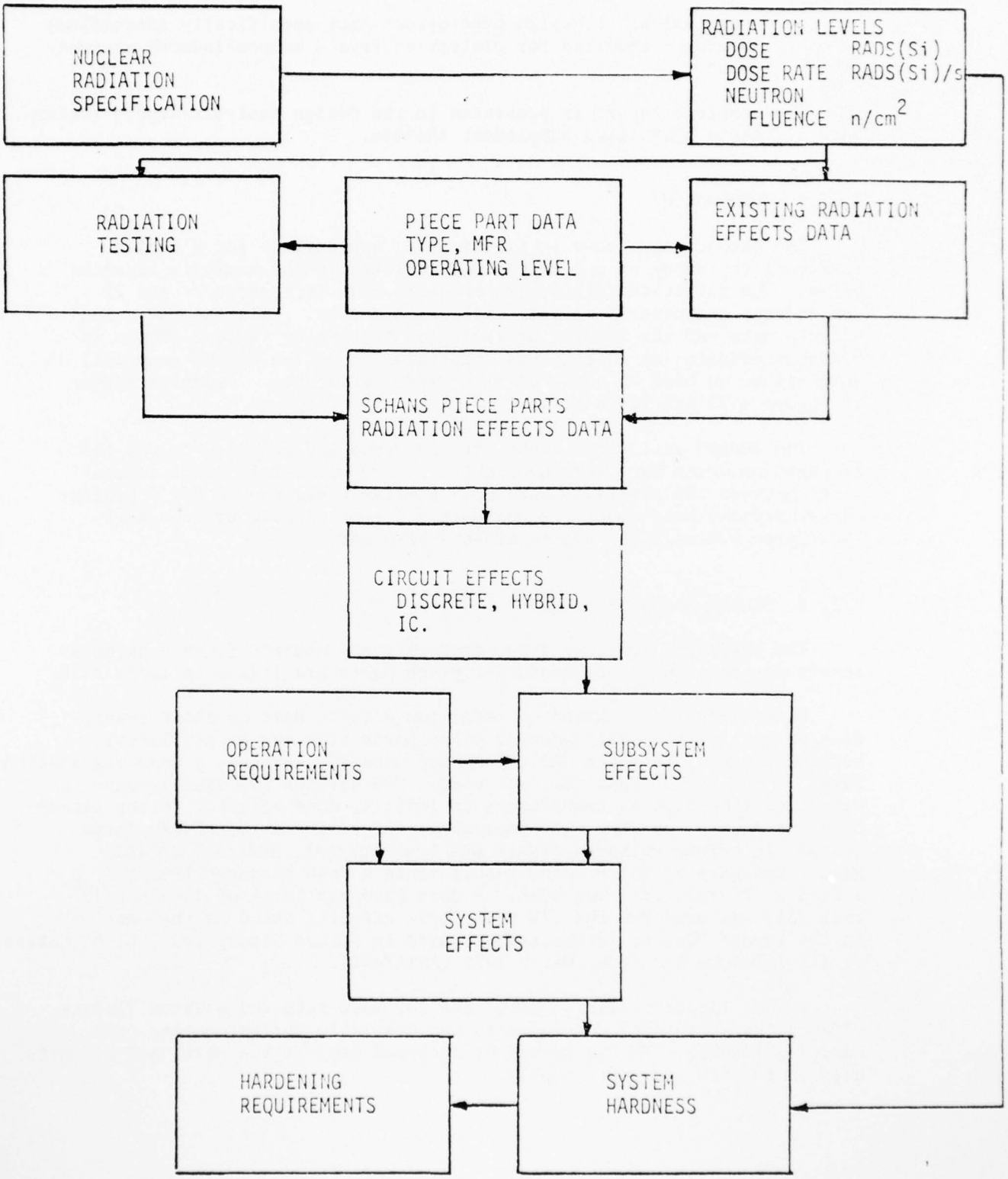


Figure 3-22. Hardness Assessment Methodology

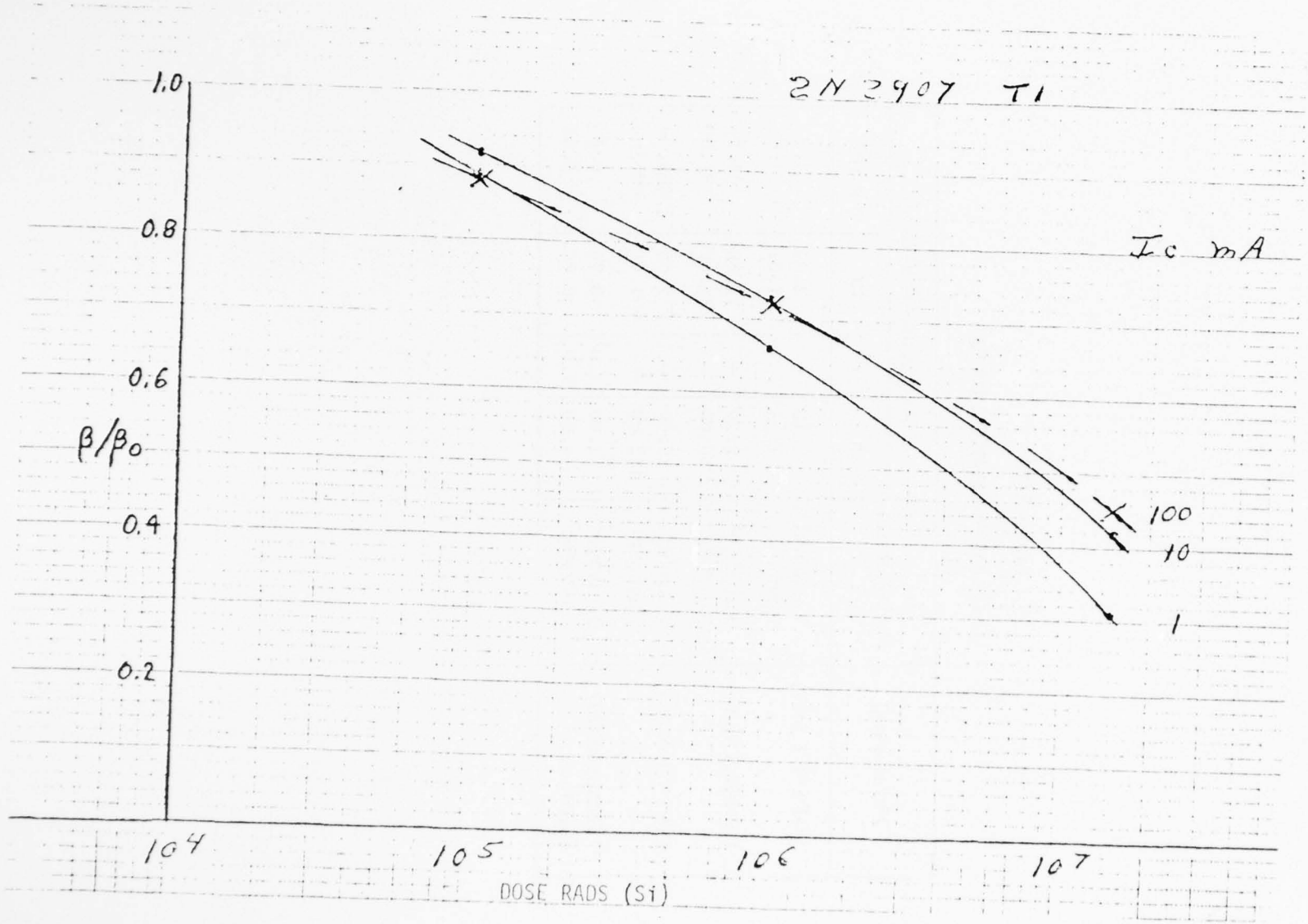


Figure 3-23. Piece Part Radiation Effects Example

Table 3-19

μA471 OP-AMP DOSE DATA

Parameter	Manufacturer	Dose Rates (rad (Si)/s)			
		0	10^5	10^6	3×10^6
VOFFSET (mV)	Fairchild	0.12	—	2.04	4.21
	Raytheon	1.24	—	1.97	1.64
IOFFSET (nA)	Fairchild	2.20	—	14.80	45.20
	Raytheon	10.00	—	34.00	34.00
INPUT IAS (nA)	Fairchild	19.60	—	712.00	1,061.00
	Raytheon	332.00	—	457.00	495.00
NORMALIZED GAIN	Fairchild	1.00	1.0	0.70	0.45
	Raytheon	1.00	1.0	0.76	0.64

Op amps used in the ILT-PCU and the power supply will malfunction for a few microseconds or more at dose rates of 10^6 to 10^7 rads (Si)/sec. In most cases, such malfunctions will have negligible effect on overall SCHANS operation. Power supply output voltages should be close to or within specifications at dose rates up to 10^8 rads (Si)/sec. Transient malfunctions in logic and memory circuits can cause significant system errors or failure unless some recovery capability is provided. Although most ICs, even those with Schottky clamp diodes, do not latch up dose rate test data for each part type from each vendor source is required at dose rates above 10^8 to 10^9 rads (Si)/sec. Burn out is usually not a problem below dose rates of 10^9 to 10^{10} rads (Si)/sec.

3.12.3 NATURAL ENVIRONMENT

Electrons and protons in the natural trapped radiation belts can cause permanent degradation of semiconductor parts from both ionizing and displacement effects. The equivalent ionizing dose in rads (Si) and the equivalent 1 meV electron fluence is dependent upon the orbit and time in intense regions of the trapped radiation belts and the shielding between the satellite surface and the semiconductor parts. For this evaluation the following assumptions were used:

- Shielding — Satellite skin: 70 mils Al
  Equipment case: 62.5 mils Al
  132.6 mils - 0.909 gm/cm^2
- Orbit
  a) Circular Synchronous: 35,966 Km
  b) MOLNIYA
     Apogee: 42,654 Km
     Perigee: 725 Km
     60^o inclination
     12-hour period

The Vette curves in Reference 22, "The Trapped Radiation Handbook", DNA 2524H, were used to estimate total dose and 1 MeV election fluence levels. Time at various altitude increments was also considered in estimating radiation levels for the MOLNIYA orbit. The radiation levels for each orbit were as follows:

Orbit	Circular Cynchronous		MOLNIYA	
Time in Orbit	1 Year	5 Years	1 Year	5 Years
Ionizing dose rads (Si)	114	570	2.3×10^5	1.15×10^6
1 MeV electrons - e/cm	3.7×10^8	1.8×10^9	6.6×10^{13}	3.3×10^{14}

The displacement damage for 3×10^{14} one-MeV electrons is approximately equivalent to a neutron fluence of 5×10^{11} to 10^{12} n/cm^2.

3.12.4 NATURAL ENVIRONMENT HARDENING

The present SCHANS design is hard to radiation levels well above those associated with the circular synchronous orbit but it would not meet the MOLNIYA orbit ionizing dose levels. Either a system design modification or additional shielding would be required to harden SCHANS to the MOLNIYA orbit dose levels. Shielding rather than redesign appears to be a better approach but the total cost and penalties of shielding should be traded off with redesign costs. An additional 1/8 inch aluminum shield would reduce the ionizing dose for the MOLNIYA orbit to approximately 5×10^4 rads (Si). Using this shielding and replacing the CA 3100T op amp with a HA 2620 op amp, a relatively easy design modification, would provide a SCHANS hardening to the MOLNIYA orbit for a 5 year mission. A more detailed shielding tradeoff study would probably provide hardness for critical parts without a full 1/8 inch additional shield on all equipment surfaces.

3.12.5 NUCLEAR ENVIRONMENT

Nuclear weapon detonations in space cause direct radiation effects and create artifical trapped radiation. The radiation associated with this threat is defined in classified document "Survivability Criteria for Representative Satellite Subsystem Development, Revised" Aerospace Document AS 7501377 (Reference 21).

Radiation levels for this environment and hardening required to meet these levels are discussed in a classified supplement to the Design Analysis Report (Reference 17).

3.12.6 HARDENING ASSESSMENT

The radiation hardness levels listed in Table 3-20 represent the best estimates that could be determined within the limited scope of this effort. The data provides a good guide to the radiation effects problems that can be expected and can be used to indicate possible hardening requirements. Before or as part of any SCHANS nuclear hardening effort a more extensive hardness assessment would be needed. Such an effort would require a detailed analysis of each section and circuit of SCHANS and possibly radiation testing of parts where inadequate radiation effects data now exists.

The following hardening would be required:

Neutron Fluence

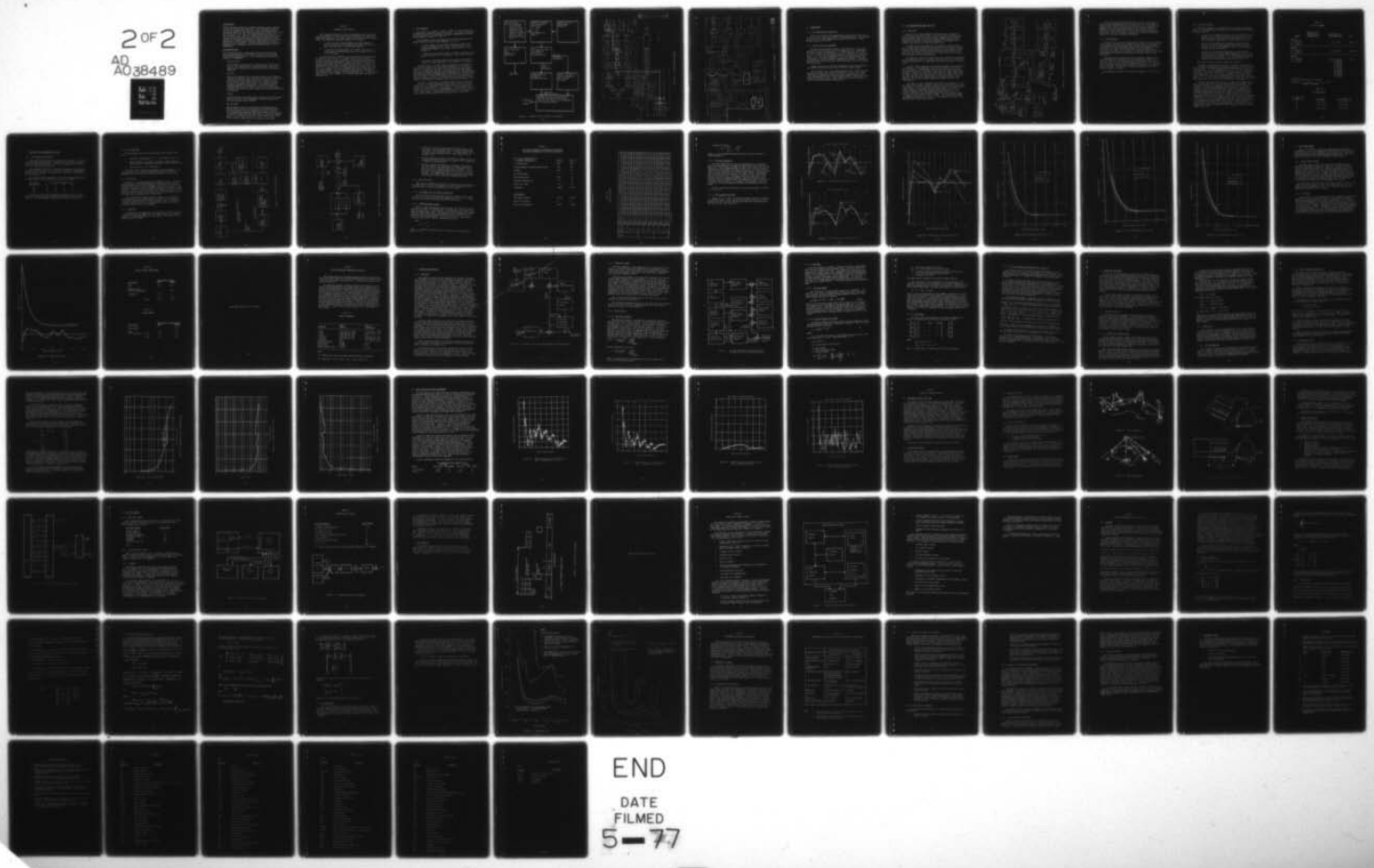
The present design should meet neutron fluence levels with no additional hardening.

Table 3-20
SCHANS ESTIMATED HARDNESS

Unit or Subunit	Dose (rad)	Dose Rate (rad (Si)/s)		Neutron Fluence (n/cm^2)
		Upset	Latchup, Burnout	
ILT	10^5	$10^6 - 10^7$	$10^8 - 10^{10}$	$10^{12} - 10^{13}$
PCU	10^5	$10^6 - 10^7$	$10^8 - 10^{10}$	$10^{12} - 10^{13}$
SPU				
I/O	10^5	$10^7 - 10^8$	$10^8 - 10^{10}$	$10^{12} - 10^{13}$
BLP-16	$10^5 - 5 \times 10^5$	$10^7 - 10^8$	$10^8 - 10^{10}$	5×10^{13}
DMCM	$5 \times 10^4 - 10^5$	$10^7 - 5 \times 10^7$	$10^8 - 10^{10}$	$10^{12} - 10^{13}$
P/S (AOU)	$10^4 - 10^5$	$5 \times 10^6 - 10^7$	$10^9 - 10^{10}$	$10^{12} - 5 \times 10^{12}$

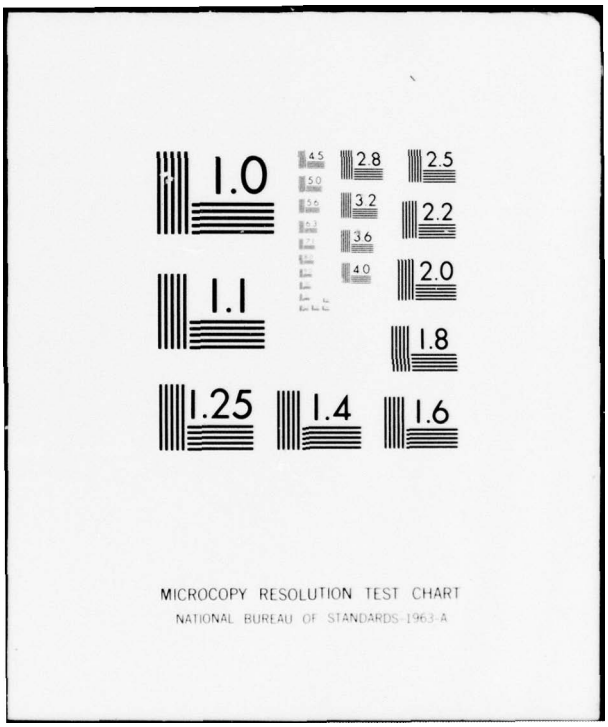
AD-A038 489 IBM FEDERAL SYSTEMS DIV OWEGO N Y F/G 17/7
SELF-CONTAINED, HIGH-ALTITUDE NAVIGATION SYSTEM STUDY: PRAIS NA--ETC(U)
JAN 77 D H ALDRICH, J W SIMMONS, N F TODA F04701-76-C-0106
UNCLASSIFIED IBM-77-D04-002S SAMSO-TR-77-57-VOL-2 NL

2 OF 2
AD
A038489



END

DATE
FILMED
5-77


1.0
1.1
1.25
1.4
1.6
1.8
2.0
2.2
2.5
2.8
3.2
3.6
4.0
4.5
5.0
5.6
MICROCOPY RESOLUTION TEST CHART
NATIONAL BUREAU OF STANDARDS-1963-A

Ionizing Dose

Without additional shielding a complete redesign would be required. It would be difficult and expensive to find and radiation qualify many of the semiconductor piece parts need to implement many of the SCHANS functions. With shielding sufficient to reduce the ionized dose to the 10^5 to 10^6 rads (Si) range hardening becomes a much more reasonable task. Many of the present parts and circuits could be used and part selection and circuit design modifications would probably be sufficient to provide the required hardness for critical applications. Some radiation testing to prove parts or circuit hardness would be required. A detailed tradeoff study of shielding approaches and of shielding versus the hardening effort is also recommended.

Ionizing Dose Rate

The ionizing dose rate is sufficiently high even with shielding that transient malfunctions of most all circuits will occur and latch-up and burnout can occur. The following dose rate hardening approach is recommended.

- Dose Rate Upset

  Circumvention - allows a halt in operation and a restart capability. This would require a dose rate detector, some hard memory such as plated wire or possibly MNOS and a reinitialize capability.

- Latch-Up

  Latch-up prescreening of all junction isolated (JI) monolithic circuits is required. Only JI circuits are now used. Dielectric isolated (DI) ICs would not require this screening testing but it would be very difficult and costly to get DI versions of some of the SCHANS circuit types. An alternate latch-up hardening approach is recommended. The dose rate detector circuitry could be used to force turn off of all power supply voltages for a period of time to assure that no latch-up conditions are sustained.

- Burnout

  Current limiting in the power supply circuitry and in the voltage buses to circuits will be required to eliminate burnout from the high dose rate levels expected.

- EMP and SGEMP

  EMP and SGEMP can cause circuit upsets and possible device burnout and will have to be addressed in any hardening effort. The total satellite system configuration as well as details of any SCHANS subsystem layout and interconnections are required to properly evaluate EMP and SGEMP effects. Since this detailed data is not now known and because of the limited scope of this effort no EMP or SGEMP hardness assessment was performed.

Section 4

LABORATORY TESTS (TASK 2)

This section describes the results of laboratory tests of certain critical components to verify that the ILT-PCU design will achieve the performance needed for the system to meet its specified accuracy requirements. The breadboard equipments tested were as follows:

- A "Time-of-Arrival Counter/Buffer" (TOA Counter/Buffer or TC/B), consisting of a 32-stage binary counter driven by a 60 MHz clock source and a 32-bit buffer register.

- A "Precision Time Measurement Unit" (PTMU), consisting of a single-channel superheterodyne receiver operating in the 2.5 to 2.9 GHz range.

The objective of the PTMU tests was to measure delays between time of receipt of an RF pulse at the antenna and the time at which a resulting video pulse crosses a threshold. By collection and analysis of several thousand such measurements, statistical data were derived for TOA delay bias (mean) and jitter (standard deviation) as a function of temperature, received signal strength, and input pulse rise time. The objective of the TC/B tests was determination of the counter error rate (i.e., the frequency with which erroneous pulse counts, equivalent to TOA, were recorded). The test setups and procedures are described in the "SCHANS Critical Component Test Plan" (Reference 18). A more detailed report of task results appears in the "SCHANS Laboratory Test Report" (Reference 19).

4.1 TEST CONCEPTS

The overall test concept is shown in Figure 4-1, which depicts the interdependencies among the various activities. The critical components listed in the upper left hand block, that were breadboarded and tested, are highlighted in Figures 4-2 and 4-3.

The breadboard circuit designated Precision Time Measurement Unit (PTMU) consists of the following components in series:

- A single channel receiver (RCVR) consisting of the RF Calibrator, RF bandpass filter, mixer, IF switch (SPST), an IF preamplifier/bandpass filter and a power divider as shown in Figure 4-2.
- A Compensated Log Amplifier (CLA), as shown in the upper right corner of Figure 4-2. Its operation is discussed in Section 3.
- An Automatic Threshold Detector (ATD), lower left corner of Figure 4-3, whose operation is also summarized in Section 3.

The PTMU tests used a Radar Signal Simulator and a programmable time interval counter. The time interval measured is that between arrival of a simulated radar pulse at the RF Calibrator and the generation of a TOA pulse by the ATD. Several thousand such measurements were made at different temperatures and signal levels. The measurements were analyzed using a Chi Square test to determine that the error distribution is normal. After verification of the statistical distribution, mean and standard deviation of the PTMU data were collected for use as inputs to the simulation program for system performance demonstration.

The TC/B is highlighted at the bottom left center of Figure 4-3. It contains a 32-stage synchronous binary counter driven by a 60 MHz clock. When it is supplied a "TOA Strobe" from the ATD, the counter content is transferred to a 32-bit register. The raw quantitization error in the 32-bit TOA tag is approximately 8.3 nanoseconds (4.8 ns 1σ) for a single reading. The purpose of the TC/B test is to measure the rate at which errors greater than the quantitization error occur.

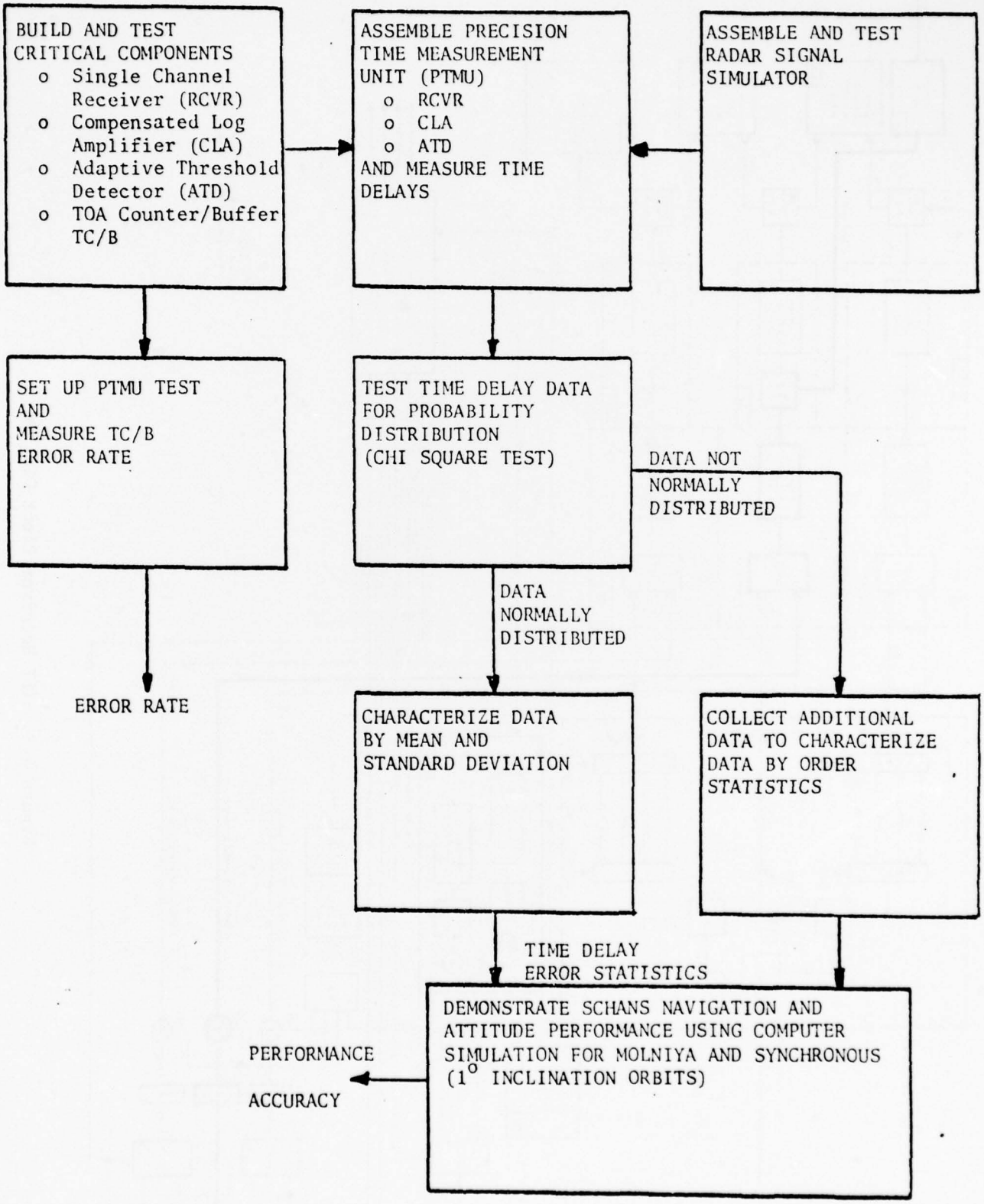


Figure 4-1. SCHANS Critical Component Test Concept

BEST AVAILABLE COPY

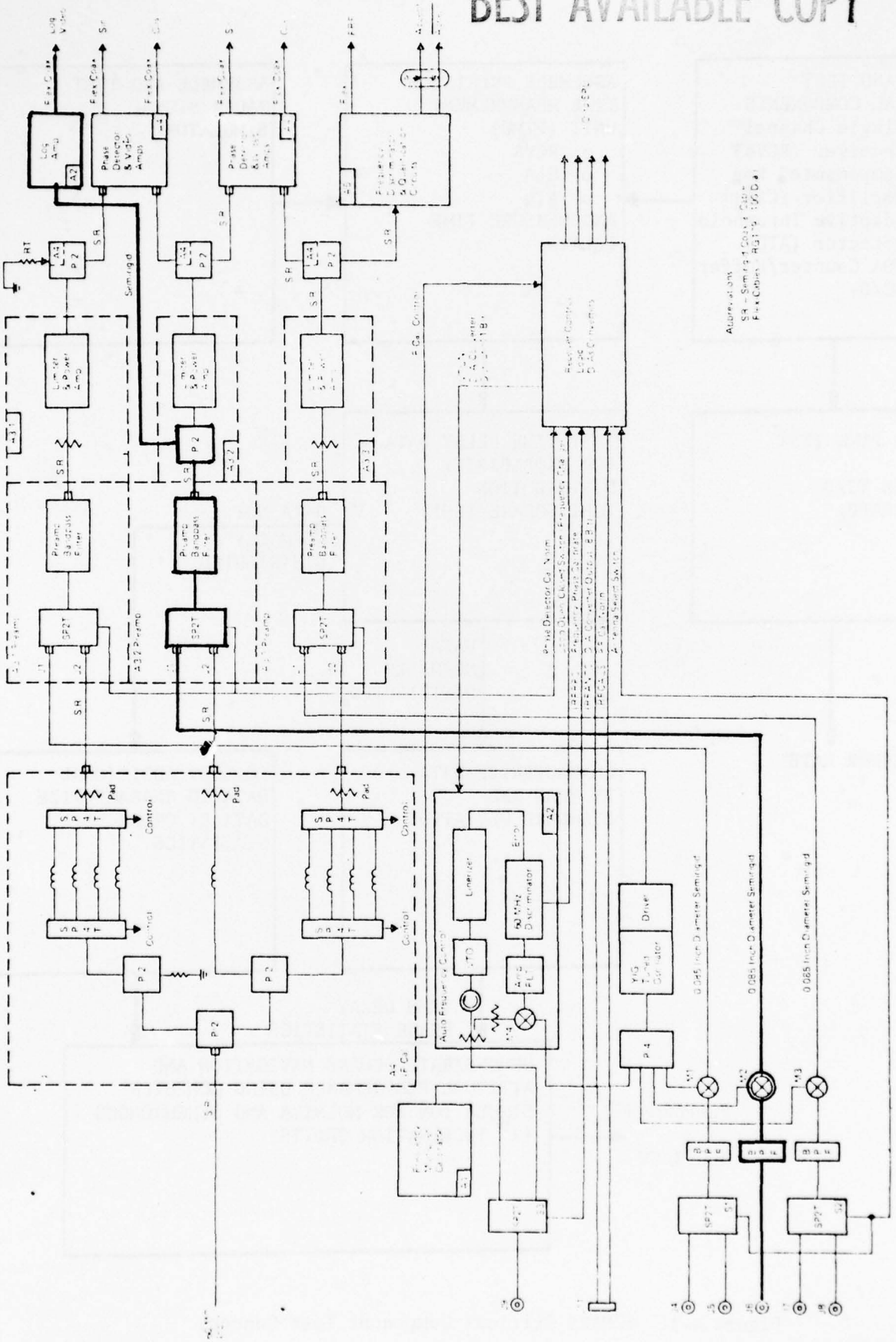


Figure 4-2. ILT Receiver Block Diagram

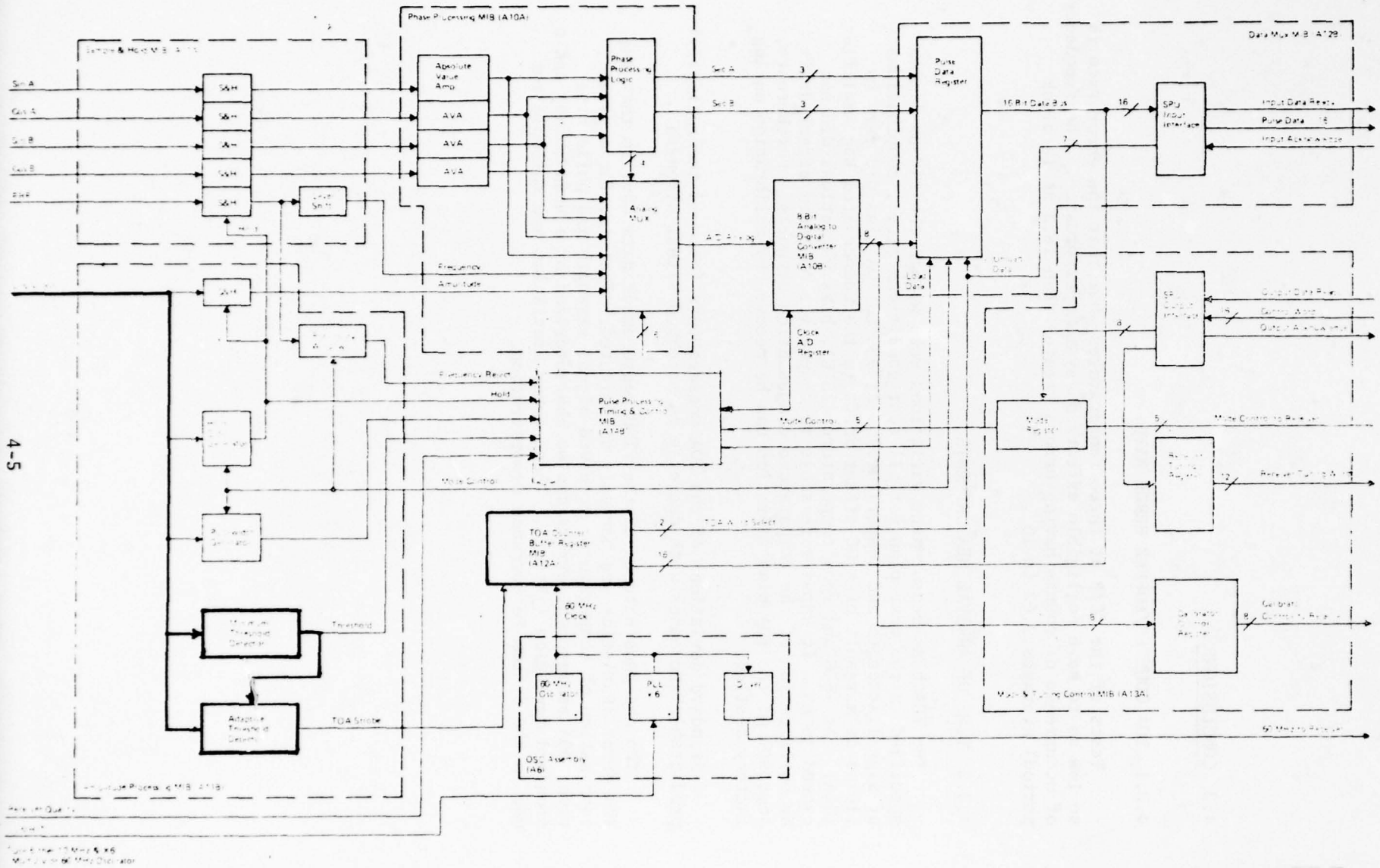


Figure 4-3. PCU Block Diagram

BEST AVAILABLE COPY

4.2 CONCLUSIONS

4.2.1 TOA COUNTER/BUFFER ERROR RATE

Tests of the TC/B at three temperatures show that the error rate is so low as to have negligible effects on system performance. The frequency of occurrence of counts having errors greater than ±8.3 ns (½ clock period) averages 2.62 in 10^6.

4.2.2 TIME OF ARRIVAL MEASUREMENTS

The TOA bias measurement variations were within the ±10 ns limits specified in the test plan for all test conditions (i.e., combinations of signal strength and temperature). At +80°C, TOA bias did vary by ±10 ns as a result of a DC offset drift in the Compensated Log Amplifier (CLA). At -5°C and room temperature (25°C), bias variations did not exceed ±6 ns. It appears feasible to reduce the observed offset drift by optimization of the temperature compensation networks. Furthermore, some 80% of the TOA bias variation can be removed by calibration during factory testing.

Standard deviations of the TOA measurements followed theoretically-predictable increases with decrease in received signal strength.

Two chi-square tests of the PTMU measurement data confirm that the TOA error statistics are normally distributed. That is, for a given combination of temperature, received signal strength and pulse rise time, TOA measurement errors can be characterized by a mean (bias) and a standard deviation (jitter). These error statistics are suitable for use in the System Performance Demonstration.

4.3 TOA COUNTER/BUFFER ERROR RATE TEST

4.3.1 TEST SETUP

Figure 4-4 is a block diagram of the test setup. The portion tested is within the dashed block. Except for the power supplies and a pulse generator (which are commercial test equipment) and the 60 MHz clock generator (which is the same reference module designed for the receiver) all the test circuitry was assembled in one chassis from standard logic modules and electrical piece parts.

In operation the pulse generator (TI Model 6613) entered pulses into an eight-stage register that generated pulses of the same characteristics as the ATD will produce in the ILT-PCU. The TOA1 pulse is taken from the first stage of the register and the TOA2 pulse from the last. Since the delay register clock rate is 12.5 MHz, the delay time between the two pulses will be 560 nanoseconds.

The TOA1 pulse causes the "TOA Strobe" to be generated, transferring the TOA counter content to its buffer, from which it will be transferred to the TOA1 Register by the "LOAD TOA1" pulse from the Timing and Control logic.

The TOA 2 pulse causes the new TOA counter reading to be transferred to the buffer. The complements of the TOA1 registers are supplied to the 32-bit adder. The TOA buffer state is also supplied to the adder. The resultant output of the adder is the difference (ΔTOA) between TOA2 and TOA1. Ideally, the ΔTOA result remaining in the adder should always be within one LSB of the register delay. After the registers and gates have had time to reach a steady state, the timing and control logic generates the TOA strobe, which transfers the adder content to the ΔTOA register.

The eight (8) least significant bits (LSB's) are displayed to show the actual ΔTOA visually (in binary form); up to 4266.66 ns of delay can be displayed. An "error window" is defined by the "error window compare" logic, which is set by upper and lower limit switches to prevent a selected number of ΔTOA values from being counted as errors. This provides flexibility for investigating possible trouble sources if initial error rate readings should be high. The "error window compare" is capable of limiting up to 8 bits of ΔTOA. The remaining bits from the adder should always be zeroes. If a one appears in any of the (24) MSB positions, an error has occurred.

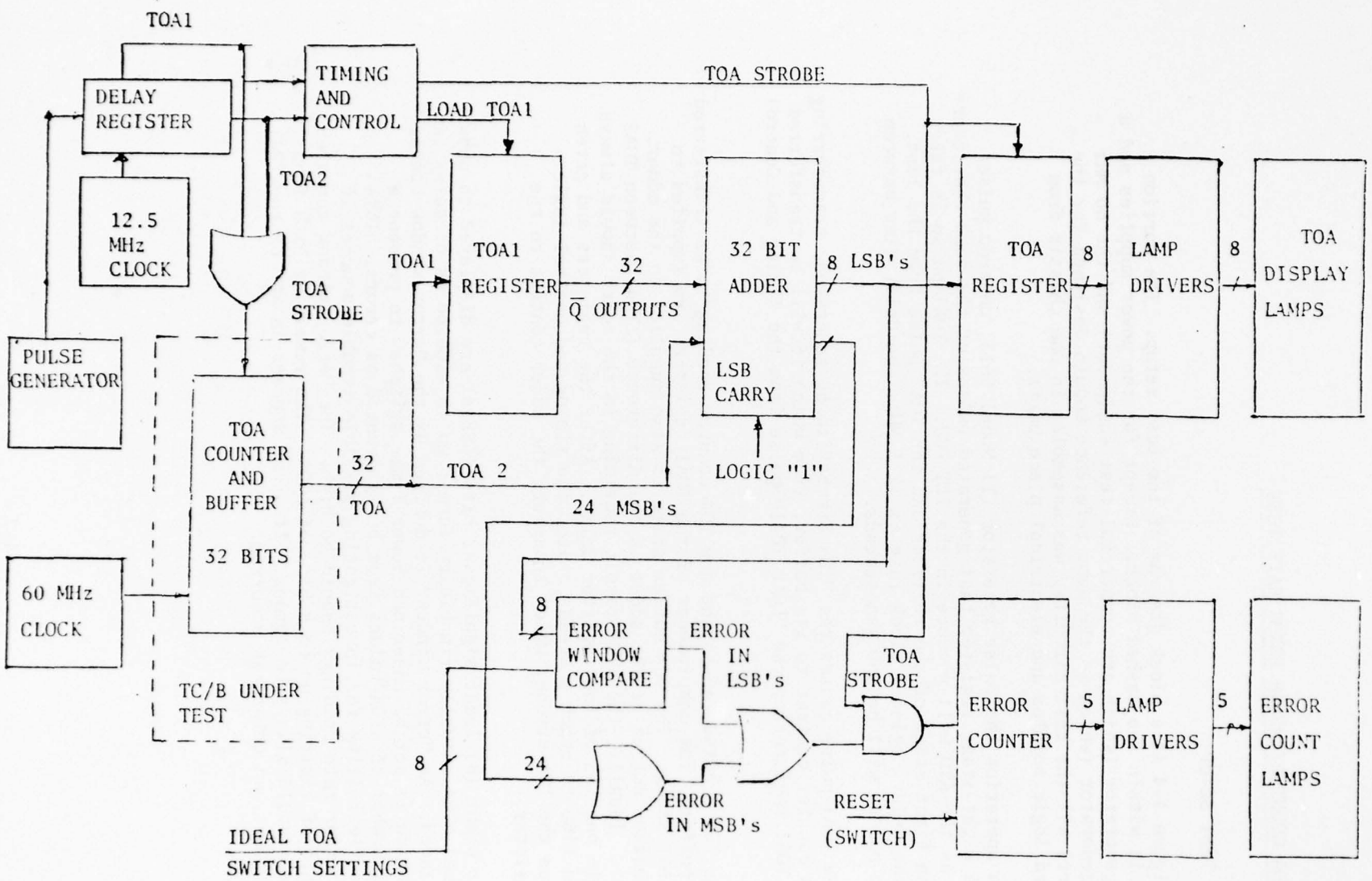


Figure 4-4. TOA Counter/Buffer Test Concept

The register delay chosen for the test is 560 ns. Since the ATD pulses are not synchronous with the 60 MHz clock, the ΔTOA reading (without error) should always show a count of 33 or 34. The ΔTOA lamps (again without error) will always show a binary count of 00100010 or 00100001. If the error window switches are set to those values, the window will prevent either 01 or 10 in the two LSB's from causing an error count. Any errors larger or smaller will result in an LSB error being sent to the error counter and displayed.

4.3.2 TEST PROCEDURE

With the test setup (as described above) operable, the test procedure simply requires that the error counter be reset, the pulse generator set to an appropriate pulse repetition rate, and the error count allowed to accumulate until some large number of pulses has been generated. The test setup was allowed to run continuously (even unattended during second and third shifts) for as long as is required. Error count readings were observed and recorded several times on the first shift of each working day.

Although the pulse repetition rate of prospective landmark radars is in the order of a few hundred to a few thousand per second, the pulses for the TC/B test can be generated at much higher rates without loss of validity. Even if the pulse repetition rate is 2×10^5 pps, the five microseconds between pulses is more than adequate for all measurements to be made. At that rate, the errors occurring in 10^{11} trials could be counted in six days.

Measurements were made at room ambient temperature, at 75°C and at -5°C.

4.3.3 TC/B TEST RESULTS

Tests were performed in accordance with the procedures described above. At each temperature tests were run at each of three error window settings as follows:

- In test #1 the acceptable window as set at 00100000 (32) and 00100011 (35). The test was run for the required time and 19 ΔTOA measurements were observed outside these limits. The ΔTOA measurements were made at a 200 KHz rate for 6 days.

- For test #2 the window was increased to a lower bound of 00011111 (31) and an upper bound of 00100100 (36). After running the test for the required time no ΔTOA measurements occurred outside these limits.

- For test #3 the window was decreased to a lower bound of 00100001 (33) and an upper bound of 00100010 (34) and it was observed that on an average 32 ΔTOA measurements were outside the window every 61 seconds. At a ΔTOA measurement rate of 200 KHz this corresponds to an error rate of 2.62×10^{-6}.

The results of these tests are summarized in Table 4-1.

The errors falling outside the limits of the least significant bit (i.e., 00100001 and 00100010) are apparently caused by noise on the TOA-2 trigger pulse. If the trigger noise is assumed Gaussian, then the error rate of 2.62×10^{-6} corresponds to $4.7\ \sigma$. For a least significant bit error of ±8.33 nanoseconds (1σ), a 4.7σ value implies a jitter of ±1.77 nanoseconds (ns). This jitter, combined with an oscilloscope jitter of ±1.1 ns, results in an expected jitter in the TOA-2 trigger pulse of 4.2 ns. Oscilloscope trace photographs confirm that the observed error rate could be due to noise on the TOA-2 test equipment pulse.

The TOA counter/buffer was placed in a temperature chamber with the test circuitry and delay circuitry mounted outside the chamber. This was done to eliminate any temperature effects of the test or delay circuits. At room temperature the time to observe 32 ΔTOA readings outside the upper bound of 00100010 and lower bound of 00100001 was recorded and the average time was 40.5 seconds. Two hundred thousand (200,000) measurements were made each second, hence the error rate is $32 \div 40.5 \times 200 \times 10^{3}$ or 3.96×10^{-6}. The tests were rerun at the temperature extremes of the commercial grade logic used in the breadboard ($0^{o}C$ and $70^{o}C$). At $0^{o}C$ the average time was 29.7 seconds and at $70^{o}C$ the average time was 44 seconds. Thus the error rates and contributions to the SCHANS error budget (ERX 16.67 ns) are as shown in Table 4-2. The increase in error rate at room temperature is attributed to noise pickup on the long lines between the test circuits and the TOA counter/buffer in the oven.

Table 4-1

TOA TEST SUMMARY

Window	Number of TOA Measurements Outside Window	Total Number of TOA Measurements	Date
Test #1 LB = 00100000 UB = 00100011	19	1.04×10^{11}	08/10 - 19
Test #2 LB = 00011111 UB = 00100100	0	0.915×10^{11}	08/24 - 30
Test #3 LB = 00100001 UB = 00100010	32	Every 60 seconds 59 seconds 59 seconds 61 seconds 75 seconds 72 seconds 68 seconds 61 seconds 58 seconds 47 seconds 52 seconds	08/31

Average of 32 errors each 61 seconds

$$\text{Error Rate} = \frac{32}{200 \text{ kHz} \times 61 \text{ seconds}} = 2.62 \times 10^{-6}$$

Table 4-2

TC/B ERROR RATES

Test Temperature (^{o}C)	Error Rate	Error Budget (ns)
0	5.38×10^{-6}	8.97×10^{-5}
25	3.96×10^{-6}	6.60×10^{-5}
70	3.64×10^{-6}	6.07×10^{-5}

4.4 PRECISION TIME MEASUREMENT UNIT TEST

4.4.1 TEST PREMISES AND CRITERIA

Three input pulse envelope rise times were to be used: 10, 140 and 200 nanoseconds (approximately). The envelope rise times at the ATD input were expected to be 233, 277 and 307 ns respectively (see reference 1 for supporting calculations).

The measurement time mean is expected to change most as a function of input pulse rise time, but it will also be affected by temperature and input signal strength. Variations due to the latter are expected to be less than ±10 ns.

The expected random timing errors (in ns) for several combinations of signal-to-noise ratio and pulse rise time are as follows:

Input Pulse	Signal-to-Noise Ratio (dB)			
Rise Time, ns	16	20	30	40
10	26	17	7	5
140	30	20	8	5
200	34	22	8	5

The entries in this table have been corrected for the 1σ timing error of 4.8 ns that will be introduced by using the TOA pulse to gate a stop pulse to the programmable counter from a 60 MHz clock source.

4.4.2 TEST CONDITIONS

PTMU measurement data were collected under the following conditions.

- Temperature (approximate, ^{o}C): -5, Room Ambient (+20), +75
- Signal strength: from -80 to -25 dBm in 5 dBm increments. Some additional measurements were taken at other signal levels
- Pulse rise time: 10, 125 and 200 ns

The radar signal simulator was operated at room temperature. The minor departure of the actual tests from the plan with respect to temperature and rise time do not affect the validity of the results.

4.4.3 TEST SET-UP

Figure 4-5 is a block diagram of the PTMU test set-up. The Radar Signal Simulator, described functionally in Reference 18, provides a simulated radar pulse to the RF Calibrator input and at the same time provides a start pulse to the Programmable Time Interval Counter. When the Adaptive Threshold Detector produces a TOA pulse resulting from that signal, it is used to gate a pulse from the 60 MHz clock source to stop the time interval counter, which records the interval between receipt of the input pulse and generation of the TOA pulse.

The simulator block diagram appears in Figure 4-6. The filters allow manual selection of three pulse rise times, and the variable attenuators allow adjustment of received signal level. The threshold detector minimizes jitter in the start pulse and reduces delay time variation as pulse rise time is changed.

4.4.4 OPERATION

Although the actual radar PRI's are expected to be of the order of a few milliseconds, the PTMU tests used a much shorter PRI in order to acquire the needed measurements in a short time. The sequence of test operations was as follows:

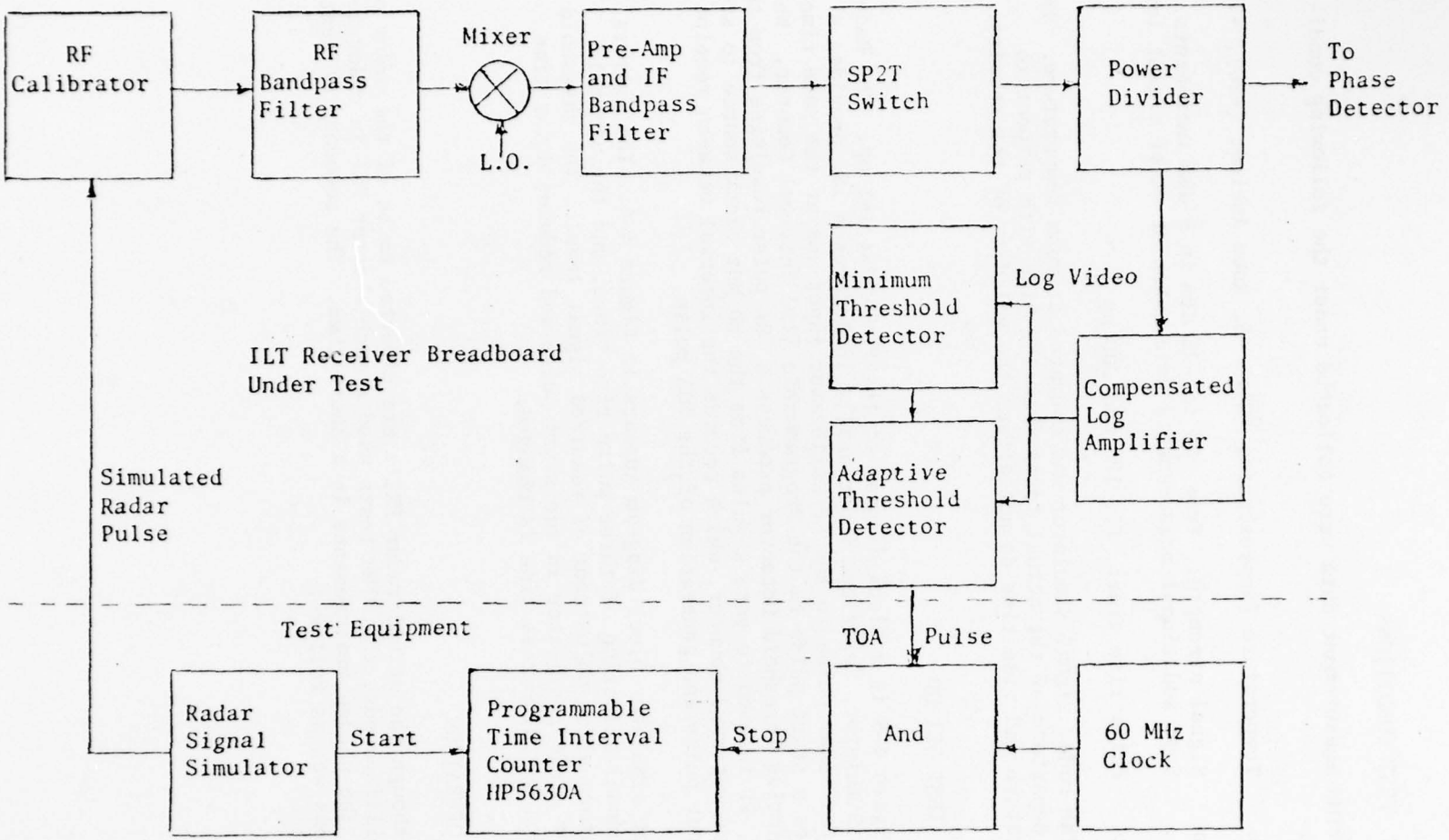


Figure 4-5. PTMU Test Block Diagram

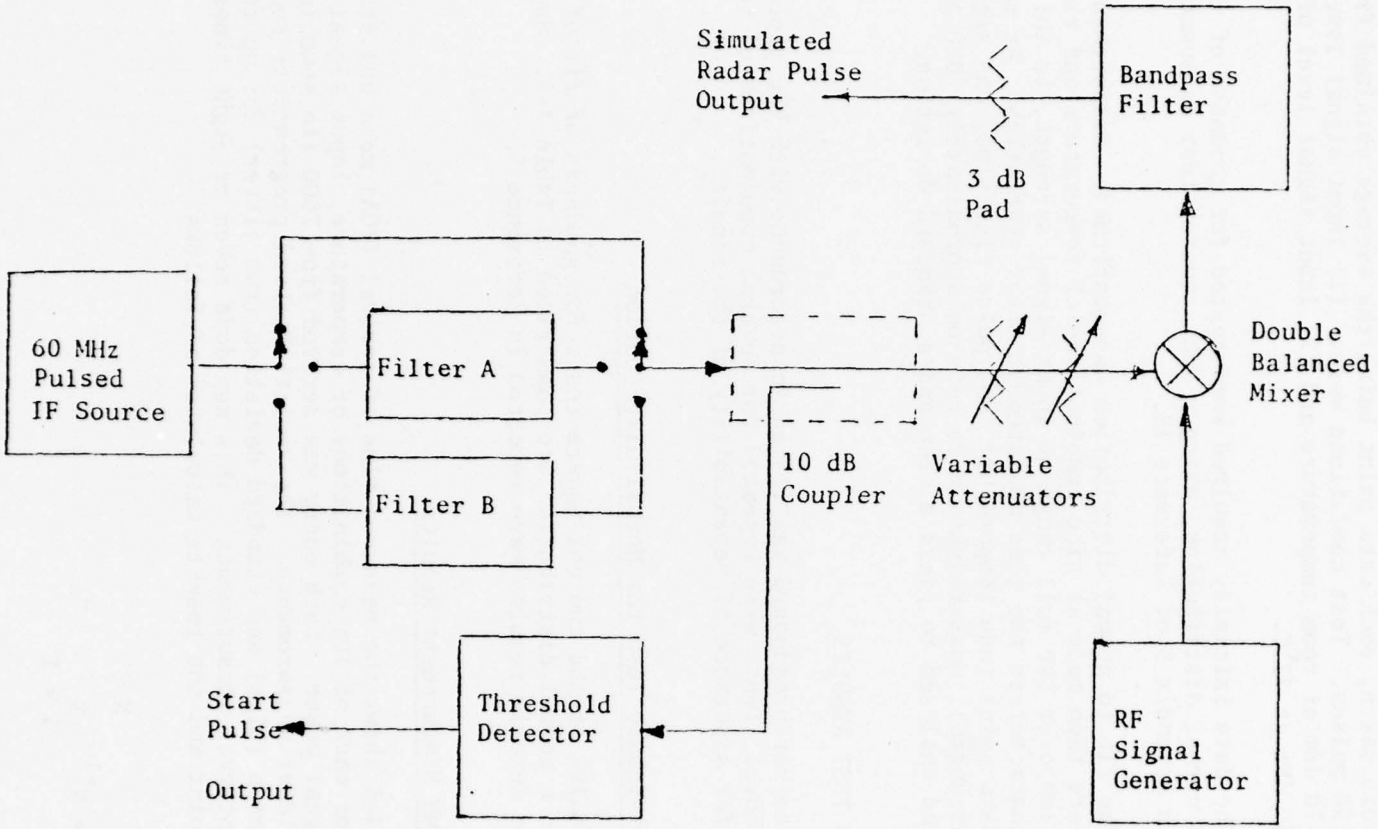


Figure 4-6. Radar Signal Simulator Block Diagram

1) Initially, two sets of approximately 1000 data points each were taken, each data point being the average obtained from 100 pulses. Test conditions were: (1) input signal level of -70 dBm at room temperature and (2) input signal level of -30 dBm at 77°C.

2) The data initially acquired were tested for goodness of fit to a normal distribution, using a "chi-square" test as summarized in Appendix B of Reference 18.

3) The fit to normal distribution was confirmed. Measurements were then made at nine combinations of temperature and rise time over the full range of input signal strength, to fully characterize the time measurement error statistics. At each data point (one temperature, one pulse rise time, one signal strength), measurements were made on approximately 7000 pulses and analyzed to yield a mean and a standard deviation.

4.4.5 PTMU TEST RESULTS

The receiver breadboard was tested in accordance with the procedures described above. Tests were repeated for several combinations of test conditions for assurance of repeatability of the results.

4.4.5.1 Chi-Square Test for Normal Distribution

The results of the two chi-square tests for goodness of fit of the test data to a normal distribution are summarized in Table 4-3. Supporting data and interim results were reported in Reference 5.

4.4.5.2 PTMU Measurement Results

Table 4-4 shows the measured time of arrival (TOA) mean and standard deviation for each of 108 combinations of temperature, input signal rise time and signal power. Each entry was derived from 7000 (in some instances 8000) individual measurements. The Hewlett-Packard programmable counter calculates mean (bias) and standard deviation (rms jitter) for up to 1000 time interval measurements. This was done seven or eight times at each data point and the results calculated as follows:

Mean:

$$\mu = N^{-1} \sum_{i=1}^{N} \mu_i$$

where μ_i is the mean calculated for the ith group of 1000 measurements and N = 7 or 8.

Table 4-3

PTMU DATA STATISTICAL DISTRIBUTION TEST RESULTS
(CHI-SQUARE GOODNESS OF FIT TEST FOR NORMALITY)

Test Signal Characteristics (Input to Receiver)	Test #1	Test #2
# of Data Points	1004	1000
TOA Measurements Averaged per Data Point	100	100
RF (MHz)	2620	2750
PW (Microseconds)	6	6
PRI (Microseconds)	1000	200
Risetime (Nanoseconds)	12	12
Power Level (dBm)	-70	-30
Temperature	$+68^{o}F$	$+171^{o}F$
Test Results		
Chi-Square Statistic	14.236	11.428
Degrees of Freedom	27	45
Level of Significance	0.975	0.995

Table 4-4

PTMU TEST RESULTS

T °C	Rise Time, ns	Statistical Parameter	Input Signal Power, dBm											
			-80	-75	-70	-65	-60	-55	-50	-45	-40	-35	-30	-25
-5	10	Mean	717.9	724.2	723.8	722.3	717.7	714.5	723.9	720.8	723.6	721.9	717.4	719.1
		S.D.	22.5	11.96	7.47	5.62	4.63	4.4	4.31	4.29	4.33	4.26	4.3	4.23
	125	Mean	713.5	722.3	723.4	722.4	718.2	715.5	724.5	719.6	721.3	718.5	713.5	713.8
		S.D.	32.1	16.9	10.03	6.64	5.27	4.50	4.42	4.32	4.36	4.21	4.26	4.33
	200	Mean	713.0	719.0	719.3	718.9	714.1	710.6	720.9	715.4	718.0	714.4	709.4	712.9
		S.D.	29.9	15.2	9.36	6.45	5.11	4.51	4.44	4.39	4.35	4.33	4.37	4.53
20	10	Mean	725.6	730.3	730.2	729.6	726.6	723.4	731.2	728.7	732	728.9	723.2	724.8
		S.D.	24.3	12.6	7.76	5.66	4.68	4.36	4.4	4.33	4.26	4.28	4.32	4.39
	125	Mean	719.8	728.3	728.5	728.9	727.2	723.8	733.2	728.9	731.8	728.5	723.6	725.2
		S.D.	31	16.21	9.8	6.57	5.23	4.66	4.49	4.39	4.37	4.39	4.39	4.52
	200	Mean	724.3	729.9	730	730.9	728.9	723.4	735.1	729.8	733.3	729.6	724.8	729
		S.D.	31	15.7	9.63	6.8	5.4	4.94	4.64	4.57	4.54	4.54	4.49	4.63
75	10	Mean	714.1	731.8	728.6	727.0	724.2	718.2	720.7	719	722.1	720.7	715.9	711.1
		S.D.	32	13.9	8.57	5.8	4.84	4.44	4.36	4.39	4.5	4.49	4.52	4.42
	125	Mean	702.7	729.7	726.9	726	724.3	718.7	724.0	724	729	728.5	724.8	721.6
		S.D.	36.3	17	10.3	6.62	5.19	4.62	4.46	4.39	4.43	4.41	4.4	4.41
	200	Mean	712	730.5	727.2	727.8	728.1	723.1	730.2	728	734.1	733	728.6	726.4
		S.D.	38	18.9	11.2	7.17	5.63	4.87	4.64	4.57	4.54	4.54	4.49	4.63

T = Temperature

S.D. = Standard Deviation

Standard Deviation:

$$\sigma = N^{-0.5} \left[\sum_{i=1}^{N} \sigma_i^2 \right]^{0.5}$$

where σ_i is the standard deviation calculated for the ith group of 1000 measurements.

4.4.5.3 TOA Bias Variations

For each combination of rise time and temperature, an "average mean" was calculated over the range of signal powers (one "Mean" row in Table 4-4). The difference between the mean at each data point and the "average mean" was termed "deviation of the mean". In actual application, this deviation would be calibrated during factory testing, and the results of the calibration used in the flight software. Approximately 80% of the deviation could thereby be removed, and the remaining 20% used as error statistics. Knowledge of received signal power (from landmark location, estimated spacecraft location and emitter power), rise time (from the landmark table) and temperature (from a calculation of whether the spacecraft is in sunlight or earth shadow) permit the program to select the appropriate residual TOA measurement error parameters.

Plots of uncalibrated deviations of the mean TOA appear in Figures 4-7, 4-8 and 4-9.

4.4.5.4 TOA Standard Deviations

Figures 4-10, 4-11 and 4-12 show TOA standard deviations following the expected trends. Note: these data include the effect of the TOA Counter LSB error since the TOA pulse from the ATD is inhibited by the TOA Counter Clock (see Figure 4-5).

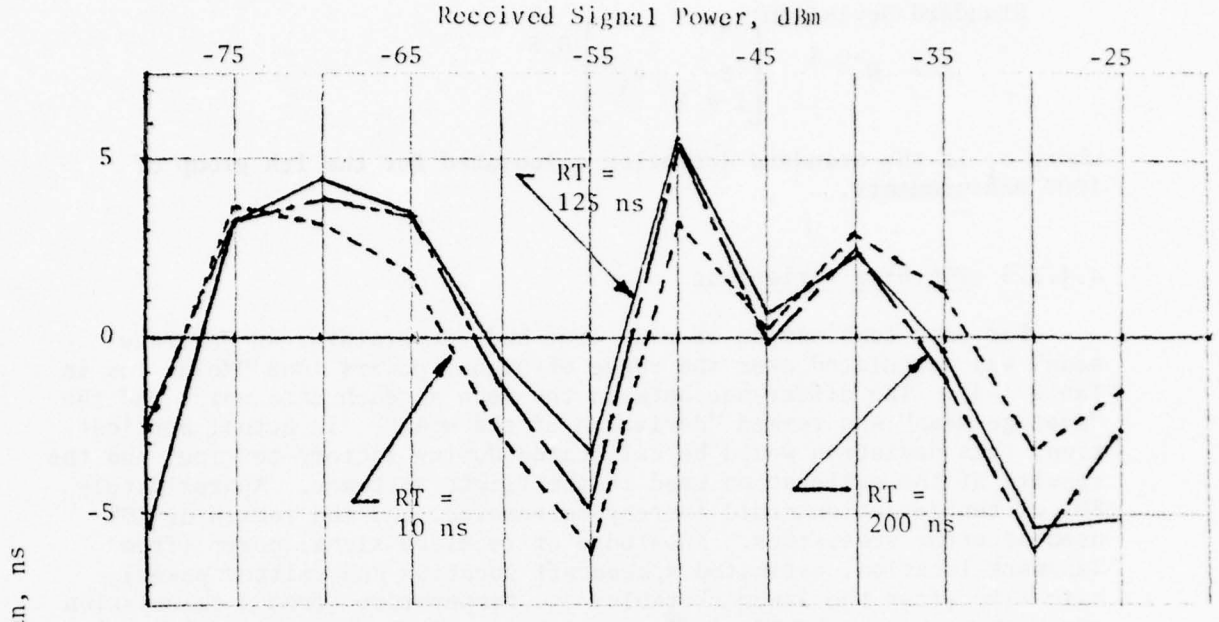


Figure 4-7. TOA Deviation of the Mean at -5°C

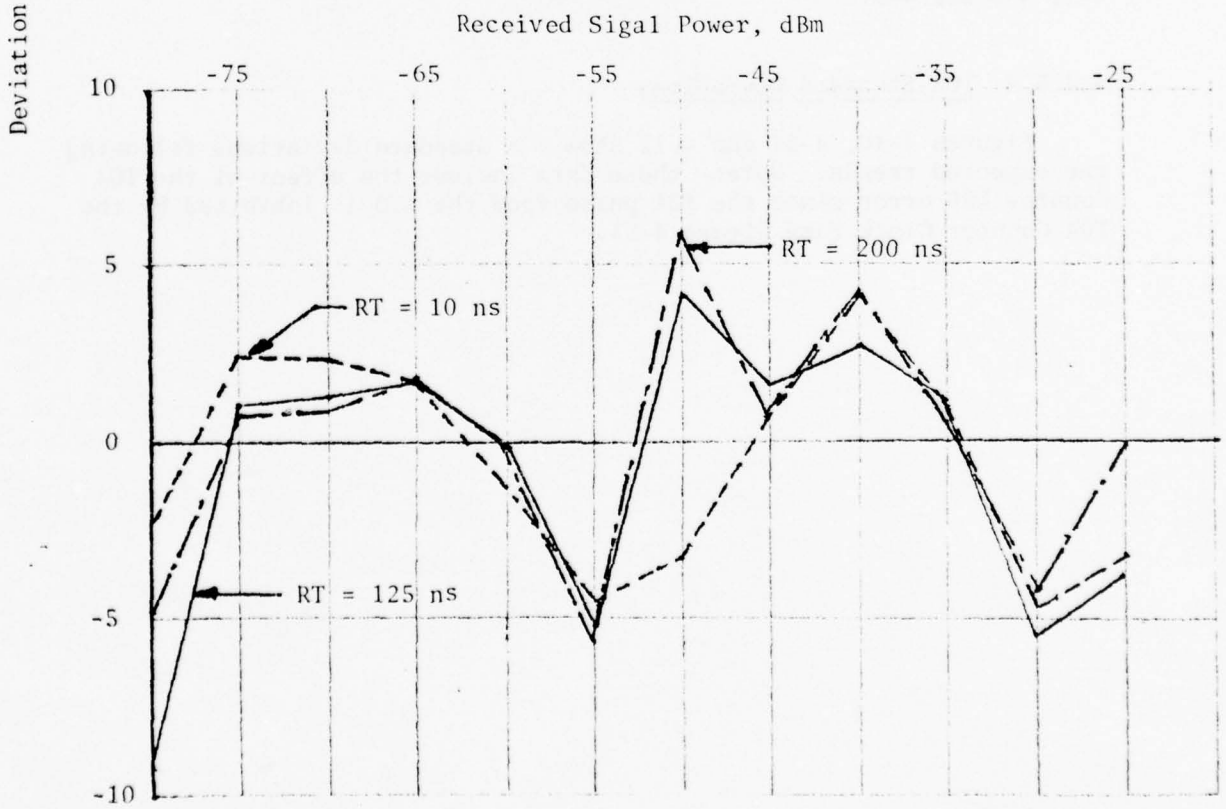


Figure 4-8. TOA Deviation of the Mean at 20°C

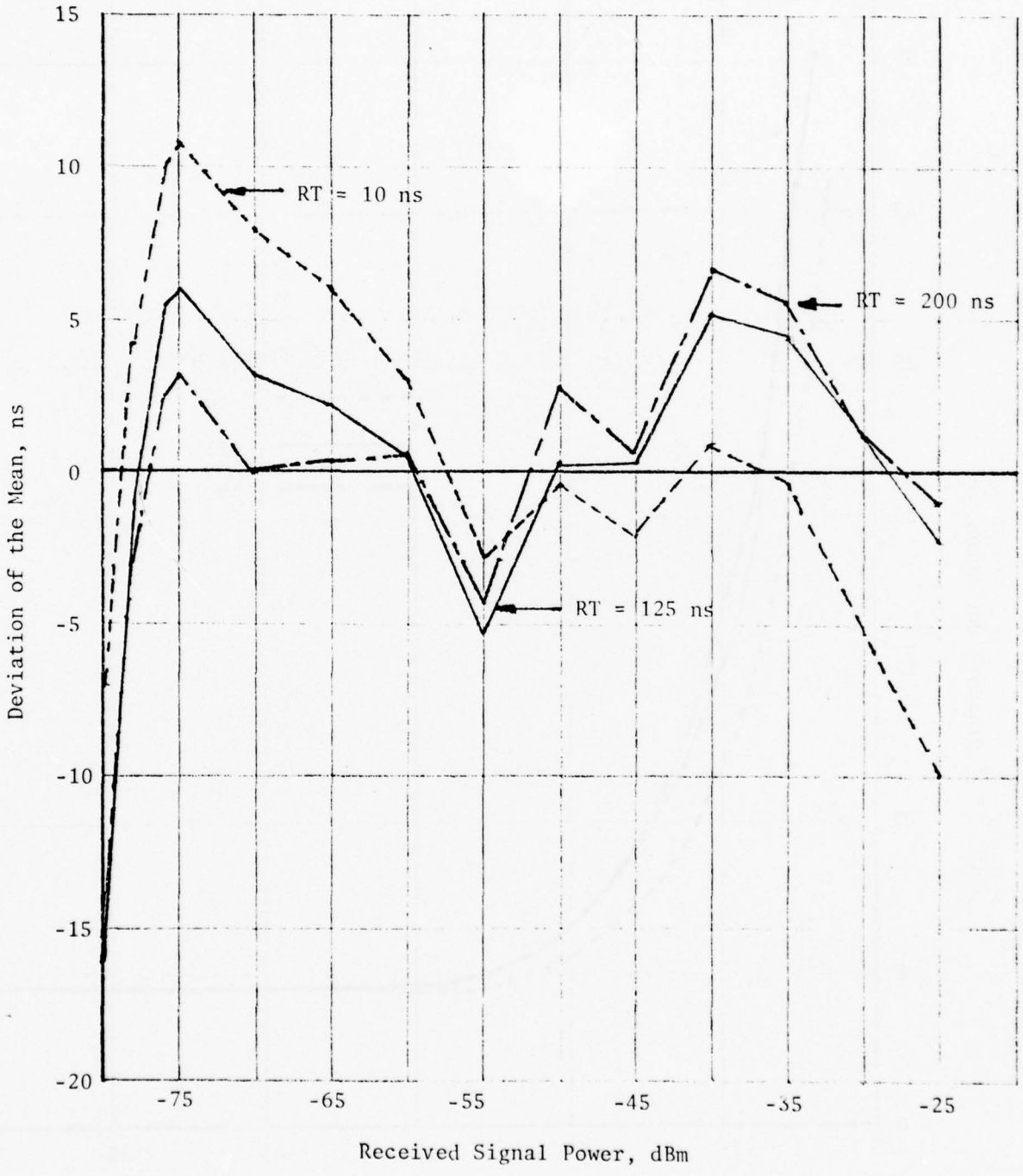


Figure 4-9. TOA Deviation from the Mean at 75°C

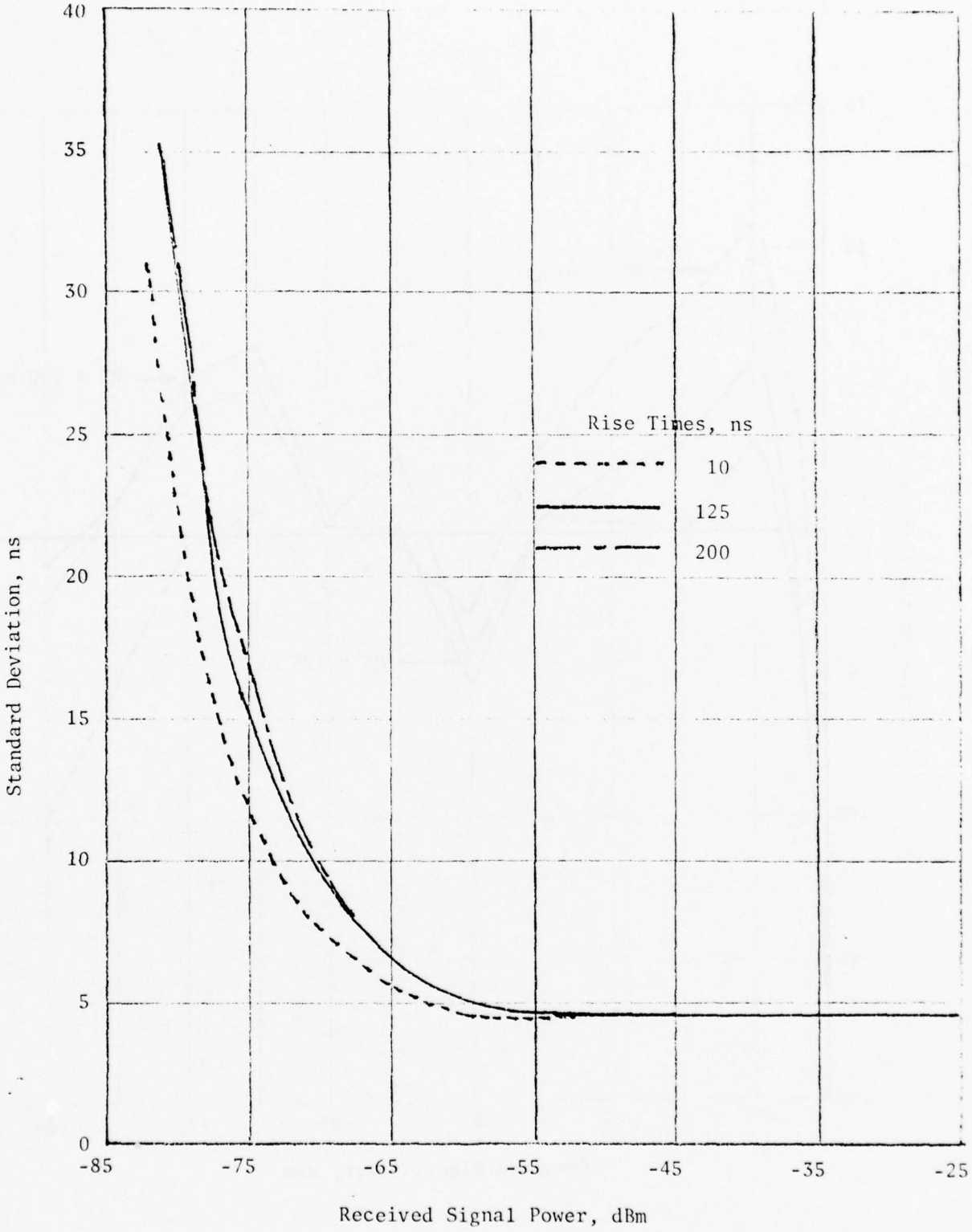


Figure 4-10. TOA Standard Deviation at -5°C

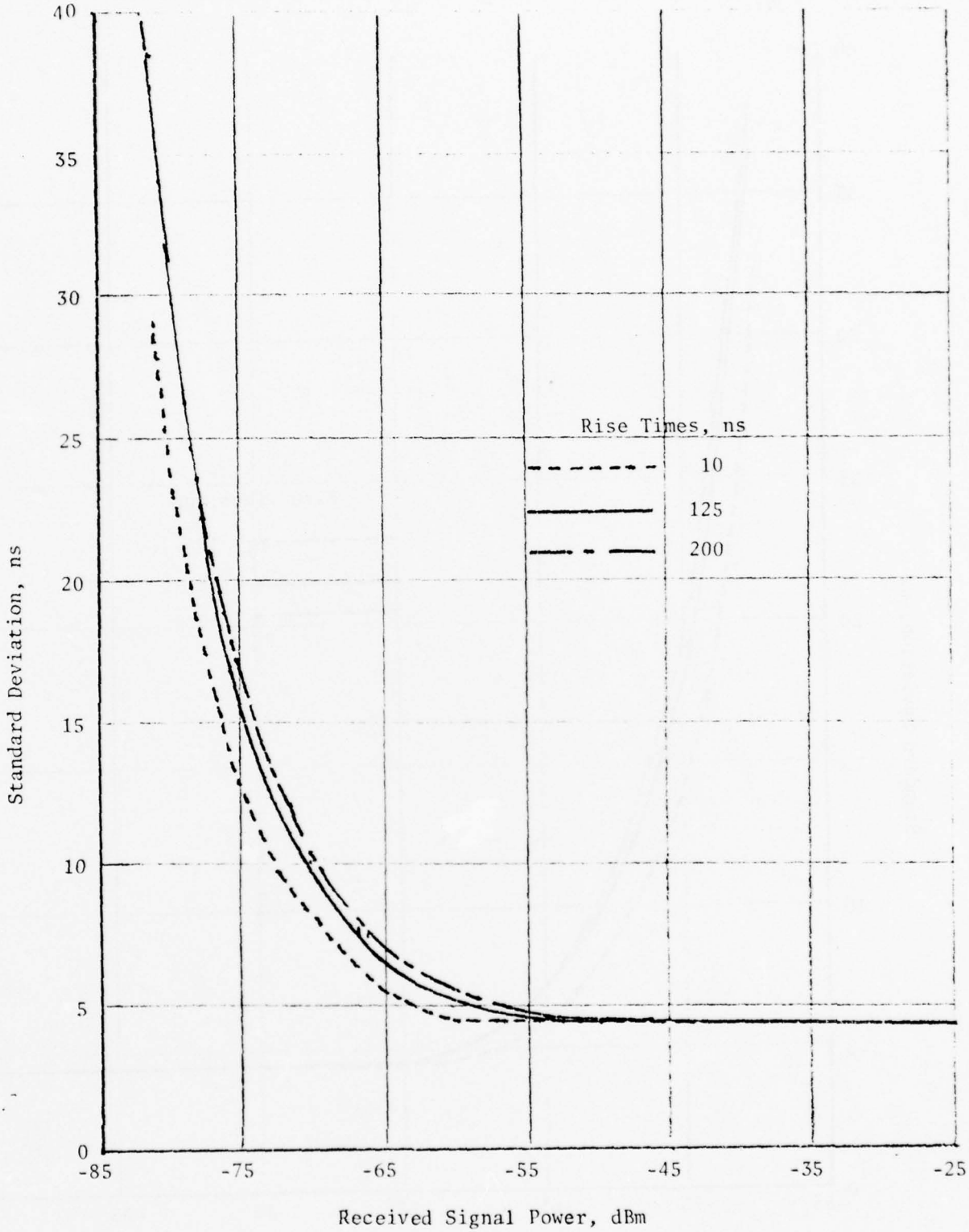


Figure 4-11. TOA Standard Deviation at 20°C

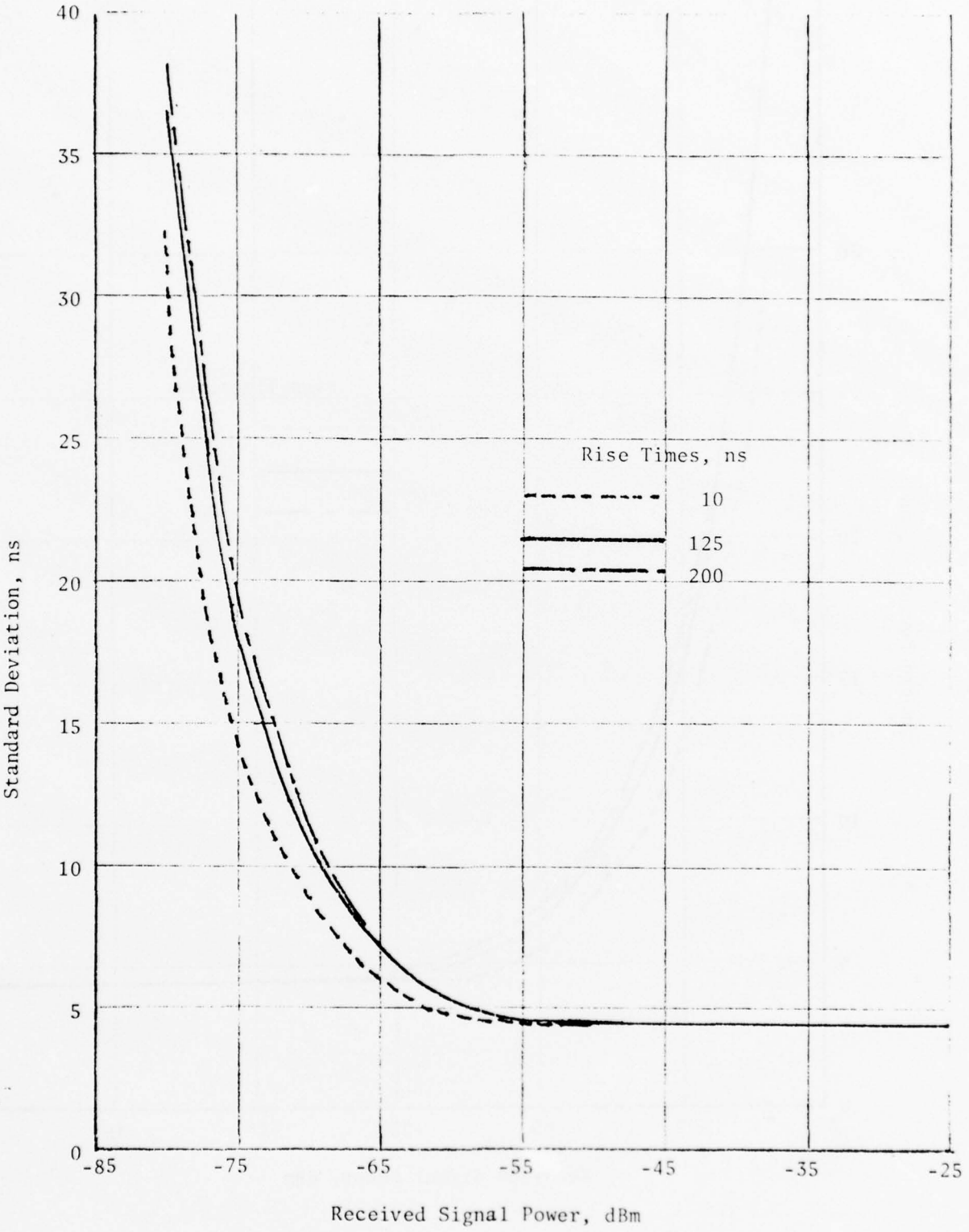


Figure 4-12. TOA Standard Deviation at 75°C

4.5 PRAIS ERROR BUDGET

Most of the PRAIS errors have been characterized by laboratory measurements. This section summarizes these measured errors, describes errors not measured in the laboratory but included in the simulation, and establishes an overall PRAIS measurement error budget. This error budget is divided into ILT errors and passive ranging errors.

4.5.1 PASSIVE RANGING ERRORS

The PRAIS time of arrival errors were fully characterized by laboratory measurements during this contract. The results of these tests are summarized in Table 4-4. These data, properly scaled, were entered into the simulation in this tabular format and assessed as a function (see Section 5.1.3.4) of range, spacecraft illumination and landmark radar pulse rise time. Figure 4-13 shows the worst case error vs. received signal strength. The random and bias errors are reduced from the tabular values by factors of 0.1414 (smoothing 50 pulses) and 0.2 (laboratory calibration of PRAIS) respectively. The PRAIS TOA errors used in the filter are 6 ns random and 0.25 ns bias.

In addition to these TOA errors, the radar landmark jitter is 25 ns $\div \sqrt{50}$ and maximum propagation error (see Section 5.1.3.4) is 2.3 ns. These errors are summarized in Table 4-5. Landmark Clock errors are modeled as described in Section 5.2.3.5.

4.5.2 ILT ERRORS

The ILT errors were also established in the laboratory (Reference 16). The ILT bias errors were entered intc the simulation by an equation empirically derived from the test data. Specifically, as a function of the angle off boresight (θ in radians) the bias error is $\sigma_{BIAS} = 0.15$ $(1 - 1.27\theta + 4.4\theta^2)$ degrees. The random error was modeled as a function of received signal strength to PRAIS noise ratio. The describing equation is given in Section 5.1.3.3. In addition, a random polarization error of 0.02 degrees phase was added to the simulation. These phase errors are summarized in Table 4-6. For the 40 inch baseline interferometer these phase errors are divided by 21π to obtain ILT pointing error.

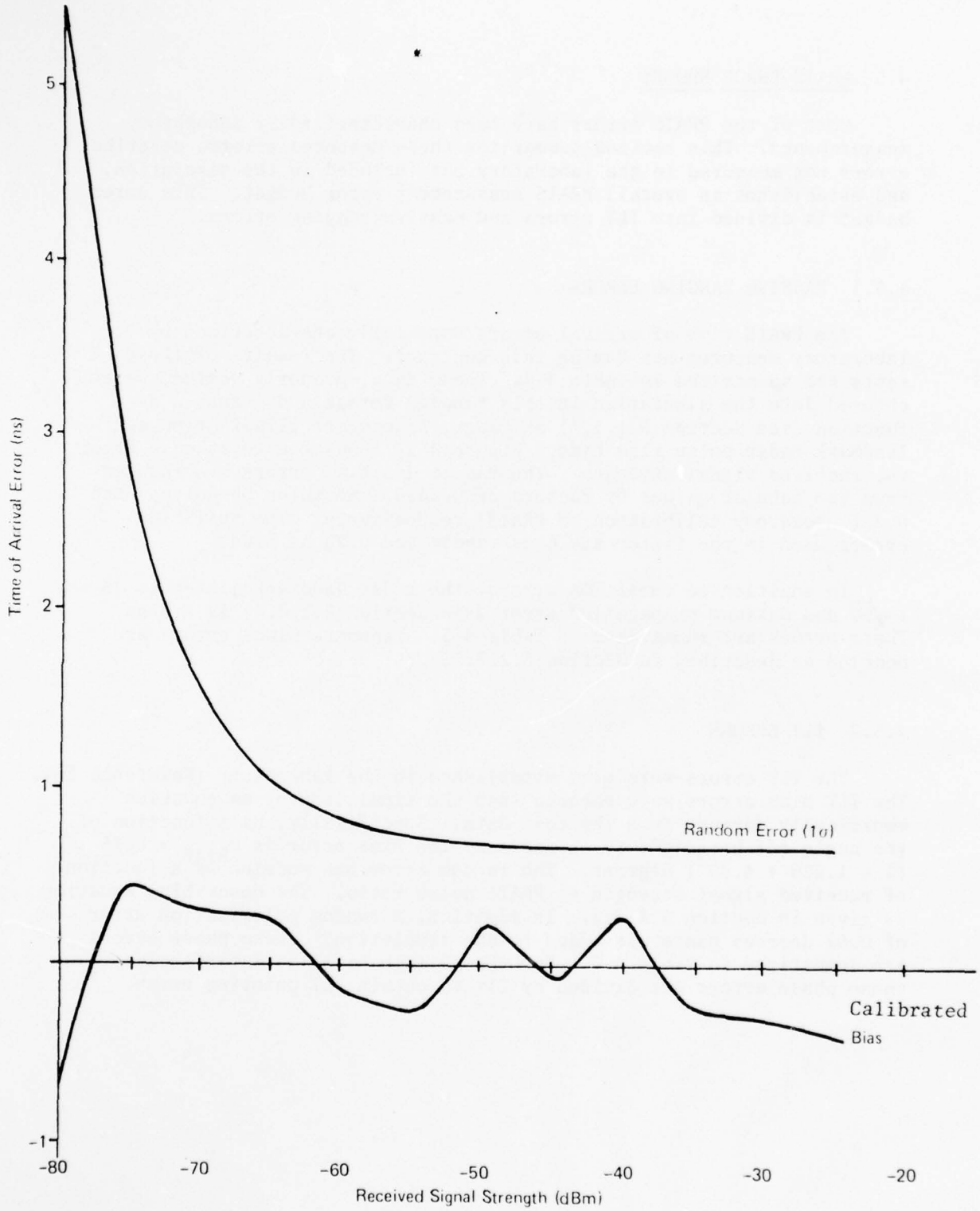


Figure 4-13. PRATS TOA Accuracy

Table 4-5

PASSIVE RANGING ERROR BUDGET

Error Source	Nanoseconds 1 Sigma Bias	Random
PRAIS	0.25	6.04
Landmark Jitter (50 pulse smoothing)		3.54
Propagation	2.30	--
Total	2.31	7.00

Table 4-6

ILT ERROR BUDGET

Error Source	Phase Error 1 Sigma Degrees Bias	Random
Polarization		0.02
PRAIS (R = 20,000 mni, E = 14^{o})	0.16	*0.31
Total	0.16	0.311

(This Page Intentionally Left Blank)

Section 5

SYSTEM PERFORMANCE DEMONSTRATION (TASK 3)

IBM's demonstration of the PRAIS Navigation System is based on two orbit simulations employing laboratory derived sensor data for the Molniya orbit and a synchronous orbit inclined at 1 degree whose parameters are listed in Table 5-1.

The simulation program is briefly discussed, with emphasis on the added attitude determination, the second order filter modification to account for measurement nonlinearities and the error sources modeled in the real and filter worlds. Some of the techniques employed to validate the program are discussed next. These techniques include the matching of two computer programs written in Fortran and APL, accuracy checks of some algorithms, observability analyses and an eigenvalues analysis to determine the adequacy of the normal extended Kalman filter algorithms. The last section discusses the results of simulations of the combined attitude/navigation system on two orbits. These results indicate that the navigation requirements are exceeded by a factor of approximately 2 in the synchronous orbit and by better than an order of magnitude in the Molinya orbit. Steady state attitude accuracies are 10 arc seconds in these orbits.

Table 5-1

ORBITAL PARAMETERS

PARAMETER	ORBIT A MOLNIYA	ORBIT B SYNCHRONOUS
X (ft)	$0.117\ 254\ 14 \times 10^{8}$	$0.240\ 316\ 85 \times 10^{8}$
Y (ft)	$-0.664\ 991\ 48 \times 10^{+8}$	$-0.136\ 292\ 66 \times 10^{9}$
Z (ft)	$0.135\ 052\ 49 \times 10^{9}$	0.0
X (ft/sec)	$0.491\ 677\ 55 \times 10^{4}$	$0.993\ 051\ 58 \times 10^{4}$
Y (ft/sec)	$0.886\ 950\ 75 \times 10^{3}$	$0.175\ 098\ 91 \times 10^{4}$
Z (ft/sec)	0.0	$0.176\ 011\ 73 \times 10^{3}$
Inclination (deg)	63.435	1
Period (sec)	43,083	86,221
Eccentricity	0.732626	0
Apogee Altitude (NM)	21,406	19,333

NOTE:

(1) Position and velocity in earth centered inertial coordinates.

(2) Epoch Date: July 4, 1976, 5 hrs., 10 min., 38.33 sec.

5.1 SIMULATION DESCRIPTION

5.1.1 BACKGROUND

The SCHANS navigation filter simulation was designed to evaluate the performance of a Kalman filter autonomous navigation system for an Earth orbiting satellite. The filter combines passive ranging and interferometer measurements to estimate current position, velocity, attitude, and gyro drifts in a recursive fashion. In addition, 4 states associated with each of the three passive ranging measurements are estimated. These states are: the time of emission of the currently received radar pulse, the nominal pulse repetition interval, and the linear and quadratic temperature coefficients of the crystal clocks employed in the passive ranging radars. A total of 24 states are therefore modeled in the filter. The current simulation is a modification and extension of an Autonomous Navigation Simulation (ANS) constructed on previous contracts. The principal modifications to the ANS simulation are (a) incorporation of attitude and gyro drift states in the filter, (b) provision for simultaneous PRAIS measurements to three landmarks, (c) modification of the conventional Kalman filter to account for quadratic non-linearities in the passive ranging measurements, and (d) incorporation of laboratory-derived measurement errors in the passive ranging sensor models. The ANS simulation had evolved over many years. There were many options, variables and techniques that were no longer employed. Consequently in addition to the new subroutines, changes were made to all subroutines and commons to simplify the program logic and speed execution. In addition, the program now runs on the IBM 370 rather than the 7094.

The four element quaternion was employed to represent spacecraft attitude rather than direction cosines or three Euler angles in order to slightly simplify the computation algorithms and obtain more accurate integration. Three infinitesimal Euler or Kelvin-Tait angles representing small angular deviations about three orthogonal body axes were employed as attitude states in the filter. This choice of filter states resulted in the minimum number of filter state variables representing spacecraft attitude, and maintained a positive definite error covariance matrix while accruing some computational advantage in attitude integration. A simple linear transformation was employed for converting filter attitude updates (corrections) to quaternion updates.

Rather than integrate both the true and estimated quaternions the "true" spacecraft was assumed to be perfectly aligned to the true RTN (radial, tangential and normal) axes.

The attitude portion of the filter included six state variables, three Kelvin-Tait angles and three constant gyro drift biases. The "real" world gyro simulation also included Gauss-Markov random noise, constant drift bias and gyro non-orthogonality errors. Figure 5-1 shows a functional flow of this gyro and estimated attitude simulation.

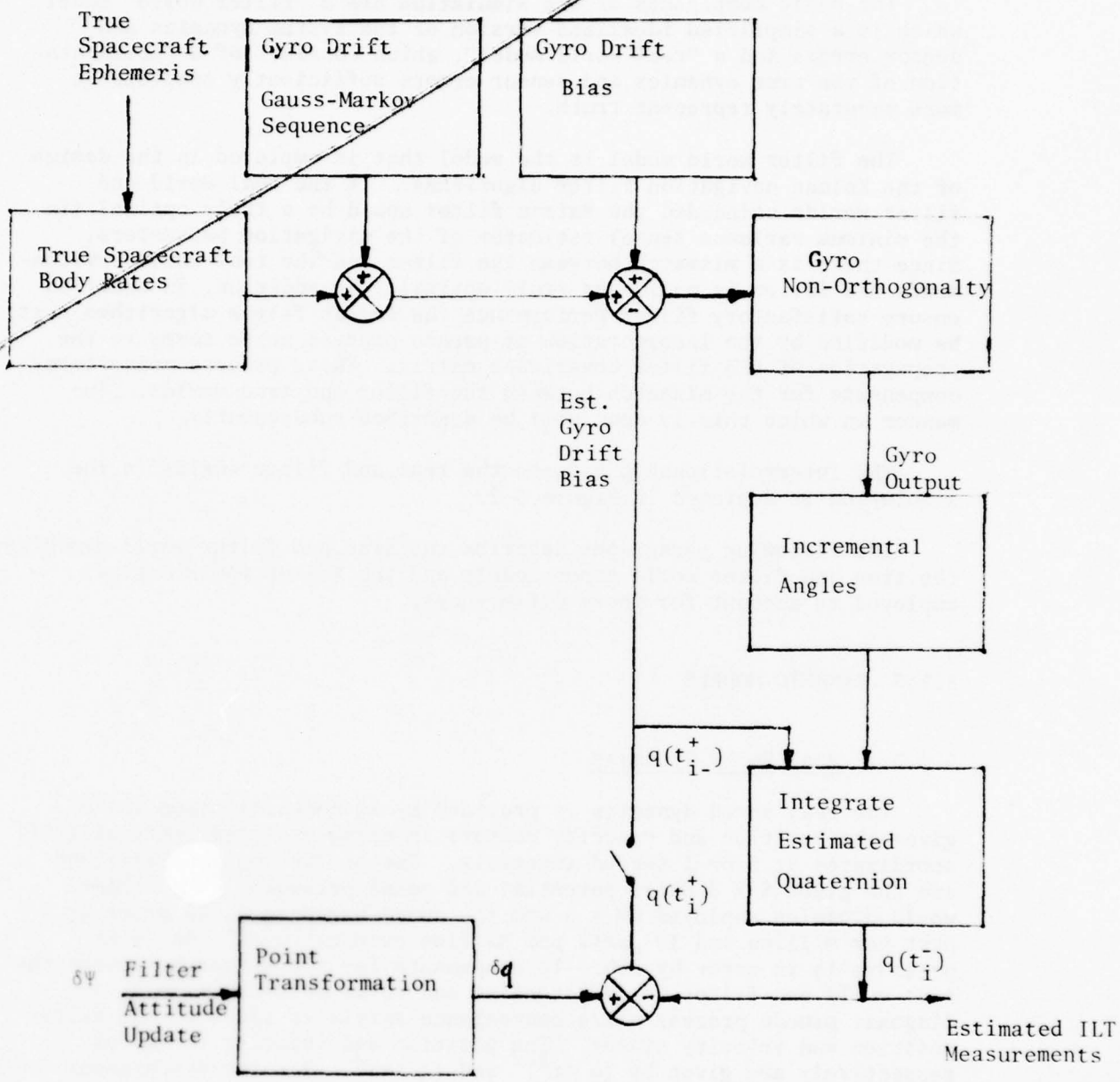


Figure 5-1. Simulation of the Gyros and Estimated Attitude Quaternion

5.1.2 SIMULATION FORMAT

The basic components of the simulation are a "filter world" model which is a simplified idealized version of the system dynamics and sensor errors and a "real world model", which consists of a representation of the true dynamics and sensor errors sufficiently complete to more accurately represent truth.

The filter world model is the model that is employed in the design of the Kalman navigation filter algorithms. If the real world and filter worlds coincided the Kalman filter would be a truly optimal (in the minimum variance sense) estimator of the navigation parameters. Since there is a mismatch between the filter and the real world environments the filter is no longer truly optimal. In addition, in order to ensure satisfactory filter performance the Kalman filter algorithms must be modified by the incorporation of pseudo process noise terms to the propagation of the filter covariance matrix. These process noise terms compensate for the mismatch between the filter and true worlds. The manner in which this is done will be described subsequently.

The interrelationship between the real and filter worlds in the simulation is depicted in Figure 5-2.

The following paragraphs describe the true and filter world dynamics, the true and filter world error models and the filter modification employed to account for these differences.

5.1.3 DYNAMIC MODELS

5.1.3.1 Real World Dynamics

The real world dynamics is provided by an ephemeris tape which gives the position and velocity vectors in earth-centered inertial (ECI) coordinates at 5 or 1 second intervals. The perturbing accelerations are the given 8 x 8 Guier potential and solar pressure. The filter world dynamics employed GM = μ and the zonal harmonic J_2 in error by 1 part per million and 10 parts per million respectively.[2] The solar pressure is in error by 50%. To compensate for the mismatch between the real world and filter world potential and solar pressure models, a diagonal psuedo process noise convenience matrix is added to the filter position and velocity states. The position and velocity variances respectively are given by $(q\ \Delta t^2)^2$ and $(q\ \Delta t)^2$. For the synchronous orbit

$$q = \frac{1.115 \times 10^{31}}{r^{4.455}} \begin{vmatrix} .8083 \\ .5001 \\ .1009 \end{vmatrix}^2_{(RTN)}$$

and for the Molniya (Q-2) orbit

$$q = \frac{1.672 \times 10^{19}}{r^{3}} \begin{vmatrix} .5912 \\ .5625 \\ .5779 \end{vmatrix}_{(RTN)}$$

where r is the distance of the spacecraft from the geocenter and Δt is the time between measurements.

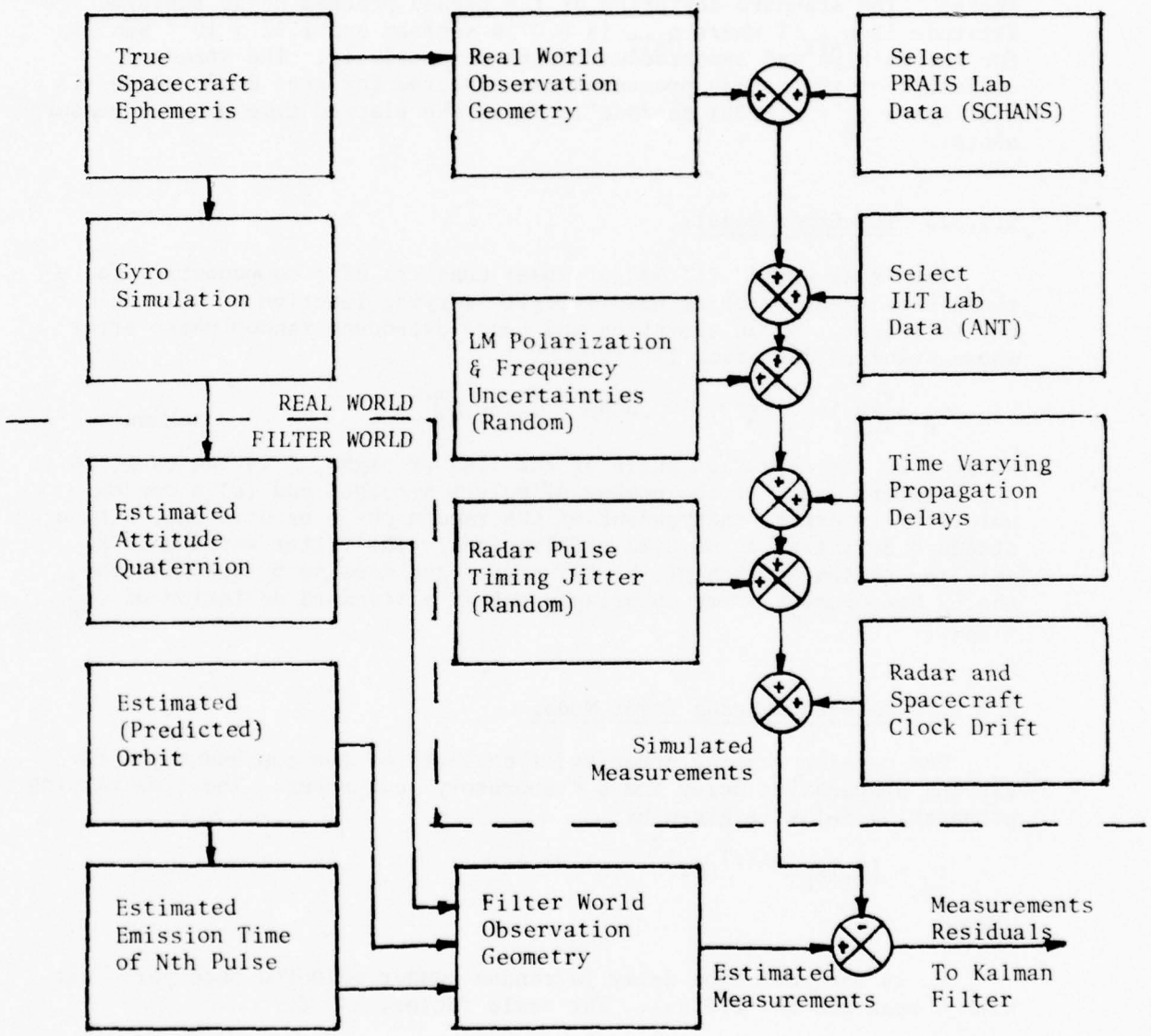


Figure 5-2. Measurement Residual Simulation Showing the Real and Filter World Representations

5.1.3.2 Gyro Model

Each gyro simulation includes a constant drift bias, a Gauss-Markov drift and non-orthogonal gyro alignment errors. The filter world estimates only the constant drift bias. The unmodeled attitude errors are compensated by pseudo process noise components to the attitude and drift states. The standard deviation of the pseudo process noise employed for attitude is $q_{ATT}\Delta T$ where q_{ATT} is 0.0716 $\widehat{sec}$/sec and 1.12×10^{-5} $\widehat{sec}$/sec for the Molniya and synchronous orbits respectively. The standard deviation of the pseudo process noise employed for gyro drift states is $q_g \Delta T$ where $q_g = 0.00001$ $\widehat{sec}/sec^2$. ΔT is the elapsed time between measurements.

5.1.3.3 ILT Error Models

The "real world" ILT sensor model consists of 3 components: (a) a phase bias error which is quadratically varying function of the angle off boresight, (b) an elevation and range dependent random phase error whose standard deviation is given by

$$\sigma_{\phi} = \left[2M \log^{-1} (12.1 - .069E - 2 \log R)\right]^{-\frac{1}{2}} \quad \text{radians}$$

where E is the elevation angle of the line of sight, R is the range to the landmark and M is the number of pulses smoothed and (c) a random polarization error, independent of the random phase error alone, with a standard deviation σ_p of 0.35 milliradians. The filter world models only the random portion of the ILT errors and does so by assuming for the ILT measurement error covariance matrix a standard deviation of $(\sigma_{\phi}^2 + \sigma_p^2)^{\frac{1}{2}}$.

5.1.3.4 Passive Ranging Error Model

The passive ranging error model consists of two components, a time varying propagation delay and a "laboratory" component. The time varying propagation delay is given by

$$t_d = |K_T| K_E e^{-(\lambda T_{LOC})^2} \quad \text{ns}$$

where

K_T is the peak time delay (a random number selected once per orbit with 0 mean and σ = 2.3 ns). The scale factor, λ = 8.

K_E is given by

K_E = secant $(\text{Sin}^{-1} (r/r+h) \text{ Cos } E)$

r = Earth radius
h = mean ionospheric height
E = Elevation angle

$$T_{LOC} = \left\{ \left| \frac{t + T_p}{P} \right| - \left[\left[\frac{t + T_p}{P} \right] \right] \right\} (1 - |\vec{e}_n \cdot \vec{e}_s|)$$

$\bar{e}_s$ = unit vector along the sun line
e_n = unit vector normal to the orbital plane
T_p = a random variable distributed uniformly over the period (-p/2, p/2) and selected once per orbit
t = elapsed mission time

The double bracket indicates the greatest integer function.

The laboratory errors (see Section 4) are incorporated in the simulation as follows. From laboratory data a table is prepared of means and standard deviation of errors as a function of pulse rise time and received signal power. Received signal power P_r is simulated by

$$P_r = 25 - .69E - 20 \log R$$

where E is the elevation angle at the landmark in degrees and R is the range from the spacecraft to the landmark in nautical miles. A rise time is then selected as a function of the landmark from which pulses are being received. By interpolation from the table described above, a mean and standard deviation for the passive ranging error is selected and a random number generated from a normal distributuon with this mean and variance. This random number represents the laboratory error contribution to the random passive ranging error. The error standard deviation employed in the filter to represent the passive ranging random error is a constant.

5.1.3.5 Clock Model

The time history of propagation of the passive ranging filter states is represented both in the real and filter worlds by

$$\begin{bmatrix} t_{N+1} \\ T_{N+1} \\ a_{N+1} \\ b_{N+1} \end{bmatrix} \begin{bmatrix} 1 & 1 & \theta_{2N}/2 & \theta_{3N}/6 \\ 0 & 1 & 0 & 0 \\ 0 & 0 & 1 & 0 \\ 0 & 0 & 0 & 1 \end{bmatrix} \begin{bmatrix} t_N \\ T_N \\ a_N \\ b_N \end{bmatrix}$$

where

$$\theta_{2N} = (2\,N + 1)\,t^2$$

$$\theta_{3N} = (3\,N^2 + 3\,N + 1)t^3$$

and t is elapsed time, in seconds after the first measurement.

5.1.3.6 Passive Ranging Measurements Bias Correction

At the initiation of the passive ranging measurements the non-linearity effects arising from the quadratic term in the Taylor series approximation to the difference between measured and estimated passive ranging measurements is comparable in magnitude to the measurement residual.

In order to reduce the effects of these non-linearities in the passive ranging measurements, the Kalman filter was modified to a Gaussian second order filter (Reference 24). This modification consisted of two parts: (1) a correction to the measurement residual to account for the bias portion of the quadratic non-linearity in the measurement residual and (2) the addition of a term to the measurement noise covariance to account for the fluctuating portion of the non-linearity. The remaining filter equations for both update and propagate are the same as for the conventional formulation.

The measurement residual correction consists of subtracting from the conventional measurement residual the additional term Trace $\frac{JP(-)}{2}$ where $P(-)$ is the filter covariance before update and J is defined by $J = \frac{\partial^2 g}{\partial X \partial X}$ where $g(X)$ is the non-linear function relating the measurement to the state vector X. Writing $g(X)$ in a Taylor series expansion and truncating at the second order term we have $g(X) - g(X-) = \frac{\partial g}{\partial X}\left[X-X(-)\right] + \left[X - X(-)\right]^T \frac{J}{2} \left[X-X(-)\right]$ where $X(-)$ is the estimate of the state vector before the measurement. We see that Trace $\frac{JP(-)}{2}$ is the expected value of $\left[X-X(-)\right]^T \frac{J}{2} \left[X-X(-)\right]$. A straightforward calculation shows that the variance of the second order correction is given by Trace $\frac{JP(-)\ JP(-)}{2}$. This term is added to the measurement noise covariance to complete the filter modification for the incorporation of second order non-linearities.

The second order correction is an especially simple extension for passive ranging since only a (3 x 3) submatrix of J is non zero.

The region of convergence for ILT measurements is much larger than for passive ranging measurements. Consequently, as an additional technique to avoid deleterious effects caused by measurement non-linearities, only ILT measurements were used during the first five hours of each mission simulation.

5.2 SIMULATION VALIDATION

In the course of development/validation of the SCHANS version of the ANS Fortran program, questions arose concerning the (1) programming, (2) accuracy of algorithms and approximations, (3) arithmetic precision and (4) observability of the 24 state variables. It was known that the covariance matrix for passive ranging measurements was nearly positive semi-definite at initialization. Thus it was not known apriori whether the normal Kalman filter algorithms in double precision arithmetic (56 bits) would preserve the positive definiteness or whether a square root filter algorithm was required. In addition, if the system was not completely observable the usual recursive filter algorithms would be suspect.

To answer these questions extensive use was made of APL. APL, a very powerful higher order language is implemented in a conversational mode. This system greatly simplifies the writing and debugging of computer programs, but execution of programs that require substantial computer time is more costly than Fortran. Two versions of the simulation were written, one in Fortran and one in APL. These will be denoted by ANS and ANS/APL. The latter has about two more decimal digits of accuracy than the double precision ANS simulation.

5.2.1 PROGRAM VALIDATION

ANS and ANS/APL were debugged by obtaining detailed numerical agreement between the two programs. This was performed on simulations where the random number generators were inactivated since different random number sequences were obtained from the Fortran and APL subroutines. Since the two programs had slightly different word length and sometimes different but equivalent algorithms agreement was not perfect. It was believed that agreement to within a foot in position was adequate after a thousand seconds of filter operation. In most variables, agreement was obtained to better than 10 digits.

5.2.2 ALGORITHMS AND APPROXIMATIONS

Previous SAMSO contracts, SPARS, ANT and HANS, had provided well tested integration algorithms for both orbit propagation and quaternion integration. The constancy of the Hamiltonian was employed as a measure of orbit integration accuracy for drag free earth orbits. In addition, the linearized Encke technique was checked by comparison with a trajectory tape generated by Aerospace corporation.

Other algorithm approximations could be quickly tested by employing ANS/APL. Typical of these was the algorithm for computing the estimated time of arrival of the Nth pulse τ_N. The "exact" value is obtained by solving a transcendental equation by a Newton-Raphson iterative technique. Several approximate methods involving perturbation techniques were tried and judged to be faster and sufficiently accurate.

A quadruple precision version of ANS was generated and found to give substantially similar filter covariance matrices, indicating that the square root filter algorithm may not be required for the simulation. An eigenvalue analysis (see Section 5.2.4) supports this conclusion. (The square root algorithm is desirable for spaceborne computers for memory conservation.)

Close agreement was also obtained in the passive ranging measurement residuals $C(\tilde{\tau}_N - \hat{\tau}_N)$. The accuracy of this measurement residual was suspect when one considers that $C\,\tau_N$ for 10^4 sec. is approximately 10^{13} and the random measurement error is 10 feet. To determine the adequacy of the arithmetic precision and algorithms simultaneously, the measurement residual was compared to the measurement matrix, (H) times the state deviation δx; i.e.,

$$C(\tilde{\tau}_N - \hat{\tau}_N) - H_{PAR}\delta x$$

For example, when τ_N = 500 sec

$$C(\tilde{\tau}_N - \hat{\tau}_N) = 6906.470\ 936 \text{ ft.}$$

$$H_{PAR}\delta x = 6906.183\ 534 \text{ ft.}$$

$$C(\tilde{\tau}_N - \hat{\tau}_N) - H_{PAR}\delta x = .287\ 402 \text{ ft.}$$

2nd order term = $\frac{1}{2}\delta x^T J \delta x$ = .287 29 ft.

Since $C(\tilde{\tau}_N - \hat{\tau}_N) - H\delta x$ is almost equal to the second order term it was concluded that the precision in the calculated measurement residual was adequate. This check also gave good assurance that the algorithms were adequate and that the passive ranging measurement matrix H_{PAR} was accurately computed.

5.2.3 OBSERVABILITY

This section discusses the observability of two systems which are subsystems of PRAIS. First the observability of the system of twelve states consisting of position, velocity, attitude, and gyro drift bias employing ILT measurements is discussed. The second subsystem employs passive ranging measurements and estimates twelve states consisting of position, velocity, and two passive ranging states per landmark, time of emission of the zeroth pulse and the pulse repetition interval (PRI).

5.2.3.1 ILT Observability

It is easily shown that with simultaneous ILT measurements to three distinct landmarks, spacecraft position and attitude may be estimated. Thus it is obvious that a sequence of measurements made at successive time instants can be employed to estimate spacecraft velocity and constant gyro drift. Hence, the 12 state ILT subsystem is observable.

5.2.3.2 Passive Ranging Observability

The observability of passive ranging is treated numerically. Passive ranging which has been shown to be equivalent to one way doppler gives excellent results in most orbits. The most difficult orbit is the near circular geosynchronous orbit with small inclination. If the inclination and eccentricity are zero it is easily shown that not all twelve states are observable. An analytical proof of observability of this subsystem would be difficult; hence IBM chose a numerical demonstration of observability.

The mere fact that the variance of all twelve state variables decreased in a Kalman filter covariance analysis is not a demonstration of observability, rather it is a necessary condition. For example, it can be shown that a system of two state variables, one of which is estimatable, can have smaller variances after processing several measurements in a filter employing a priori data.

A batch filter valid for circular orbits was constructed where the state was referred to a common epoch; i.e.,

$$\underset{(n \times 1)}{\delta y} = \underset{(n \times 12)}{H_{epoch}} \underset{(12 \times 1)}{\delta x \text{ (epoch)}}$$

Observability is equivalent to the invertability of $H^{T}_{epoch} R^{-1} H_{epoch}$ where R is the measurement noise covariance matrix. For establishing observability, landmarks 29, 35 and 2 were employed. The orbit was a 1^{o} circular geosynchronous orbit.

Since this batch filter was constructed by another analyst, the batch filter covariance analysis could also be employed as an independent check of the Kalman filter covariance analysis. This was accomplished by employing a priori data. The RMS position error checked to within 1% after taking measurements every 500 seconds over an interval of 5000 seconds.

Thus, this batch filter was employed to (1) numerically demonstrate the observability and (2) provide an independent check of the Kalman filter simulation for passive ranging.

5.2.4 EIGENVALUE ANALYSIS

Previous HANS experience indicated that the covariance matrix could lose its positive definiteness for single precision arithmetic. Initialization of the covariance matrix for each new passive ranging (PAR) landmark would result in a positive semi-definite matrix (zero eigenvalue) if the variance of PAR measurement noise were zero. In addition, a sequence of PAR measurements is expected to further reduce

the lowest eigenvalue. This condition coupled with the filter algorithms executed with finite word length arithmetic and a poorly observable PAR system (in the geosynchronous orbit) may cause the filter covariance matrix to lose its positive definiteness (have a negative eigenvalue). A change to one of the "square root" filter algorithms would be indicated if this were the case.

Since the one degree inclination, nearly circular, synchronous orbit is nearly non-observable for the passive ranging measurements a "worst case" investigation was used. The ANS/APL program was run out to 47,000 seconds using ILT observations only. The ILT and passive ranging observations were then initialized and at each update of each of the three trackers, the corrected covariance matrix was stored on tape. This data was stored from 47,000 seconds to 60,000 seconds. This interval covers the transient region as seen in the position RMS curve shown in Figure 5-3.

The data were then used in an APL program which determines the eigenvalues of the symmetric matrix using the Jacobi-VonNeumann diagonalization method. The covariance matrices were first scaled such that a matrix of correlation coefficients (R) is established

$$R = \begin{bmatrix} 1 & p12 & p13 & \cdots & p_{1n} \\ p12 & 1 & \cdots & & p_{2n} \\ \vdots & & & & \vdots \\ \cdots & & & & \cdots \\ p_{1n} & & & & 1 \end{bmatrix}$$

to determine the smallest eigenvalue. A negative or zero eigenvalue would immediately indicate the loss of positive definiteness whether due to computer roundoff or a programming error. Thus, the minimum eigenvalue was found for the scaled covariance matrix and is plotted in Figure 5-4. It can be seen that the minimum eigenvalue was always greater than zero which is a necessary and sufficient condition that the covariance matrix is positive definite. Furthermore, the curve indicates that the minimum eigenvalue approaches an asymptotic value of 10^{-7}.

Figure 5-5 shows the condition number of the scaled covariance matrix. The condition number is defined as the ratio of the largest eigenvalue to the smallest. The condition number is a popularly used measure of computational error.

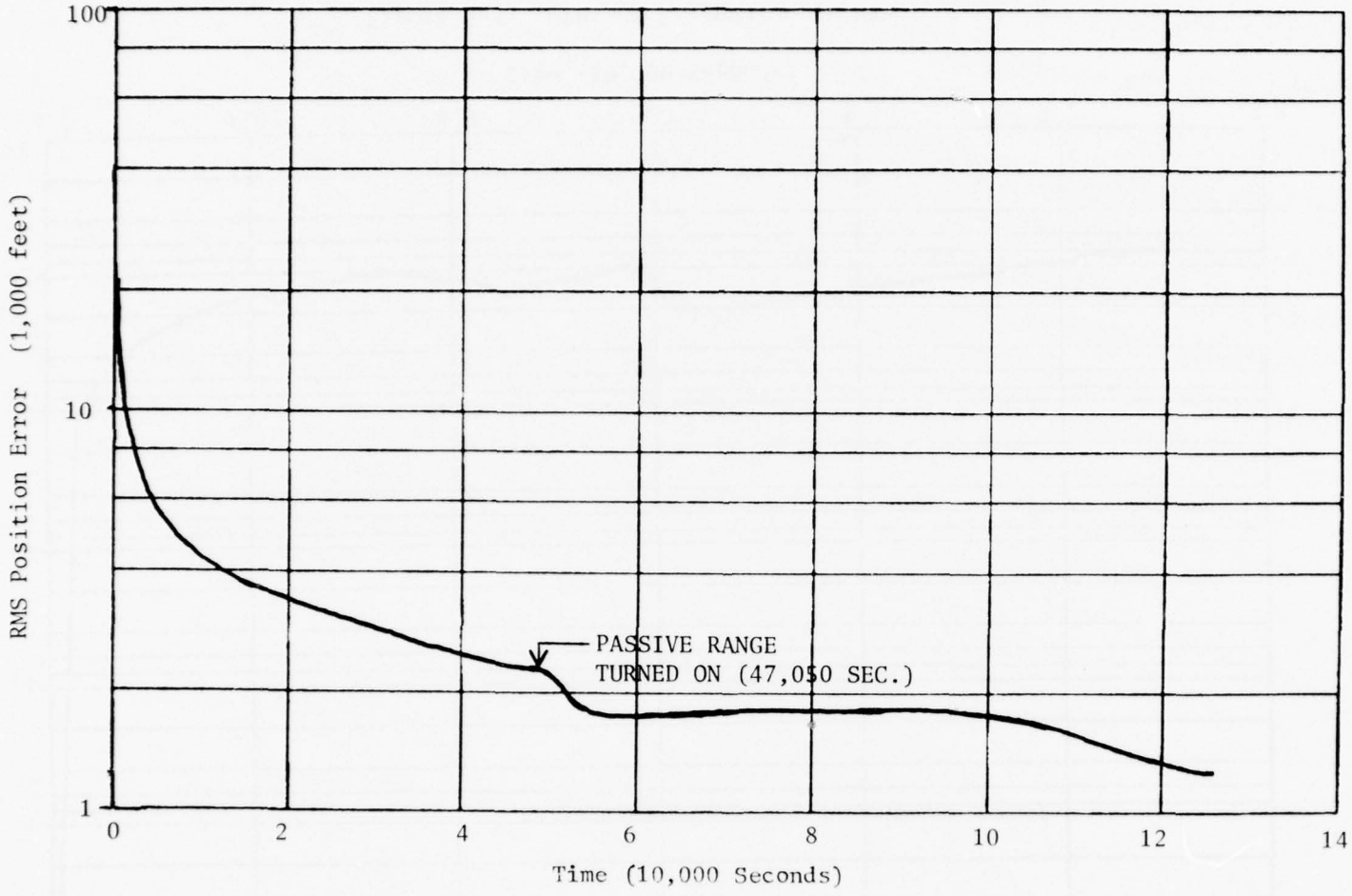


Figure 5-3. RMS Position Error, Synchronous Orbit

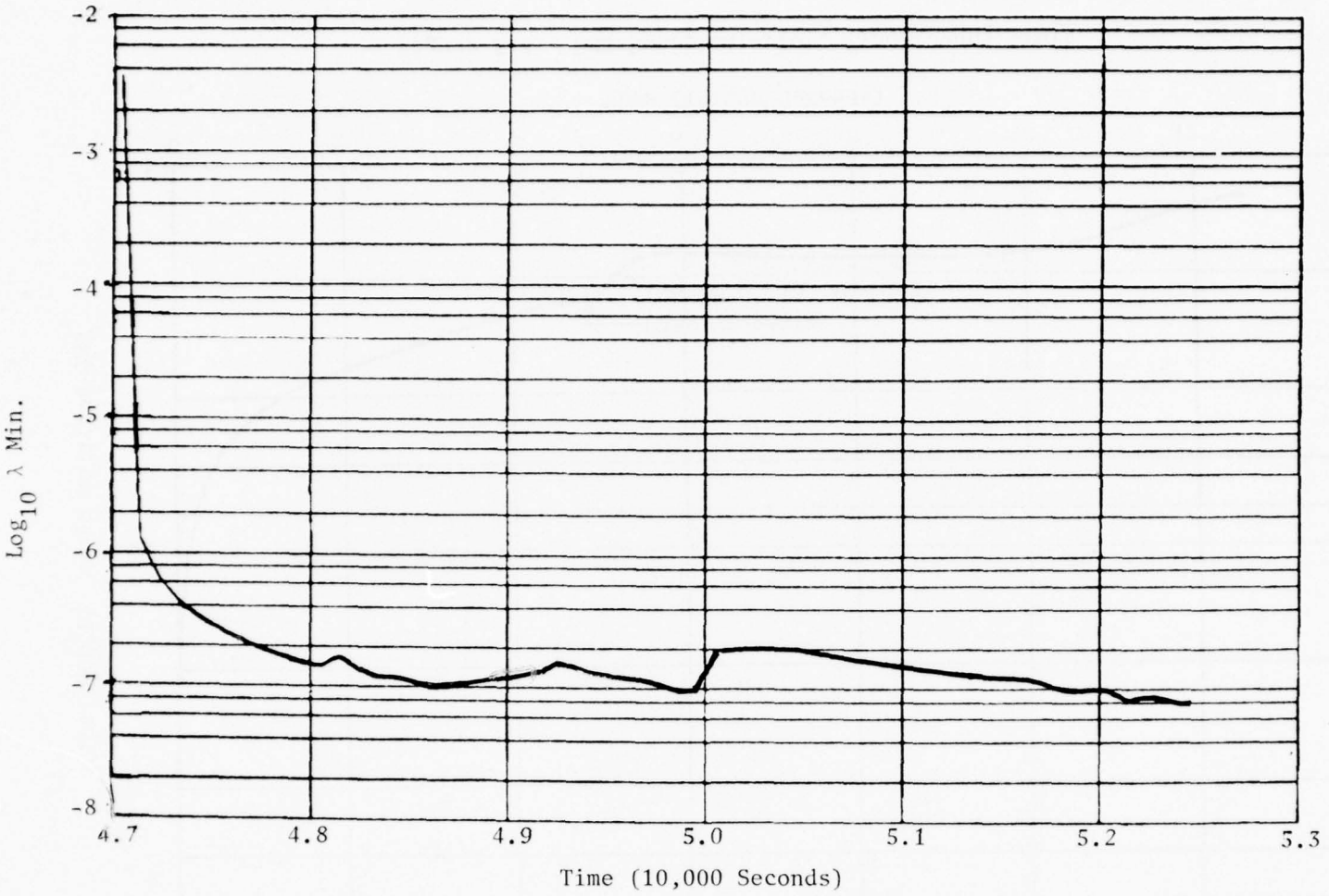


Figure 5-4. Minimum Eigenvalue (λ Min.)

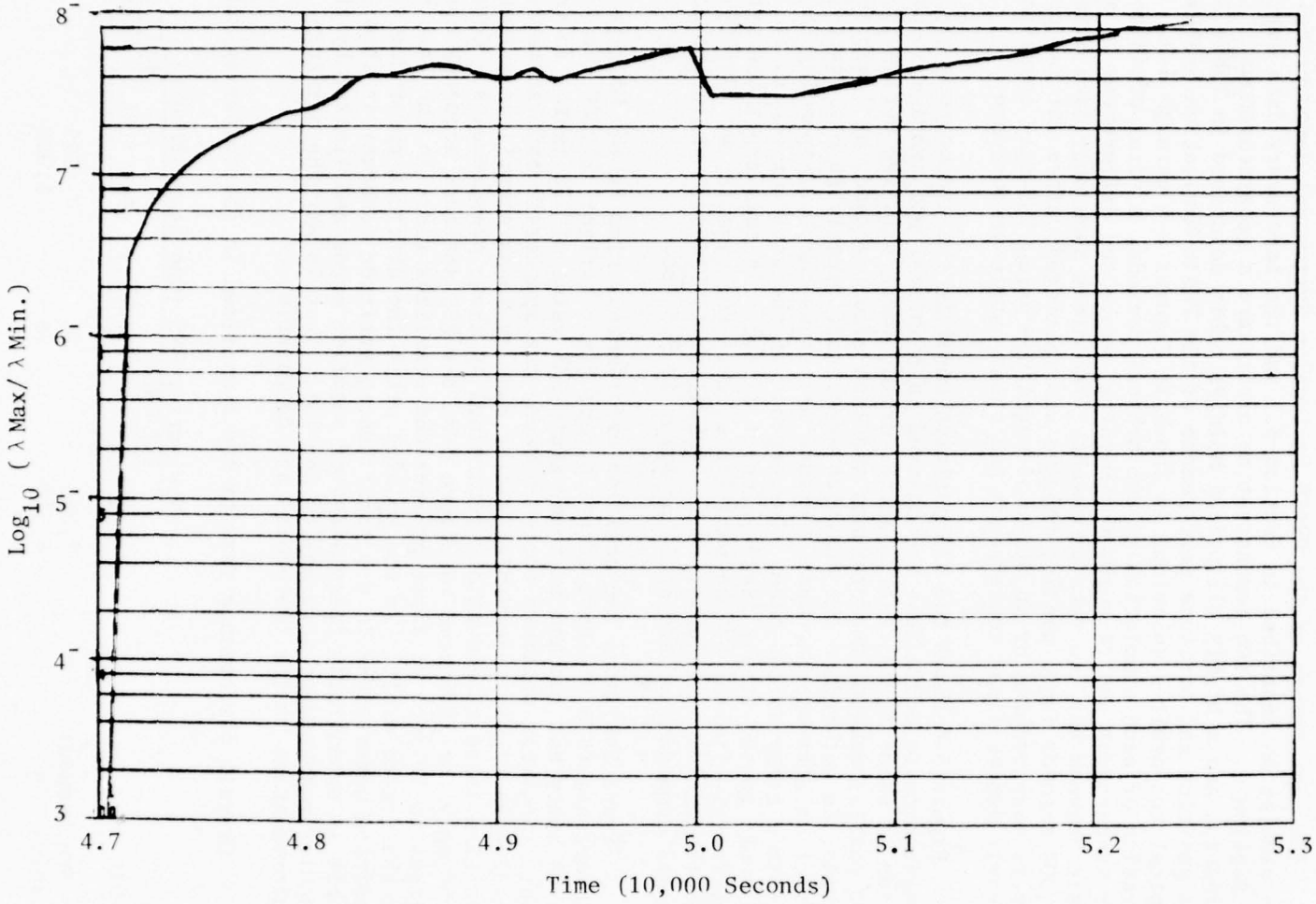


Figure 5-5. Condition Number (λMax/ λMin.)

5.3 PRAIS NAVIGATION SYSTEM PERFORMANCE

The performance of the PRAIS Navigation System was demonstrated using the simulation described in Section 5.1 and the laboratory data described in Section 4. The two demonstration orbits are a geosynchronous 1^{o} inclination and a highly elliptical Molniya orbit described in Table 5-1. The position and attitude performance of the PRAIS Navigation System for typical two orbit simulations is shown in Figures 5-6 through 5-9. The duration of each simulation is two orbital periods, a total of 48 hours for synchronous and 24 hours for Molniya, hence the differences in abscissa scale between the two sets of graphs. The plots show only data after 18,000 seconds (when passive ranging was initiated, after initial position errors were reduced by an order of magnitude using ILT-only operation) to clearly depict final convergence and steady state performance.

Figure 5-6 shows the RSS position error in the synchronous (1^{o}) orbit. Convergence to 6,000 feet is achieved in 36 hours, and average steady state error is about 3,000 feet. In this orbit, where relative motion is small, the passive ranging measurements are less effective and, at least for two orbits, do not reduce the position error sufficiently to eliminate its effect on attitude accuracy. Figure 5-7 shows the corresponding RSS attitude error versus time. Convergence of the attitude occurs at 29 hours to the steady state value of 12 $\widehat{\text{sec}}$. In this orbit the attitude accuracy is limited by the position error. For example, at 170,000 seconds the tangential position error is equivalent to 7.4 $\widehat{\text{sec}}$. while the corresponding normal component of the attitude error is 9.3 $\widehat{\text{sec}}$.

Figure 5-8 shows the position error versus time in the Molniya orbit. Convergence to 6,000 feet occurs before first perigee (21,000 sec.) and at 24 hours has reached a steady state RSS value of 225 feet. In this orbit the large relative motion between the spacecraft and landmarks results in highly observable passive ranging measurements; as a result position error is accurately determined by these measurements. Correspondingly, as indicated in Figure 5-9, the RSS attitude accuracy converges to 10 $\widehat{\text{sec}}$. at first perigee and stablizes there in the last half of the second orbit. In the Molniya orbit the attitude error due to position uncertainty is 0.3 $\widehat{\text{sec}}$.; hence, attitude accuracy in this orbit is essentially independent of position error and limited by the angular measurement accuracy of the ILT. That is why the attitude uncertainties in the two orbits are comparable.

Overall performance results are summarized in the following table:

	Navigation RMS (One-Sigma Errors)			
	ILT ONLY		PRAIS	
Orbit	Pos. (ft.)	Att. ($\widehat{\text{sec}}$.)	Pos. (ft.)	Att. ($\widehat{\text{sec}}$.)
1^{o} Synchronous	7,080	26	225	12
Molniya	8,316	16	3,000	10

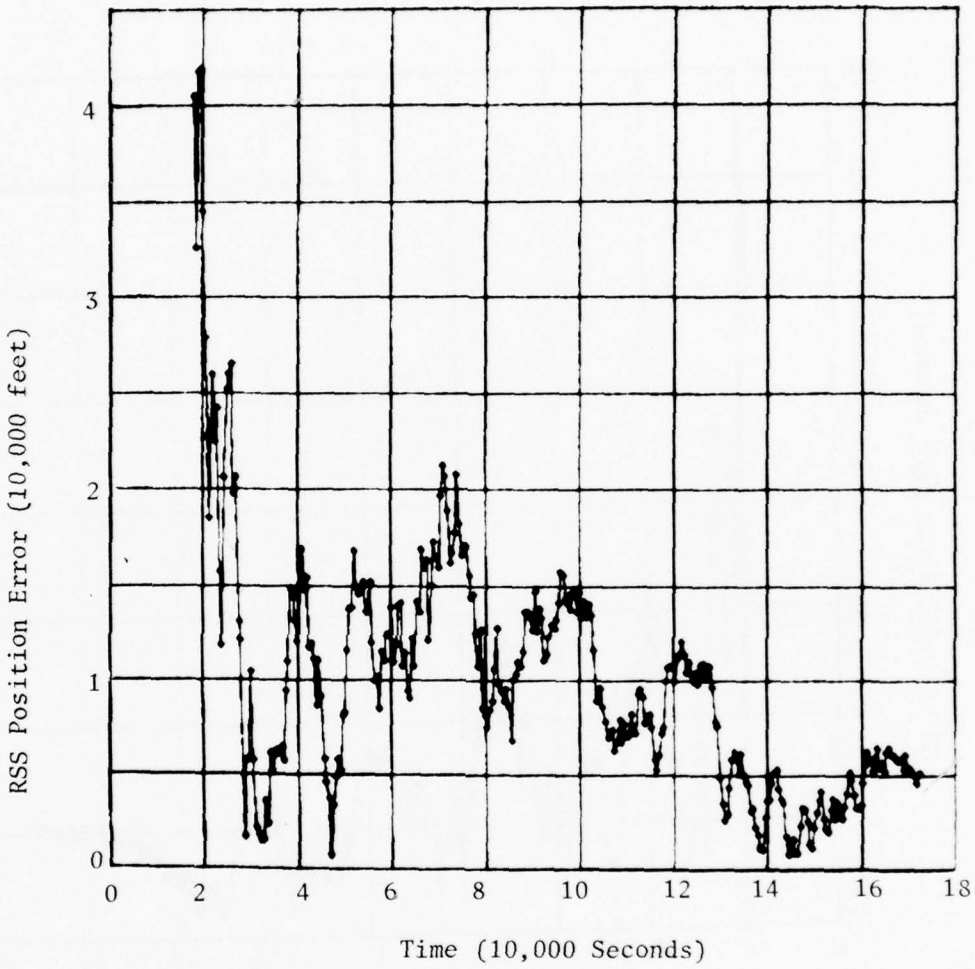


Figure 5-6. PRAIS Navigation System, RSS Position Error in Synchronous (1^{δ}) Orbit

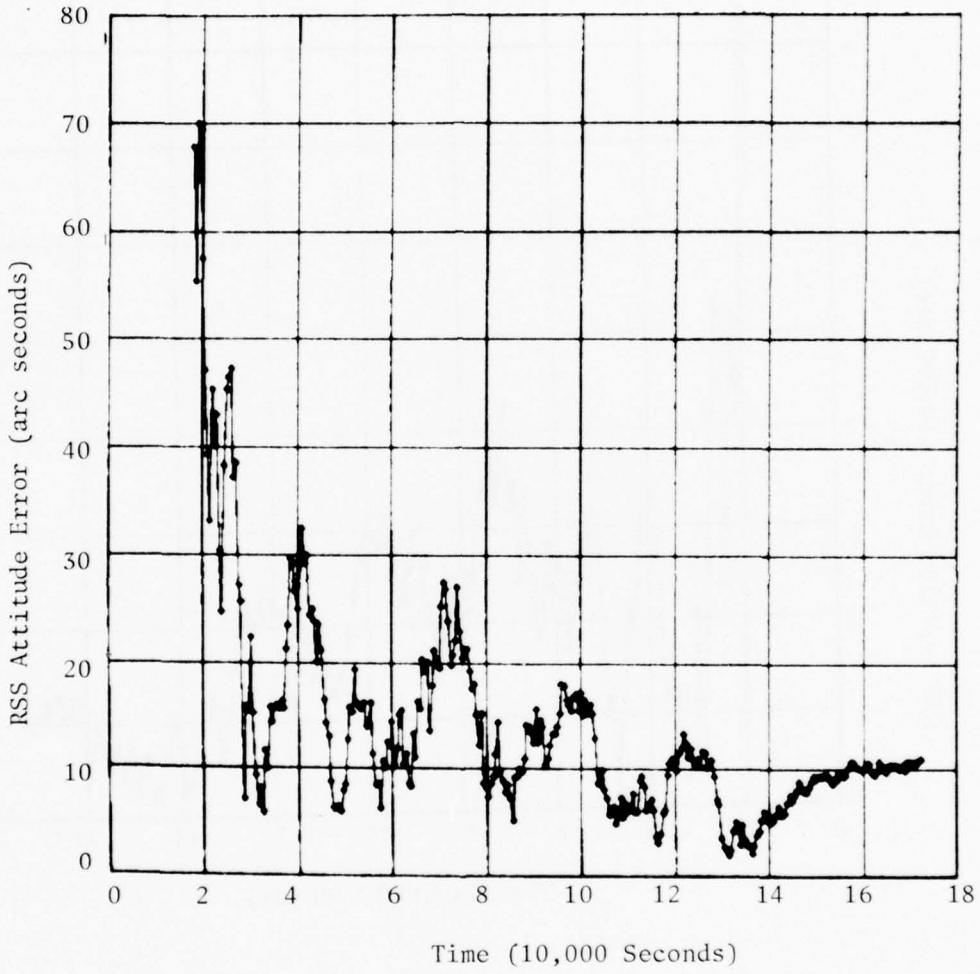


Figure 5-7. PRAIS Navigation System RSS Attitude Error in Synchronous (1^{o}) Orbit

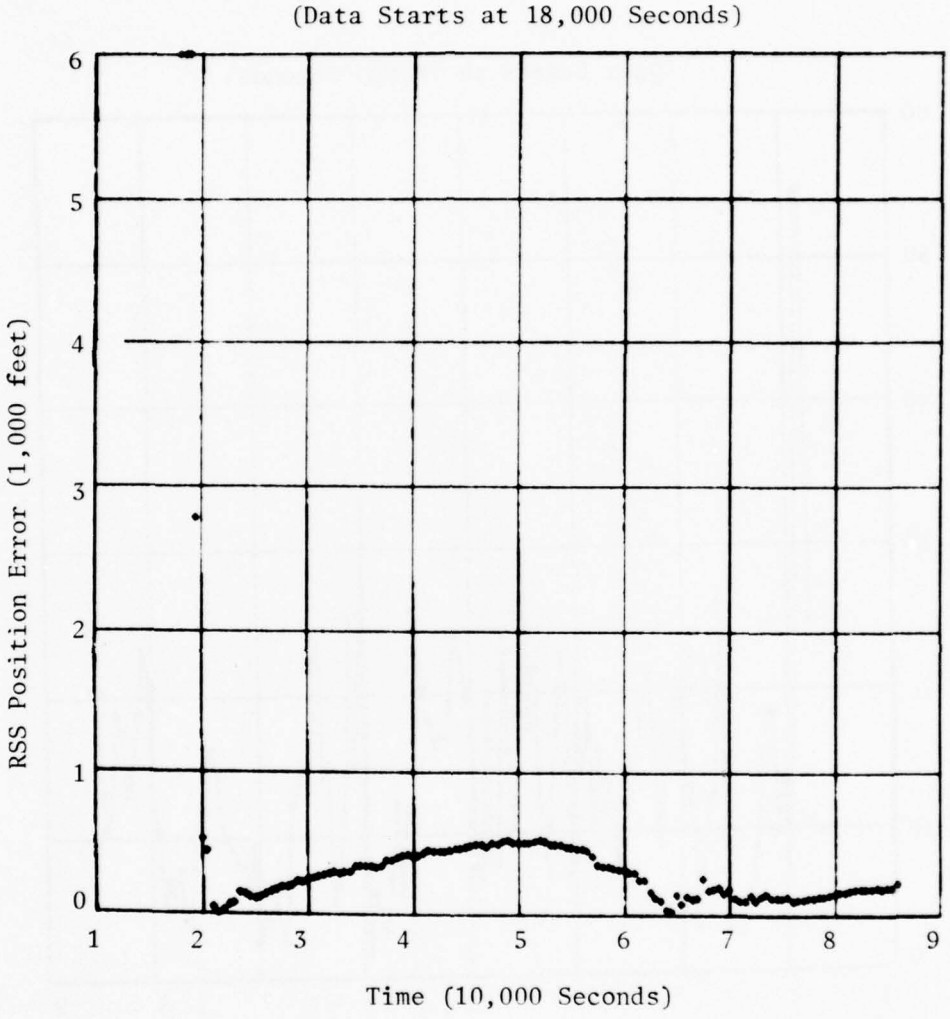


Figure 5-8. PRAIS Navigation System RSS Position Error in the Molniya Orbit

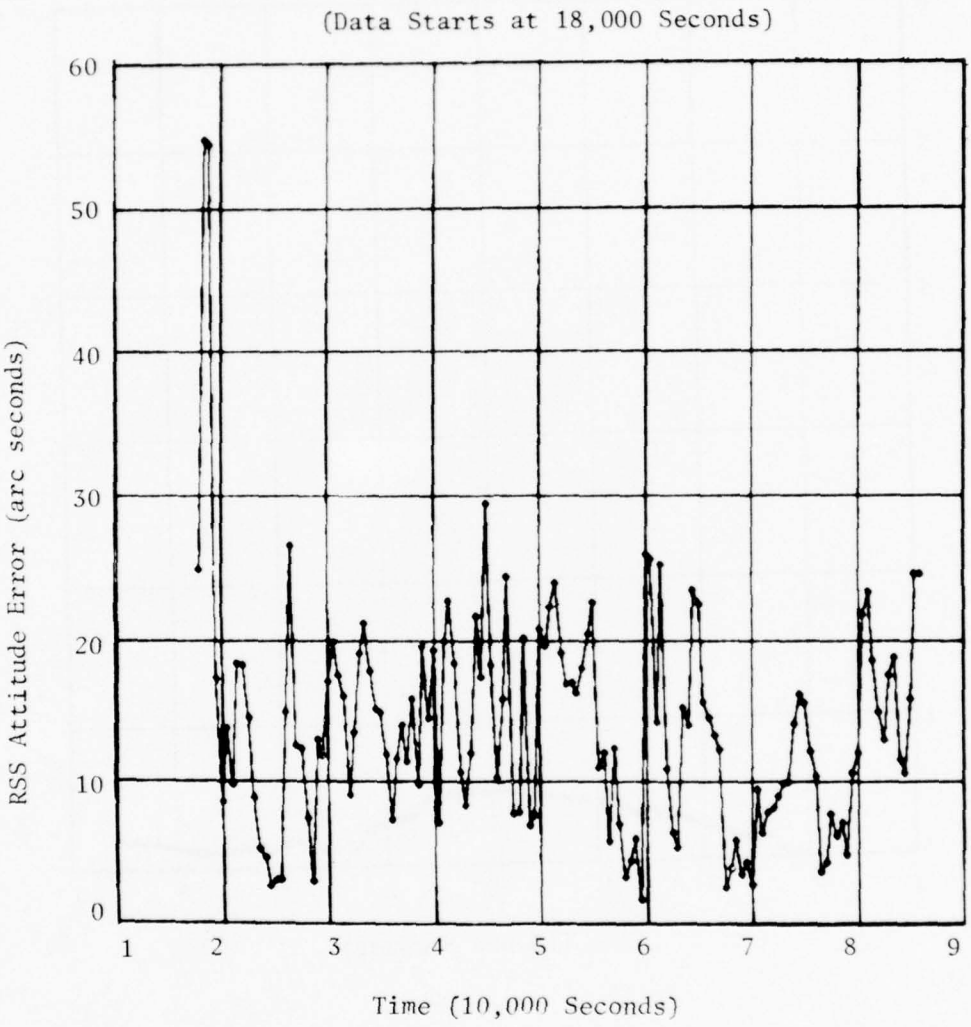


Figure 5-9. PRAIS Navigation System RSS Attitude Error in the Molniya Orbit

Section 6

FLIGHT TEST PLANNING (TASK 4)

6.1 PRELIMINARY FLIGHT TEST PLAN

The results of this task are reported in a preliminary flight test plan submitted separately as CDRL Item A014 (Reference 20). The report is in the form of a response to a Space Test Program (STP) payload requirements questionnaire (See Reference 23). The plan is based on tentative assignment of the SCHANS payload to a host vehicle scheduled for flight late in 1978. It incoporates results of a payload accommodation study performed in 1976 by the host vehicle integration contractor, Lockheed Missile and Space Company (LMSC), Sunnyvale, California. The payload assignment was not confirmed, however, and the flight test plan is to some extent no longer applicable. It is useful as a baseline document that can be readily revised to be compatible with assignment to another host vehicle. The SCHANS payload was to consist of the PRAIS, it's associated SPU and (optional) IRU.

Experience in this preliminary flight test planning clearly indicates the necessity of early identification of the host vehicle, prompt completion of a payload accommodation study by the host vehicle integration contractor (HVIC), and establishment of close liaison among the sponsoring agency (SAMSO), the HVIC and the payload contractor. This is more important from a design standpoint than it is for effective flight test planning. Operational, physical and functional constraints imposed upon the payload equipment and software have potentially far reaching design impacts.

Highlights of the preliminary flight test plan are as follows.

6.2 FLIGHT TEST CONCEPT

The flight tests were to be performed in a high-inclination near-circular low earth orbit (100-400 Nm). The SCHANS payload was to begin intermittent operation (two consecutive orbits per day) thirty days after launch. This intermittent operation was intended to continue for up to 120 days after launch. Data collected during operation was to be stored in the SPU and "dumped" at the end of each orbit (or at the end of the second orbit) when a telemetry ground station is in sight.

6.2.1 NORMAL OPERATION

The normal mode of operation is shown in Figure 6-1. As landmarks come into view, their pulses are received by the PRAIS, pre-processed and used as inputs to the Navigation and Attitude Determination Program. That is, measurements made on pulses from one, two or three landmarks are used to update the Kalman Filter. After each update, the processed navigation data (filter state variables, mission time, and other supporting data) are stored for later transmission.

The number of processed data samples that can be stored depends upon the SPU memory capacity available (approximately 9000 16-bit words). When the HV becomes visible to a ground station, an uplink command is used to initiate telemetry transmission. Another command is used to terminate operation for the day.

6.2.2 REAL TIME OPERATION

Normal operation provides results of SCHANS payload operation. It is desirable also to have access to the raw landmark measurements as well as the results of processing those measurements. To this end, a real time operating mode was conceived, to be initiated by command when all the following conditions exist (as depicted in Figure 6-2).

- o One, two or three landmarks are in view
- o A telemetry downlink is operable
- o No normal-mode data remain in memory.

In this mode, every set of landmark pulse measurement data transferred to the SPU (phase angles, time of arrival, etc.) is kept in storage until all measurements have been made and the navigation filter updated. Then all raw measurement data and the processed data are transmitted to the ground station. This total cycle is performed six or more times.

6.3 INSTALLATION

The tentative installation in the HV is shown in Figure 6-3. The PRAIS (ILT-PCU) and SPU are shown mounted on a mechanically-isolated, thermally-controlled pallet. The HVIC would prefer to "stack" the two units to conserve pallet area. This would be mechanically awkward but feasible. The thermal condition would require additional analysis.

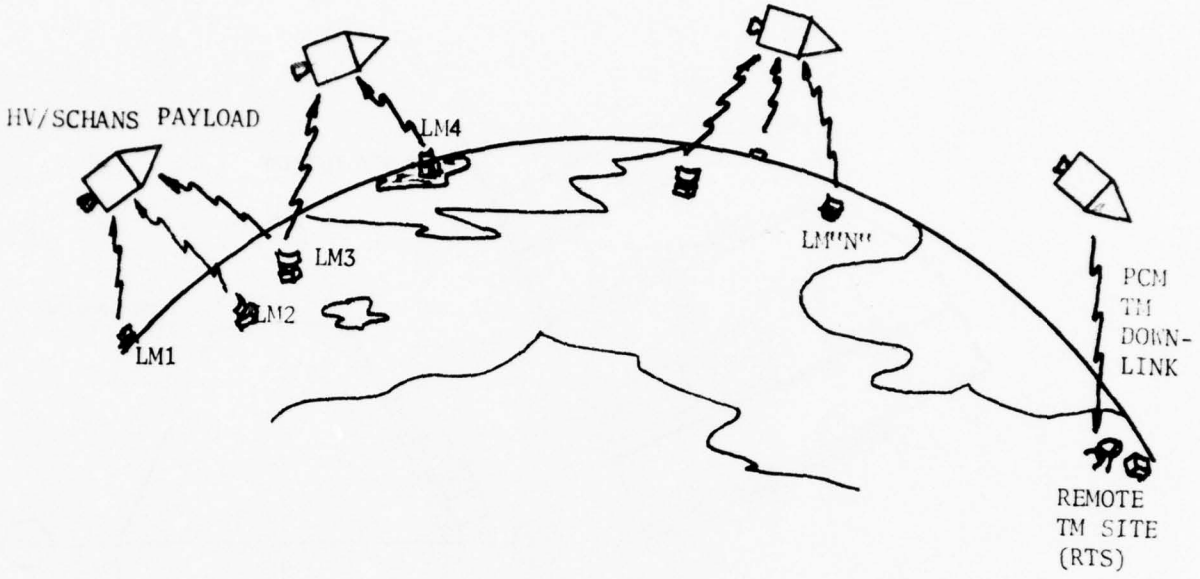


Figure 6-1. Normal Operation

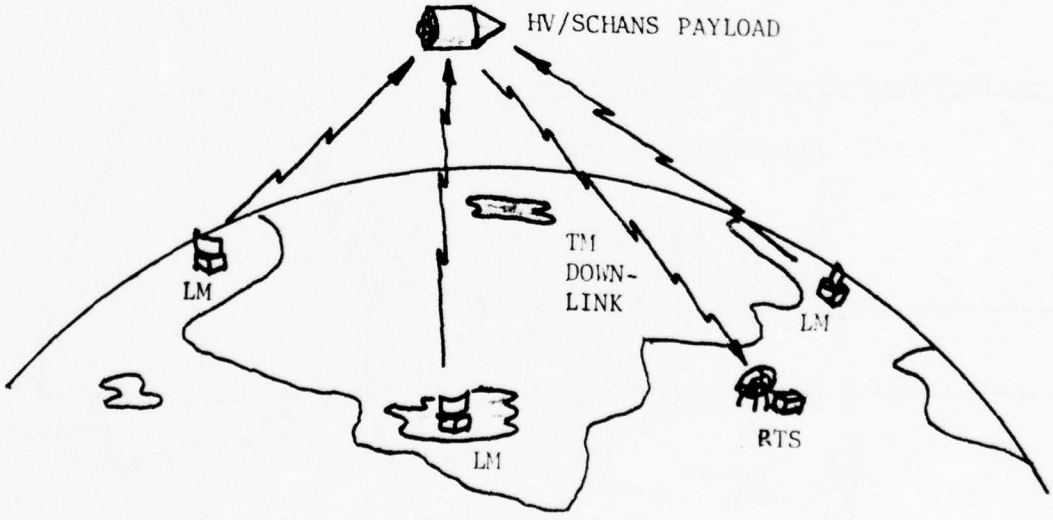


Figure 6-2. Real Time Operation

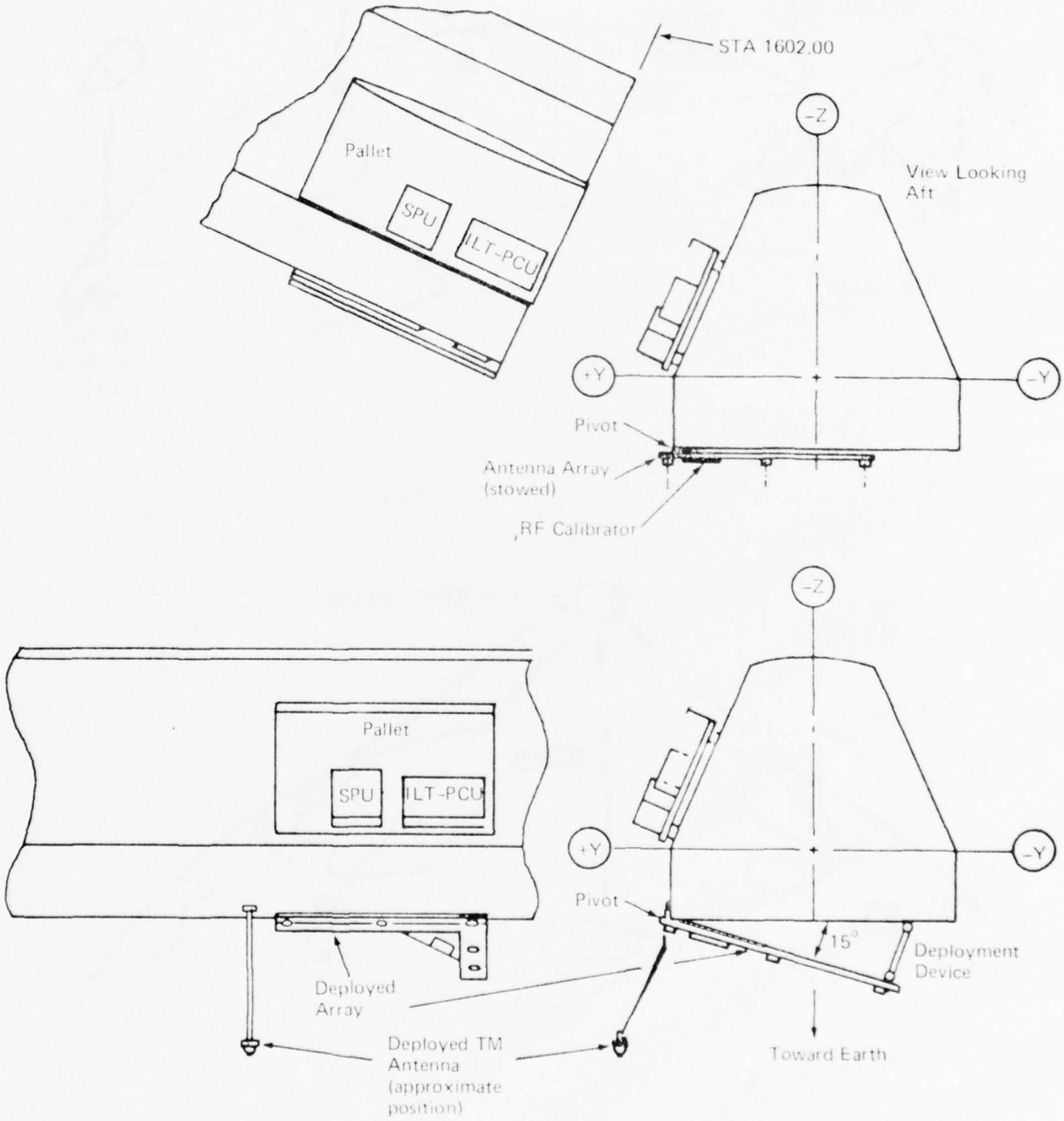


Figure 6-3. Prospective Host Vehicle Installation

Subsystem support provided by the HV includes mechanical, thermal, electrical power, command and telemetry. The proximity of the pallet telemetry antenna in its deployed position has not been found, at least in a preliminary worst-case analysis, to cause any electromagnetic interference. It may create adverse multipath effects that would have to be tested and calibrated out in an anechoic chamber.

The interferometer antenna array is mounted for best earth viewing capability. Mechanical deployment from the stowed position to a 15^{o} (to 30^{o}) offset is made necessary because of other equipment operating nearby. This arrangement was suggested by the HVIC.

The SCHANS system cabling is shown in Figure 6-4. The External clock connector would not be used.

6.4 COMMAND REQUIREMENTS

The Extended Command System in the Host Vehicle provides three types of commands, of which two would be used by SCHANS: discrete and variable. The discrete command is a single pulse, 100 to 110 Ms wide, 22 to 35 volts in amplitude capable of providing a current of up to 150 Ma. Isolation of both the command line and its return are required. The variable command consists of a seven-bit word, equivalent to seven discretes in parallel with a validation signal.

At least one discrete command is needed to turn the system on at the beginning of an operating period. All other commands can be implemented as variable commands. They are as follows:

- Telemetry Transmit
- Real Time Operation
- Normal Operation
- Ambiguity Resolution Method (by baseline switching or by a priori estimation of the LM line of sight)
- Navigation Filter Initialization: Initial position of the HV at the time of receipt of the last variable command in a sequence of 14 variable commands
- Turn Off.

In order to initialize the filter by variable command, the 96 bits representing position would have to be transmitted as 14 seven-bit bytes or as 16 six-bit bytes, each accompanied by a parity bit. Software in the SPU would reassemble the bits into the appropriate format. Once this capability is implemented, it could be used to re-load small sections of the SPU memory if diagnostic routines showed the need for it.

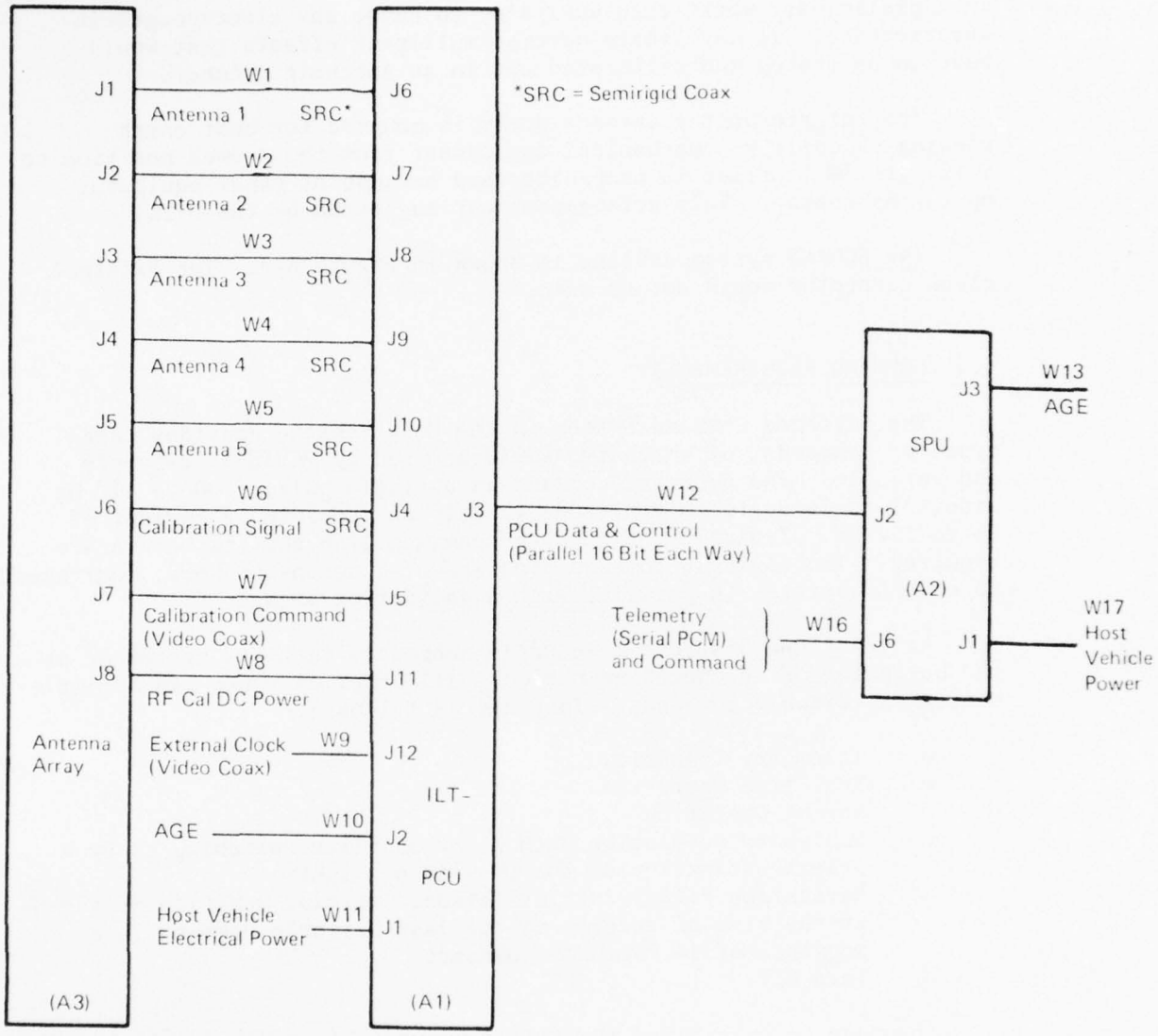


Figure 6-4. SCHANS Space Flight Test System Cabling

6.5 DATA ACQUISITION

6.5.1 PULSE DATA SAMPLES

Data interfaces are shown in Figure 6-5. The "pulse data" transferred to the SPU by the PCU consists of the following for every valid landmark pulse received.

Data (One Sample)	16-Bit Words
Sin/Cos (phase A)	1
Sin/Cos (phase B)	1
Calibration (phase A)	1
Calibration (phase B)	1
Amplitude	1/2
Frequency	1/2
Time of Arrival (TOA)	2
Total	7

6.5.2 NAVIGATION DATA SAMPLES

Each time the navigation filter is updated a "navigation data sample" is stored in the SPU memory for later transmission via telemetry. Table 6-1 shows the desired composition of each such sample, and Figure 6-6 depicts how it is generated.

6.5.3 TELEMETRY

The primary flight test data in the normal mode consists of all the navigation data (i.e. processed data) accumulated during one or two orbits. In real time operation it consist of up to six navigation data samples and up to 600 pulse data samples for every navigation data sample. For both modes, the primary data should be transmitted serially by a Pulse Code Modulation (PCM) downlink, using the pallet telemetry transmitter.

The PCM data frame consists of 69 sixteen-bit words, of which a half word at the beginning of the frame indicates the mode of operation (real time or normal) and the kind of data (pulse, navigation, diagnostic or idle) in the frame. Two words at the end are used for frame synchronization (one spare bit plus the 31-bit Barker pattern suggested by Inter-Range Instrumentation Group Document 106-73). This leaves 66.5 words for data, which could be one navigation data sample (Table 6-1) or nine pulse data samples. The preferred code is Bi-Phase L (Manchester). A transmission rate of 128 kbps is satisfactory. No subcommutation or supercommutation are required.

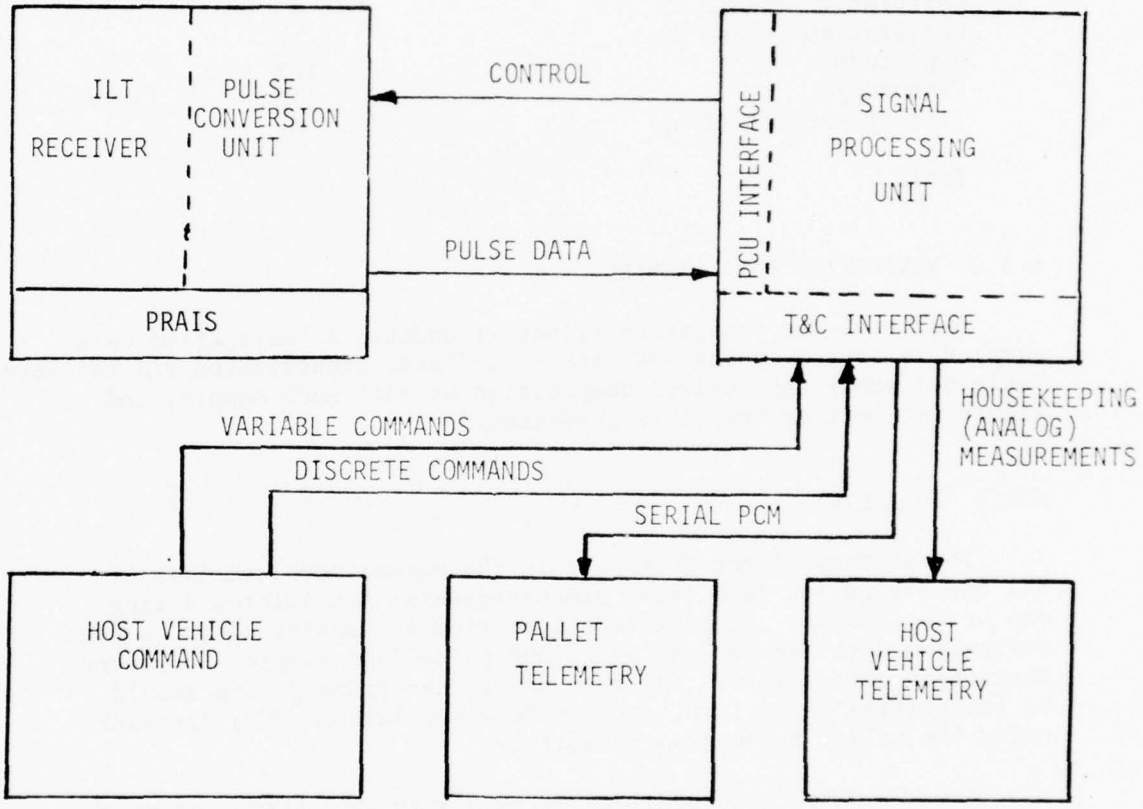


Figure 6-5. Space Flight Test Data Interfaces

TABLE 6-1

NAVIGATION DATA SAMPLE

DATA (ONE SAMPLE)	16-BIT WORDS
LANDMARK IDENTIFICATION (3)	1.5
ILT PHASE A (3 LM's)	3
ILT PHASE B (3 LM's)	3
PULSE FREQUENCY & AMPLITUDE (3 LM's)	3
MISSION TIME TAG	2
NAVIGATION STATE ESTIMATES	48
TOA (3 LM's)	6
	66.5

EACH SAMPLE DERIVED FROM 200 PULSE DATA SAMPLES FROM EACH OF 3 LANDMARKS

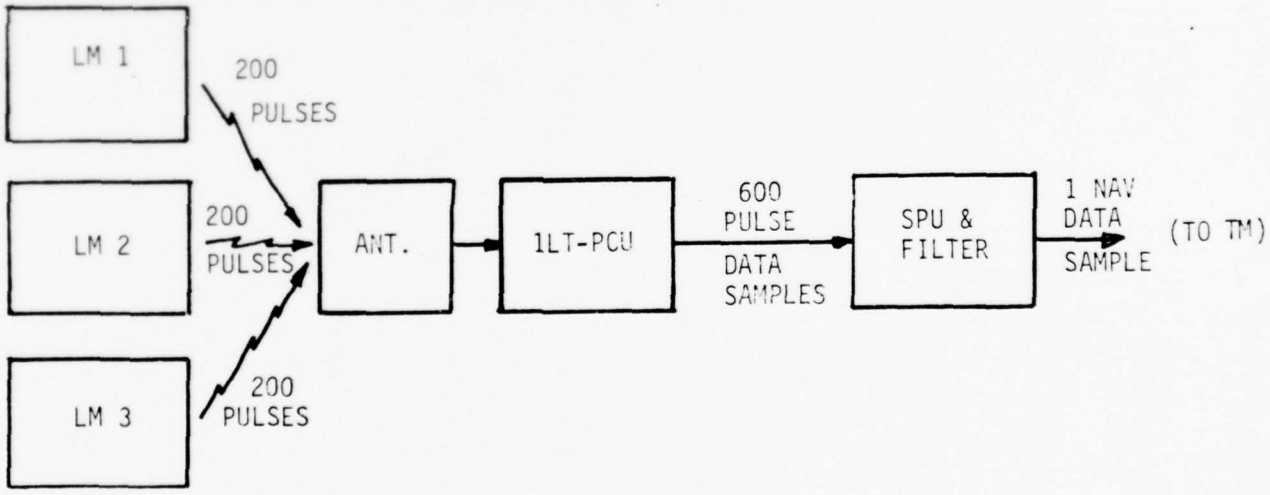


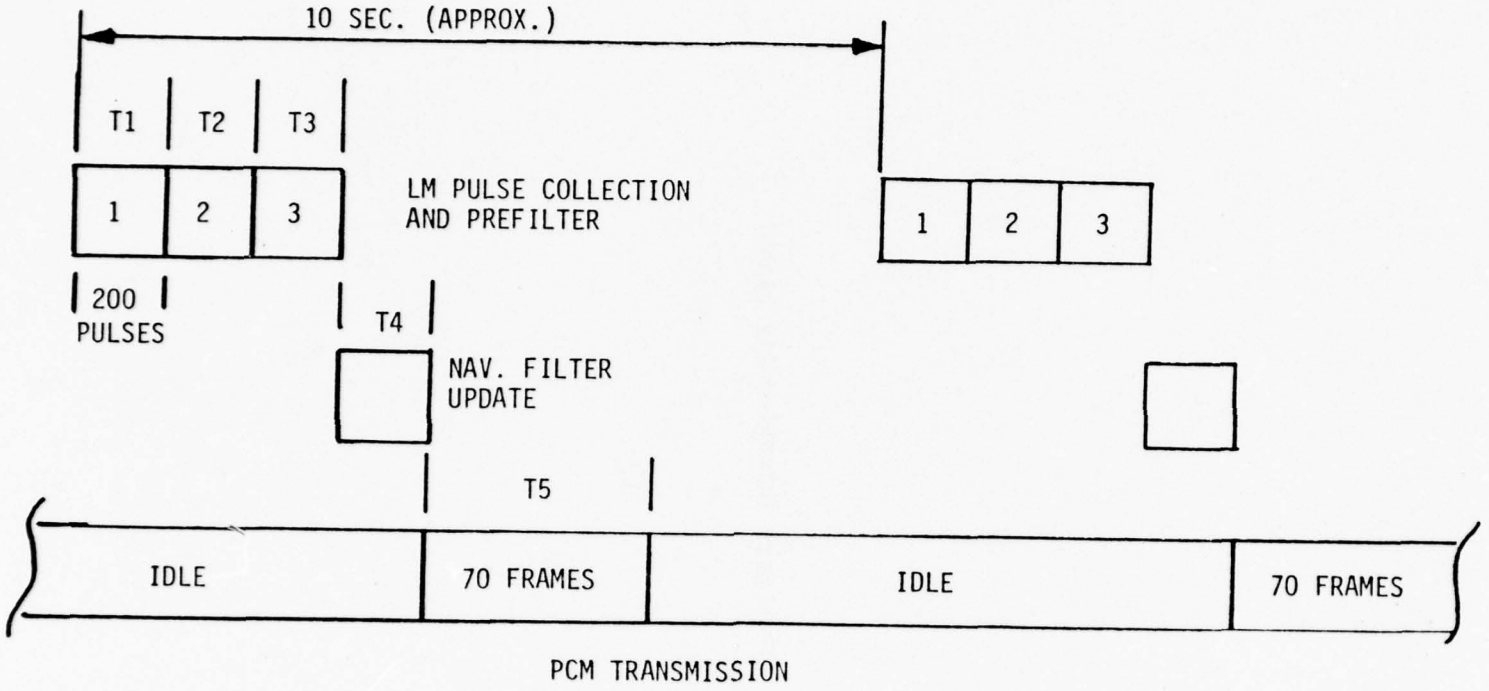
Figure 6-6. Navigation Data Sample Generation

The serial PCM telemetry interface operates under software control. The HV would turn on the transmitter some ten seconds before valid data are to be transmitted. In normal operation, each frame contains one navigation data sample. The entire sequence of frames should be transmitted two or three times before the transmitter is turned off. In real time operation, data transmission would be accomplished as indicated in Figure 6-7.

Housekeeping (analog) measurements were tentatively identified as several supply voltages and temperatures in the 1LT-PCU and the SPU. However, since the payload must provide signal conditioning (to a range of 0 to +5 volts DC), most of them would probably not be implemented. If they were, the lowest sample rate (one sample every 6.4 seconds) in the HV master telemetry system would suffice.

6.6 DATA REDUCTION

If diagnostic routines are used for SCHANS self-test during space flight, the results could be transmitted by PCM telemetry, and "quick look" (same day) analysis would be desirable. For other data, a tape should be delivered to IBM for reduction and analysis in Owego. Supporting ephemeris/tracking data will also be needed.



T1, T2 AND T3 DEPEND ON TRANSMITTER PRI

Figure 6-7. Real Time Data Transmission

(This page intentionally blank)

Section 7

FLIGHT TEST SOFTWARE (TASK 5)

The Flight Test Software task produced a Computer Program Development Specification that is submitted as Appendix C, Volume III of this report. It provides functional descriptions and top-level flows expressing flight test software requirements. The principal components of the SCHANS Operational Program are indicated in Figure 7-1.

The Executive Routine, including its called subroutines, performs system power sequencing, initialization, calibration and interface data transfer control. Specific tasks of the Executive Routine and its called subroutines are as follows:

- Control system power-up sequencing from the power off and standby power conditions.
- Initialize the RF Signal Processing and Executive Program, NADP and hardware control registers.
- Calibrate Local Oscillator
- Calibrate phase detectors.
- Keep real time.
- Service Telemetry.
- Control system power-down sequencing from the power-on to stand-by conditions.
- Process hardware interrupts.
- Load memory via command uplink.
- Dump memory via telemetry.

The Pulse Processing Routine, including its called subroutines, performs all processing functions required to reduce signals intercepted by the PRAIS to landmark-report data suitable for input to the Navigation and Attitude Determination Program (NADP). The Pulse Processing Routine also provides PRAIS tuning and control as required for intercept of desired landmark signals. The Pulse Processing routine and its called subroutines perform the following functions:

- Tune LO to search for and center landmark frequency in IF passband; compute landmark RF.
- Measure landmark signal pitch and roll phase angles; sort and qualify signals based on these measurements.

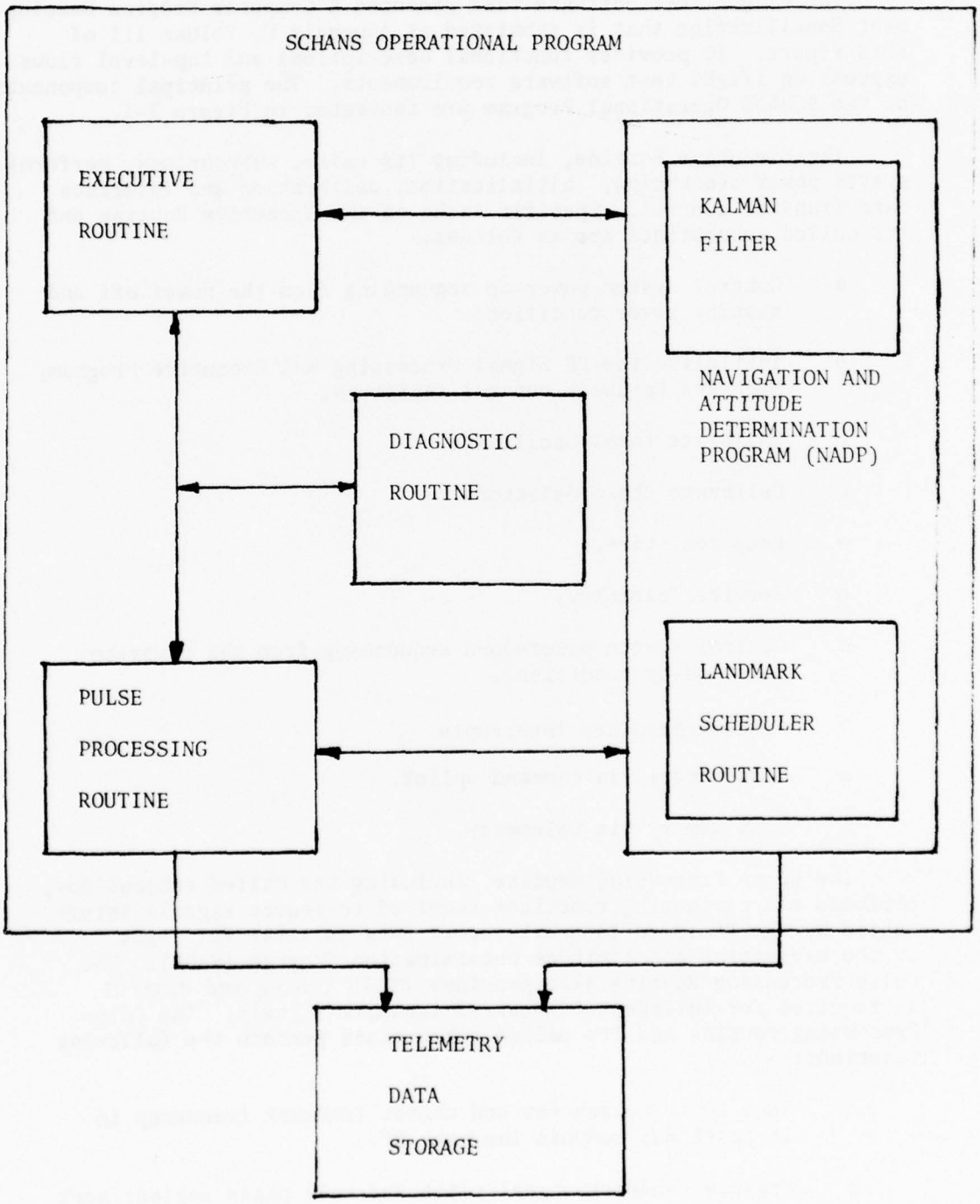


Figure 7-1. SCHANS Operational Program Structure

- Measure landmark pulse TOA. Sort and qualify stable PRI and staggered PRI signals based on this measurement.
- Control long/short baseline antenna switching to collect phase angle data required for phase ambiguity resolution.
- Measure landmark signal amplitude.
- Average and store parameter measurements for input to the NADP.

The Diagnostic Routine, including its called subroutines performs hardware control and data analysis to accomplish internal self-test of the system. Within system configuration constraints, the Diagnostic Routine maximizes failure isolation and reports the results of the self-test. The Diagnostic Routine performs the following functions:

- Checksum memory testing.
- IF calibrator testing.
- Channel testing.
- RF phase calibrator testing.
- Failure word determination and reporting.

Two major processes operate simultaneously in the Navigation and Attitude Determination Program. The first process consist of a series of functions performed by a Kalman filter. These functions include:

- Propagation of the state vector and set-up of the State Transition Matrix (STM).
- Propagation of the Covariance Matrix.
- Calculation of estimated measurements and measurement gradient.
- Calculation of filter weights.
- Update of the estimated state vector.
- Update of the Covariance Matrix.

These functions are exercised sequentially whenever there are measurements available.

The second process is performed by a Landmark Scheduler Routine. The Landmark Scheduler Routine, on the basis of spacecraft landmark geometry, initiates the tracker observations which provide the filter with PRAIS measurements.

Prior to starting the program, tables of landmark data, initial estimates of the ephemeris and the Covariance Matrix, and tables of constants required for navigation computations must be loaded into memory.

For detailed descriptions of inputs, processing functions and outputs by subroutine, the reader is referred to Appendix C, Volume III.

Section 8

ATTITUDE DETERMINATION DESIGN (TASK 7)

8.1 APPROACH

Spacecraft attitude can be measured using the angle measurements from the PRAIS. When these landmarks are continuously in the field of view and ILT measurements can be made at rates compatible with spacecraft angular rates, only the PRAIS is needed for attitude determination. However the addition of an IMU will improve performance and reduce PRAIS measurement frequency.

Attitude estimation is accomplished by optimal filtering of angle data with no hardware changes required. Vehicle attitude is specified by means of quaternions. By Euler's theorem, the rotation of a rigid body may be defined by the direction of the axis of rotation and the magnitude of the rotation. A quaternion is a four element vector $q = q_1 + q_2 i + q_3 j + q_4 k$ which specifies the magnitude u of the rotation and direction cosines cos a, cos b, cos c, of the axis of rotation by $q_1 = \cos u/2$, $q_2 = \cos a \sin u/2$, $q_3 = \cos b \sin u/2$, $q_4 = \cos c \sin u/2$.

Specification of attitude by means of quaternions rather than more familiar direction cosines has at least two advantages: (1) only 4 rather than 9 parameters are required and (2) to minimize round off errors encountered in the numerical integration of the attitude differential equations only a periodic renormalization is required. That is, the computed quaternion $q_c(t)$ is forced to have unit magnitude by dividing its elements by the quaternion norm $\left[\sum_{i=1}^{4} q_c^{\,2}(t)\right]^{\frac{1}{2}}$. In contrast, when direction cosines are employed both periodic renormalization of the rows (columns) of the direction cosine matrix and a periodic reorthogonalization of the rows (columns) are required.

In theory, quaternions could be employed directly as components of the filter state vector. In practice, if quaternions were employed directly as filter state variables, the differential constraint would make the filter attitude covariance matrix positive semidefinite instead of positive definite. Small computational errors could convert this into an indefinite matrix, that is, one possessing both positive and negative eigenvalues. The presence of negative eigenvalues could lead to eventual filter instability.

In addition to position and velocity state variables, the filter will employ as attitude state variables the 3 component vector $\vec{\psi}$ representing the infinitesimal rotation vector needed to bring the true body axes on which the gyros are mounted into coincidence with the computed body axes. This filter formulation also has the obvious advantage of reducing the number of components of the filter state vector by one. The operation of the attitude filter proceed as follows: Six filter states, the 3 infinitesimal rotations $\vec{\psi}$ and 3 gyro drift states constitute the attitude portion of the Kalman filter. Interferometer measurements (prefiltered)* are differenced with predicted measurements. These differences are multiplied by the Kalman filter gain matrix and the gyro drift and infinitesimal rotations updated along with the navigation states. The updated infinitesimal rotations are then converted into equivalent quaternion updates. The gyro outputs are corrected by the the gyro drift estimates. In addition, the covariance of the errors in the filter estimates is updated. The updated quaternion will reinitialize the attitude quaternion differential equations which are then integrated, using the corrected gyro outputs, to the time of the next measurement.

Only the modifications to the navigation filter algorithms required to incorporate attitude estimation are described in this report. It is convenient to decompose the description of these modifications into three parts, (i) attitude propagation (ii) filter update and (iii) covariance propagation.

8.2 ATTITUDE PROPAGATION

The differential equation yielding the time history of the attitude quaternion is

$$(2.1) \qquad \frac{d\vec{q}}{dt} = \tfrac{1}{2} \quad (t)\ \vec{q}$$

$\Omega(t)$ is the 4 x 4 skew symmetric matrix of body rates (obtained from the body mounted rate gyros.)

$$\Omega = \begin{bmatrix} 0 & W_3 & -W_2 & W_1 \\ -W_3 & 0 & W_1 & W_2 \\ W_2 & -W_1 & 0 & W_3 \\ -W_1 & -W_2 & -W_3 & 0 \end{bmatrix}$$

* A suggested algorithm for the interferometer prefilter is described and analyzed in AUTONOMOUS NAVIGATION TECHNOLOGY STUDY SAMSO TRTR No. 7288, pp. 4-29 to 4-33 (Reference 12).

In actuality, the angular rates themselves are not utilized in the differential equations, but the filter corrected (for gyro drift) incremental angles.

$$\delta\theta_i = \int_{t_{i-1}}^{t_i} W_i(t)dt - \hat{b}_i(t_i - t_{i-1})$$

The w_i are the measured angular rates and the b_i are the filter estimates of the gyro drifts. The quaternion differential equation is integrated by the numerical integration algorithm

$$\vec{q}\ (t_{i+1}) = (1 - \frac{CT}{8})\ \vec{q}\ (t_i) + GT\ \vec{q}\ (t_i)$$

where

$$CT = \sum_{i=1}^{3} \delta\theta_i^2$$

$$2\ GT = \begin{bmatrix} 0 & \delta\theta_3 & -\delta\theta_2 & \delta\theta_1 \\ -\delta\theta_3 & 0 & \delta\theta_1 & \delta\theta_2 \\ \delta\theta_2 & -\delta\theta_1 & 0 & \delta\theta_3 \\ -\delta\theta_1 & -\delta\theta_2 & -\delta\theta_3 & 0 \end{bmatrix}$$

The integration is performed in single precision increments with double precision accumulation. The quaternion is normalized just prior to incorporation of a new interferometer measurement.

8.2.1 FILTER UPDATE

We begin with the specification of the estimated ILT measurement. Define the 3 component vector $\hat{A}ILT = (\vec{i}_B.\vec{e}_p)$, $(\vec{j}_B.\vec{e}_p)$, $(\vec{k}_B.\vec{e}_p)$ where $\vec{i}_B$, $\vec{j}_B$, $\vec{k}_B$ are unit vectors specifying the computed body frame and $\vec{e}_p$ is a unit vector from the spacecraft to the landmark. The estimated T baseline interferometer measurement is $\hat{A}_T = (\vec{j}_B.\vec{e}_p)$ and the computed N

baseline measurement is $\hat{A}_N = (\vec{k}_B \cdot \vec{e}_p)$. The components of the unit vectors defining the computed body frame are calculated from the attitude quaternion.

The difference $\tilde{A}_T - \hat{A}_T$ and $\tilde{A}_N - \hat{A}_N$ between measured and computed data are utilized to update the Kalman filter. The attitude components of the measurement (gradient) matrix are:

H [attitude N] = [-AÎLT [2],AÎLT[1],0]

H [attitude T] = [-AÎLT [3], 0,-AÎLT[1]]

The filter update yields new estimates of the infinitesimal rotation $\delta\vec{\Psi}$ and the gyro drift. The gyro drift estimates are used to compensate the gyro outputs. The estimates of $\delta\vec{\Psi}$ are used to update the attitude quaternion by

$$q^*(t_i+) = q(t_i-) + \delta q(i)$$

$$\delta q(i) = -\frac{1}{2} \begin{bmatrix} -q_4 & q_3 & -q_2 \\ -q_3 & -q_4 & q_1 \\ q_2 & -q_1 & q_4 \\ q_1 & q_2 & q_3 \end{bmatrix} \begin{bmatrix} \delta\Psi_x \\ \delta\Psi_y \\ \delta\Psi_z \end{bmatrix}$$

8.2.2 FILTER COVARIANCE PROPAGATION

The filter covariance propagation algorithm modification required to estimate the attitude states via the Kalman filter consists of the generation of the transition matrix corresponding to the $\delta\Psi$ and b states and the calculation of the process noise covariance matrix. We turn to the transition matrix first. In describing the generation of the transition matrix it is convenient to introduce some new notation. Denote by $\left[\vec{X}\right]_{B(t)}$ and $\left[\vec{X}\right]_{I}$ respectively, the components of a vector $\vec{X}$ in the body frame at time t and in the Earth centered inertial (I frame). Define T_{B2I} to be the orthogonal matrix relating the components of x in the two frames.

$$[\vec{x}]_{I} = T_{B2I}\,[\vec{x}]_{B}$$

$$[\vec{x}]_{B_t} = T_{B2I}\,[\vec{x}]_{I}$$

(We note that $T = T^{-1}$ since T is orthogonal). The vector $\vec{\Psi}$ is related to the gyro drift vector vector $\vec{b}$ by $\left.\frac{d\vec{\Psi}}{dt}\right|_{I} = \vec{b}$ where $\left.\frac{d}{dt}\right|_{I}$ denotes differentiation with respect to the inertial frame. Integrating in the inertial frame yields

$$[\vec{\Psi}(ti)]_{I} = [\vec{\Psi}(ti-1)]_{I} + \int_{t_{i-1}}^{t_i} \vec{b}(u)\,du$$

Now

$$[\vec{\Psi}(t)]_{I} = T_{B(t)2I}\,[\vec{\Psi}(t)]_{B(t)}$$

hence

$$[\vec{\Psi}(t_i)]_{B(t_i)} = T_{B(t_{i-1})2B(t_i)}\,[\vec{\Psi}(t_{i-1})]_{B(t_{i-1})}$$

Assuming $[\vec{b}(u)]_{B(ti)}$ is constant yields after some algebra

$$[\vec{\Psi}(t_i)]_{B(t_i)} = T_{B(t_{i-1})}\,[\vec{\Psi}(t_{i-1})]_{B(t_{i-1})} + T_{B(t_{i-1})2B(t_i)} \int_{t_{i-1}}^{t_i} T^{t}_{B(t_{i-2})2B(u)}\,\vec{b}_d$$

This expression must be transformed into one computable from the attitude quaternions. To accomplish this we define

$$T_Q(t) = T_{2B(t)}$$

where the elements of the direction cosine matrix are computable from the attitude quaternion by

$$T_Q(t) = \begin{bmatrix} q_1^2 - q_2^2 - q_3^2 + q_4^2 & 2(q_1q_2 - q_3q_4) & 2(q_1q_3 + q_2q_4) \\ 2(q_1q_2 + q_3q_4) & (-q_1^2+q_2^2-q_3^2+q_4^2) & 2(q_2q_3 - q_1q_4) \\ 2(q_1q_3 - q_2q_4) & 2(q_2q_3+q_1q_4) & (-q_1^2-q_2^2+q_3^2+q_4^2) \end{bmatrix}$$

Now

$$T_{B(t_{i-1})2B(t_i)} = T_{Q(t_i)}\, T_Q^{\,t}\,(t_{i-1})$$

and

$$\left[\vec{\Psi}(t_i)\right]_{B(t_i)} = T_Q(t_i)\, T_Q^{\,t}(t_{i-1}) \left\{\vec{\Psi}(t_{i-1})\right\}_{B(t_{i-1})} + T_{Q(t_i)} \int_{t_{i-1}}^{t_i} T_Q^{\,t}(u)\, du\, \vec{b}$$

Thus if the transition matrix is given by the partioned matrix

$$\begin{bmatrix} \phi_{11} & \phi_{12} \\ 0 & I \end{bmatrix}$$

then

$$\phi_{11}\,(t_i, t_{i-2}) = T_Q(t_i) T_Q^{T}(t_{i-1}) \qquad \phi_{12}(t_i, t_{i-1}) = T_Q(t_i) \left[\frac{T_Q(t_i)+T_Q^{T}(t_{i-1})}{2}\right] \Delta t$$

(trapezoidal integration)

Finally the process noise accounting for the random error in gyro drift is computed as follows. Assuming a random walk gyro drift model the attitude and gyro drift states propagate according to

$$\begin{bmatrix} \vec{\psi}(t_i) \\ \vec{b}(t_i) \end{bmatrix} = \begin{bmatrix} \phi_{11} & \phi_{12} \\ 0 & I \end{bmatrix} \begin{bmatrix} \vec{\psi}(t_{i-1}) \\ \vec{b}(t_{i-1}) \end{bmatrix}$$

$$+ \begin{bmatrix} T_Q^T(t_i) \int_{t_{i-1}}^{t_i} T_Q(u) \left(\int_{t_{i-1}}^{u} n(s)ds \right) du \\ \\ \int_{t_{i-1}}^{t_i} n(s)ds \end{bmatrix}$$

Assuming n(s) is white noise, the process noise covariance matrix becomes

$$Q = \begin{bmatrix} \frac{c}{3}(\Delta t)^3 & \frac{c}{2}(\Delta t)^2 \\ \\ \frac{c}{2}(\Delta t)^2 & c\Delta t \end{bmatrix}$$

Where C is the power spectral density of the process.

8.3 IRU DESCRIPTION

The Inertial Reference Unit Characteristics were shown in Table 2-3. The IRU performance shown was used in the simulation during the SCHANS contract. As indicated, this performance can be met with either a laser gyro package or with conventional gyros. To meet reliability goals on long missions the laser gyro is preferred but even this unit will require redundancy.

Analysis of operation with only the interferometer in a low earth orbit and estimating spacecraft attitude rates instead of using gyros showed that gyros improved navigation accuracy by only 8% and attitude accuracy by only 20%. These results indicate that in orbits where measurements can be made to three landmarks at a rate compatible with spacecraft attitude rates, a gyro package is not required. Alternately, if rate gyros are used in the spacecraft attitude control system, that gyro data could be used to provide attitude memory to reduce the PRAIS measurement frequency.

The IRU is therefore considered an optional system element.

Figures 8-1 and 8-2 summarize the position and attitude results of this covariance analysis. Note that time axis starts at 250 seconds and plot of data begins after first observation of the three landmarks. The attitude accuracy on the SCHANS demonstration orbits is shown in Section 5.

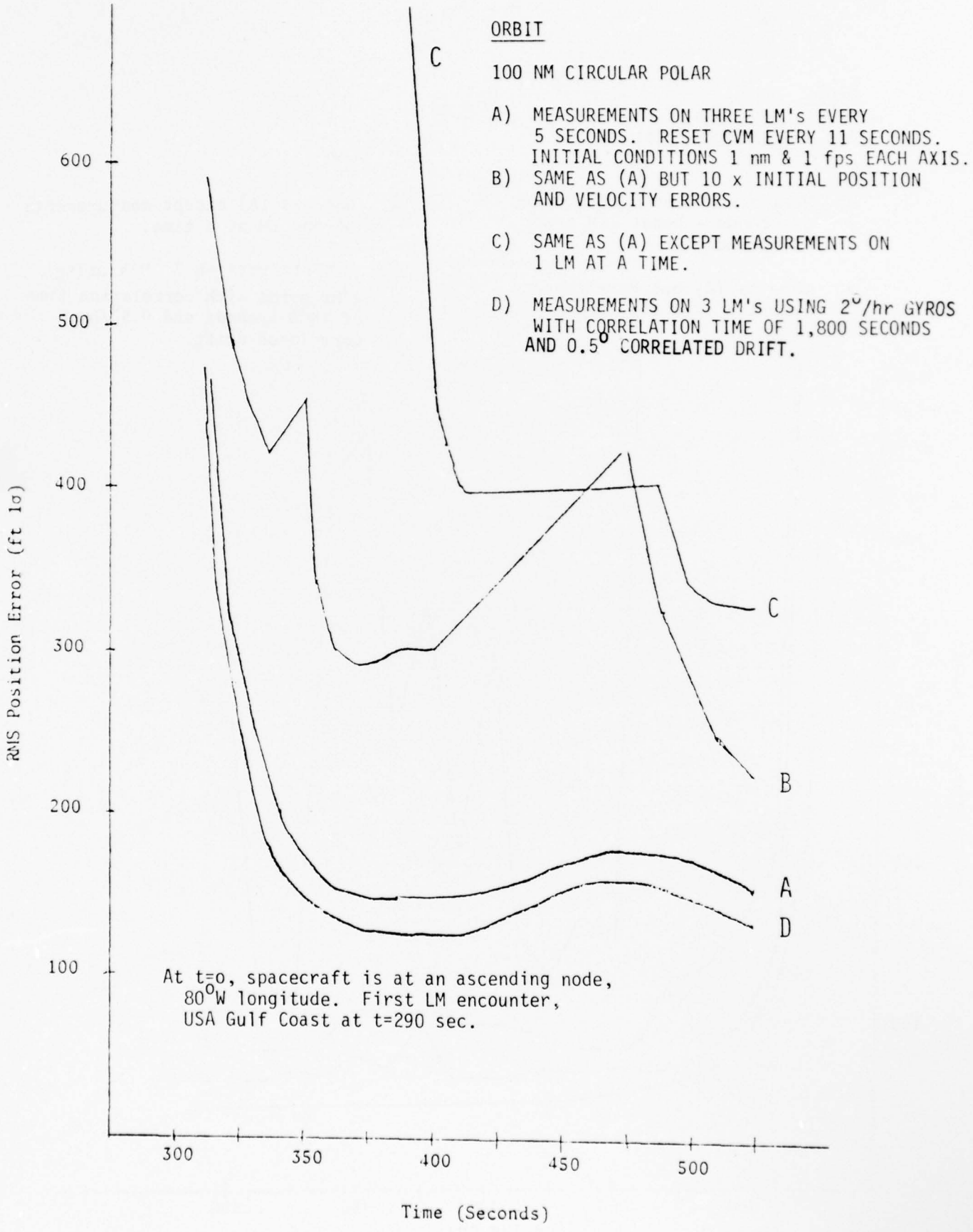


Figure 8-1. Navigation Error

ORBIT

100 Nm Circular Polar

A) Measurements on 3 LM's every 5 seconds - Reset CVM every 11 seconds.

B) Same as (A) but Position and Velocity IC x 10.

C) Same as (A) except measurements on one LM at a time.

D) Measurements on 3 LM's using 2^{o}hr gyros with correlation time of 1800 seconds and 0.5^{o}/hr. correlated drift.

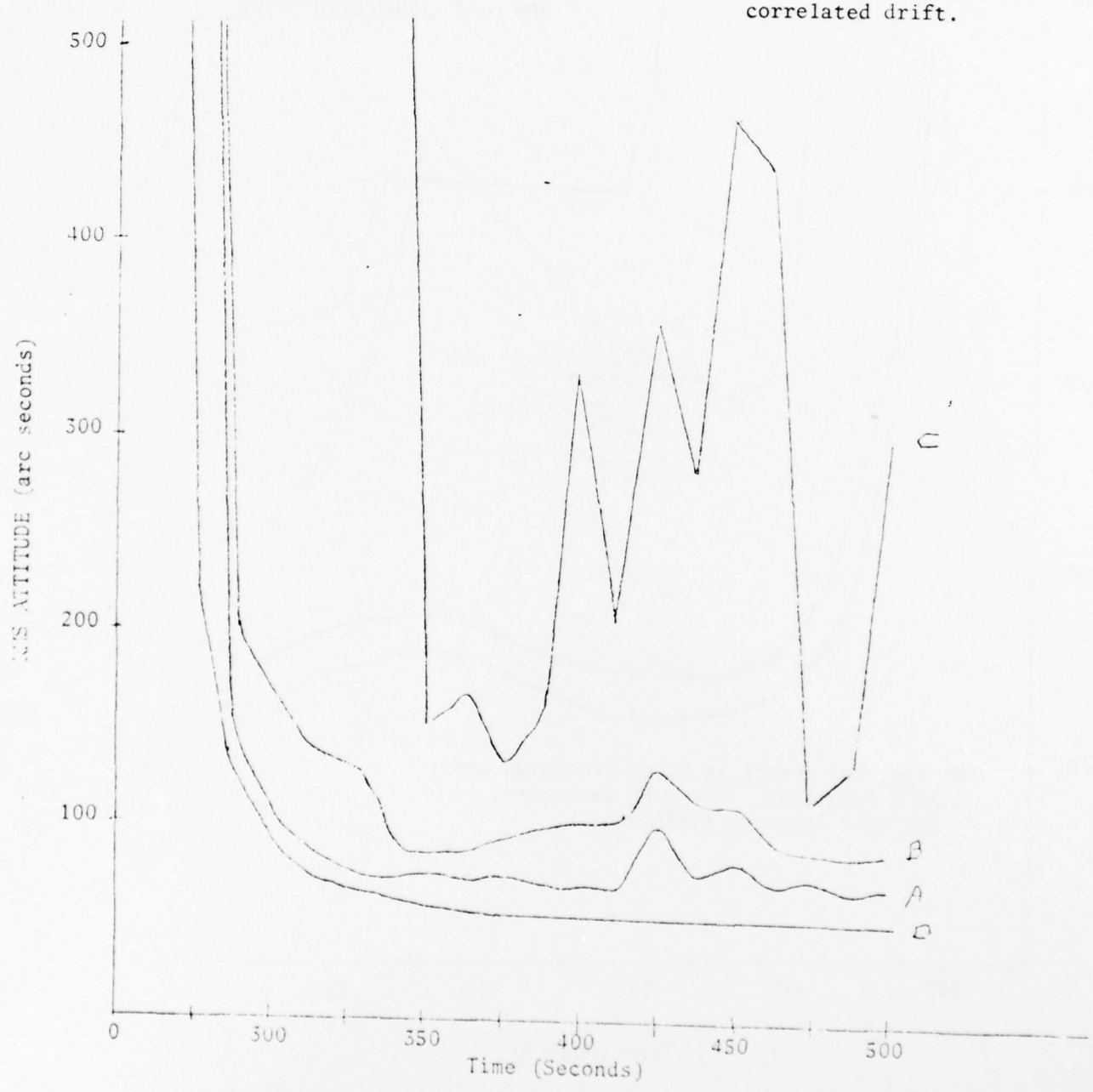


Figure 8-2. Attitude Error

Section 9

RECOMMENDED ADDITIONAL DEVELOPMENTS

The study, analysis, laboratory tests, simulation and design activities performed under a series of SAMSO contracts since mid-1971 have resulted in an excellent foundation for continued development of the PRAIS Navigation System concept. There is a baseline of design documentation, a flight test software development specification. laboratory test data and simulation results. There is also an accumulation of experience that provides insight into the special technical considerations, or key technical issues, involved in planning and performing subsequent phases. Those key issues are identified by program phase in the following paragraphs.

9.1 COMPLETION OF DESIGN

The scope of the SCHANS contract did not embrace design of the entire subsystem, because much of the design depends upon the spacecraft installation and operational constraints, and the spacecraft was not designated at the time the scope was defined. Additionally, a suitable (or at least readily adaptable) antenna array design was expected to be the end product of another program. The next phase should be to complete system, hardware and software designs to a point suitable for fabrication and qualification for space flight test. The key technical issues are as follows.

9.1.1 OPERATIONAL SYSTEMS DESIGN

There are significant differences between the PRAIS operational and space flight test subsystem requirements. The principal differences are indicated in Table 9-1. This design phase is intended to meet the space flight test objectives, with continuous attention to providing growth potential to meet long-range requirements. The differences have the most effect in the area of reliability. Previous multiyear reliability studies show that considerable redundancy will be required at modular levels. Any redundancy implemented in the space flight test subsystem will be limited to the minimum needed for confidence in a successful space flight test. With respect to nuclear survivability, the approach is not to harden or shield the space flight test subsystem, but to monitor the design so that it can be hardened and/or shielded without significant redesign.

Table 9-1

COMPARISON OF SPACE FLIGHT TEST AND OPERATIONAL REQUIREMENTS

Requirement Category	PRAIS Navigation System Requirement	
	Space Flight Test	Operational
Orbital Altitude	Low (100-400 nmi)	High (>5,000 nmi)
Observation Time/LM	<6 min/encounter	30 min — continuous
IRU	Not needed (1)	May be required
Signal/Navigation Processor	SPU	FTSC or other
Telemetry (Downlink)	Serial PCM @128 kb/s • Processed Data • LM Measurements • Diagnostic Results	None required
Command (Uplink)	1 to 3 discretes 7-bit variable	1 to 5 control discretes
Time Reference	Internal 60-MHz Crystal Clock	External 10-MHz Atomic Clock (optional)
Spacecraft	STP Host Vehicle (2)	Unknown
Reliability	To be specified for 120-day mission	7 years mean lifetime
Duty Cycle	<5%, 3 h/day	<3%, up to 24 h/day
Nuclear Survivability	Not required	Required

NOTES: (1) IRU not required in a local vertical stabilized spacecraft having low attitude rates.

(2) Most probable; others, such as Space InfraRed Experiment (SIRE) Spacecraft could be used.

9.1.2 EARLY SPACE FLIGHT TEST PLANNING

Experience in SCHANS shows clearly the importance of early identification of the prospective flight test vehicle and early establishment of liaison among the host vehicle integration contractor, SAMSO and the PRAIS Navigation System contractor. This is more important from a design standpoint than it is for planning the flight test itself. System, hardware and software are affected in the following ways:

- Overall unit configurations and inter-unit cable length are affected by host vehicle (HV) installation provisions and mechanical (launch) environments.
- Antenna array configuration, deployment provisions and RF cable selection criteria are highly dependent upon mounting space allocated by the HV integration contractor and other equipment in its vicinity.
- Thermal design is affected by HV temperature control of mounting surfaces and expected profile of exposure to solar radiation, earth albedo, and deep space.
- Electrical design of the SPU is affected by HV telemetry and command interfaces.
- Attitude stabilization accuracy and rates determine if an IRU is required in space flight test. This in turn affects SPU interface design and has a significant impact on software.
- Operational constraints, such as limitations on operating periods because of different payload priorities, affect software.
- Prime power supply characteristics affect unit power supply selection/design.
- Special requirements are imposed on payloads and payload contractors by each integration contractor. These usually affect EMC, safety, quality, AGE design, personnel access to integration areas and control of support equipment brought into the facility.

9.1.3 ANTENNA ARRAY DEVELOPMENT

The major design considerations in antenna array development are the following:

- Suitability of the antennas in the planned installation in a space environment.

- o Selection of a material for the array supporting structure that is limited in temperature coefficient of expansion or predictable in this respect, low in density yet capable of supporting five antennas and an RF calibrator through the launch environment.

- o Definition of a stable mounting and deployment interface that is stress free after deployment.

- o Specification of coaxial cables suitable for the space environment, low in insertion loss, light in weight, and capable of some flexure (in antenna array deployment) without change in phase shift characteristics.

- o Calibration of the array in an anechoic chamber on a mockup of the portion of the spacecraft to which it will be mounted.

9.1.4 RELIABILITY AND EQUIPMENT REDUNDANCY

In contracts previous to SCHANS, reliability analyses had been confined to identifying system configurations for multiyear missions, and they (not surprisingly) yielded recommendations for hardware redundancy at appropriate levels: circuit, module, and unit. In the current contract, a reliability prediction was calculated near the end of the performance period, based on a baseline space flight test system configuration, without inertial reference sensors. The result indicated a probability of successful operation 120 days after launch of less than 0.9. System and unit-level redundancy were quickly ruled out because of limitations in host vehicle accommodations with respect to payload volume and weight.

The need for an analysis to identify appropriate module- and circuit-level redundancy is apparent. A review of estimated failure rates shows that redundancy could be beneficial in power supplies for the PRAIS and the SPU, in the receiver local oscillator, and in cross-switching arrangements that could take advantage of the redundancy inherent in a five-antenna interferometer array. A redundant memory in the SPU has been considered, but diagnostic software and the ability to reload a portion of memory by command uplink could obviate that. Additionally, redundancy in the RF calibrator was considered, but the additional switchover hardware needed to implement the scheme would in itself impose a reliability penalty and make the net gain marginal.

The current contract could not accommodate such an analysis. It is essential that a selective-redundancy reliability analysis be performed in the design-completion phase.

9.1.5 FLIGHT SOFTWARE DEVELOPMENT

Special attention should be given to development of flight and ground software for the space flight test. No major problems are expected so long as a disciplined, carefully planned and managed approach is followed. The flight software should be developed for the Signal

Processing Unit, which contains a fixed-point microprocessor (designated ML-0). The experience gained previously in working with the navigation software contained in the Autonomous Navigation System (ANS) simulator would be beneficial, but the actual flight software should be developed "from scratch". This permits application of a top-down, structured program development approach and yields adequate documentation. The ground software should be developed entirely in Fortran IV; flight software could be mainly in Fortran IV, with the possibility that some modules may be in ML-0 assembly language.

9.1.6 SYSTEM ENGINEERING

Successful continuation of PRAIS Navigation System Development requires a continuing system engineering effort to maintain interface control, adequate documentation and a coherent system design. The following subject deserves special attention.

In SCHANS and preceding efforts, copious data have been compiled concerning ground-based radars usable as autonomous navigation landmarks. The published data on the various types of radars and their performance characteristics indicate that ample landmarks of known location will be in operation and that satisfactory PRAIS measurements can be made on them. However, there are additional facts that appear not to be readily accessible that are essential to complete the PRAIS flight test plan. These are tolerances -- frequency stability, power variations, antenna pattern accuracy, location accuracy, pulse repetition interval (PRI) stability, pulse rise time tolerances, etc. -- and operational variations: frequency change schedules, PRI stagger patterns, power reductions, pulse shape modifications, etc. All these parameters are expected to vary from one radar installation to another.

It is necessary that the above data be collected on the landmark selected for the flight test and their impact on flight software assessed. Accumulation of these additional facts should primarily be accomplished by SAMSO through government sources, supplemented by some SAMSO/contractor survey trips.

9.2 SUBSEQUENT PHASES

Two sets of hardware should be fabricated and functionally tested. One set should be subjected to qualification tests. The qualification set should then be refurbished and both sets subjected to acceptance tests, including appropriate burn in. The qualification hardware can then serve as flight test spares. This fabrication and test program should be paralleled by:

- o flight test software development
- o flight test planning
- o supporting Aerospace Ground Equipment (AGE) design, fabrication and checkout.

After space flight test, operational system design would incorporate appropriate equipment redundancy, shielding and hardening for long operational life. Software would also have to be modified for operational applications.

REFERENCES

1) SCHANS Program Plan, CDRL Item A001, Contract F04701-76-C-0106 (IBM No. 76-L74-001S), February 1976.

2) Interferometric Landmark Tracker (ILT) CEI Specification Part I, CDRL Item A008, Contract F04701-74-C-0106 (IBM No. 76-L74-003S "A").

Monthly Progress reports, Self Contained High Altitude Navigation System, Contract F04701-76-C-0106.

	Number	Month, 1976	IBM Report No.
3)	3	February	76-L74-006S
4)	4	March	76-L74-008S
5)	5	April	76-L74-009S
6)	6	May	76-L74-010S
7)	7	June	76-D04-002S
8)	8	July	76-D04-003S
9)	9, 10	August, September	76-D04-006S
10)	11	October	76-D04-007S
11)	12	November	76-D04-010S

12) "Autonomous Navigation Technology Study Final Report", SAMSO TR No. 72-88, May 1972 (Contract F04701-71-C-3337).

13) "High Altitude Navigation Study Final Report", six volumes, March 1975, SAMSO TR No. 75-72, Contract F04701-74-C-0565 (IBM No. 75-L74-H1-H6).

14) Autonomous Navigation System (ANS) Simulation Description and Specification (HANS Version), IBM No. 75-L74-H3, March 1975 (delivered under Contract F04701-74-C-0565).

15) ANS Simulation User's Manual (HANS Version), IBM No. 75-L74-H4, March 1975 (delivered under Contract F04701-74-C-0565).

16) ILT Flight Test Model Receiver Design (Autonomous Navigation Technology Phase IB Final Report), SAMSO TR No. 75-298, November 1975.

References (Continued)

17) SCHANS Design Analysis Report, CDRL Item A006, Contract F04701-76-C-0106 (IBM No. 76-D04-008S), November 30, 1976.

18) SCHANS Critical Component Test Plan (Nonsystem), CDRL Item A009, Contract F04701-76-C-0106, (IBM No. 76-L74-007S "B"), September 10, 1976.

19) SCHANS Laboratory Test Report, CDRL Item A007, Contract F04701-76-C-0106 (IBM No. 76-D04-009S), December 1976.

20) SCHANS Flight Test Plan, CDRL Item A014, Contract F04701-76-C-0106, (IBM No. 76-L74-001A), December 10, 1976.

21) "Survivability Criteria for Representative Satellite Subsystems Development, Revised" (U), Aerospace Document AS 75-01377 (S), IBM CD No. 3-076-5678.

22) "The Trapped Radiation Handbook", Defense Nuclear Agency Document 2524H.

23) "Payload Planner's Guide for DoD Space Test Program", Aerospace Report No. TOR-0073(3481-01)-2, October 15, 1972.

24) Widnall, W.S., "Enlarging the Region of Convergence of Kalman Filters Employing Range Measurements," AIAA Journal, Volume 11, No. 3, March 1973, pp. 283-287.

GLOSSARY

Term or Acronym	Definition
ACS	Attitude Control System
A/D	Analog-to-Digital
ADC	Analog-to-Digital Converter
AGC	Automatic Gain Control
AM	Amplitude Modulation
ANARS	Autonomous Navigation and Attitude Reference System (or Sensor)
ANS	Autonomous Navigation Simulation
ANT	Autonomous Navigation Technology
ARS	Attitude Reference Sensor
ATD	Adaptive Threshold Detector
BLP	Basic Logic Page
BOM	Bill of Materials
BPF	Bandpass Filter
BVTCW	Binary Vehicle Time Control Word
bps, b/s	Bits per second
CAL	Calibration/Calibrator
CDRL	Contractor Data Requirements List
CEI	Contract End Item
CG	Center of Gravity
CI	Configuration Item
CLA	Compensated Logarithmic Amplifier
CPU	Central Processing Unit
D/A	Digital-to-Analog
DAC	Digital-to-Analog Converter
dB	Decibel
dBm	Decibels referred to One Milliwatt
DF	Direction Finding

Term or Acronym	Definition
DI	Data Item
DIU	Device Interface Unit
DMCM	Double Modular Core Memory
DME	Distance Measuring Equipment
DoD	Department of Defense
EMC	Electromagnetic Compatibility
EMI	Electromagnetic Interference
FAT	Factory Acceptance Test
FM	Frequency Modulation
FOV	Field-of-View
FTP	Flight Test Plan
FTSC	Fault-Tolerant Spaceborne Computer
GFE	Government-Furnished Equipment
GMT	Greenwich Mean Time
HANS	High-Altitude Navigation (Sub) System
HPF	High-Pass Filter
HV	Host Vehicle
HVIC	Host Vehicle Integration Contractor
ICD	Interface Control Document
IF	Intermediate Frequency
ILT	Interferometric Landmark Tracker
IMU	Inertial Measuring Unit
INS	Inertial Navigation (Sub) System
I/O	Input/Output
IPL	Initial Program Load
IRG	Integrating Rate Gyro
IRIG	Inter-Range Instrumentation Group
IRU	Inertial Reference Unit
kbps, kb/s	Kilobits per second

Term or Acronym	Definition
LM	Landmark
LO	Local Oscillator
LOG AMP	Logarithmic Amplifier
LOS	Line-of-Sight
LPF	Low-Pass Filter
LSB	Least-Significant Bit
MAB	Missile Assembly Building
MDS	Minimum Discernible Signal
MFR	Manufacturer
MIB	Multilayer Interconnection Board
MSB	Most-Significant Bit
MTS	Microprogrammed Test Set
MUX	Multiplexer
nmi	Nautical mile
NRZ	Nonreturn to Zero
NRZL	Nonreturn to Zero, Level
ns	Nanosecond(s)
PAR	Passive Ranging
PCM	Pulse Code Modulation
PCU	Pulse Conversion Unit
PLL	Phase Lock Loop
PMPAG	Parts, Materials, and Processes Advisory Group
PMPCB	Parts, Materials, and Processes Control Board
pps	Pulses per second
PRAIS	Passive Ranging Interferometric Sensor
PRF	Pulse Repetition Frequency
PRI	Pulse Repetition Interval
PTMU	Precision Time Measurement Unit
PTR	Precision Time Reference

Term or Acronym	Definition
QA	Quality Assurance
RF	Radio Frequency
R&M	Reliability and Maintainability
RMS (or rms)	Root mean square
RTC	Real-Time Command
RTS	Remote Telemetry Station
SAW	Surface Acoustic Wave
SCF	Satellite Control Facility
SCHANS	Self-Contained, High-Altitude Navigation System
SDL	Software Development Laboratory
SGLS	Space-Ground Link System
SIRE	Space Infrared Experiment
SIU	Special Interface Unit
SNR	Signal-to-Noise Ratio
SPC	Stored Program Command
SPU	Signal Processing Unit
SPVC	Stored Program Variable Command
STF	Satellite Test Facility
STP	Space Test Program
SYNC	Synchronization
TC/B	TOA Counter/Buffer
TM	Telemetry
TOA	Time-of-Arrival
TSP	Twisted Shielded Pair
TT&C	Telemetry, Tracking, and Command
TTL	Transistor-Transistor Logic
VDC	Vandenberg
VST	Vehicle System Time
VTO	Voltage-Tuned Oscillator

Term or Acronym	Definition
VTS	Vandenberg Tracking Station
WTR	Western Test Range
XMTR	Transmitter
μs	Microsecond